Energy based visualisation of a Brayton cycle power conversion unit for the purpose of condition monitoring

H Neser

orcid.org/0000-0001-5355-7513

Thesis submitted in fulfilment of the requirements for the degree *Doctor of Philosophy in Computer and Electronic Engineering* at the North-West University

Promoter:	Prof G van Schoor
Co-promoter:	Prof KR Uren

Graduation ceremony July 2019

Student number: 12826294

Declaration

I, Henri Neser, hereby declare that the thesis titled “Energy based visualisation of a Brayton cycle power conversion unit for the purpose of condition monitoring” is my own original work and has not already been submitted to any other university or institution for examination.

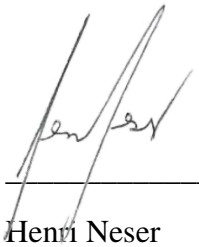

Henri Neser

Signed on the 23th day of May 2019 at Potchefstroom.

To my wife, may we reap the rewards of the sacrifices made to complete this journey.

Acknowledgements

This was a life changing journey for me, moulding and shaping me more than I could have imagined. All the honour and glory to God.

To my promoters, Prof. George van Schoor and Prof. Kenny Uren, thank you for your continued guidance, support, understanding and motivation.

I would like to thank M-Tech Industrial (Pty) Ltd for the financial support and access to the Flownex® Simulation Environment software. This study would not have been possible otherwise.

Thank you to my fellow researchers in the McTronX Research Group for your contributions in various degrees.

To my family and my family-in-law, I appreciate all the encouragement. To my parents specifically, thank you for all the support and assistance.

Lastly, I could not have completed this journey without the love, support and motivation from my wife. Love you.

"Helping one person might not change the whole world, but it could change the world for one person." Anon

Abstract

The efficient operation of industrial plants has been the subject of many studies, due to an increased awareness of greenhouse gas emissions and dwindling natural resources. Condition monitoring is key to the efficient operation of a plant. Part of condition monitoring is fault detection and isolation (FDI). Various methods have been developed and implemented for the purpose of FDI in industrial plants. These methods are mostly based on process monitoring, requiring large amounts of data.

Based on the fact that an industrial plant can be viewed as an energy transformation process, energy has been proposed as a non-domain specific monitoring parameter for the purpose of FDI. An energy-based representation of the industrial plant will, therefore, be required. Energy-based representations are commonly used during the design phase to optimise the plant or to monitor the plant's efficiency during its lifespan, but not for FDI.

In this study, a basic Brayton cycle power conversion unit (PCU) is used as a case study to determine the suitability of an energy-based approach to FDI. The PCU is completely characterised by an attributed graph matrix in terms of energy and exergy. Exergy was identified as being part of the energy characterisation of a thermodynamic power cycle, such as a Brayton cycle. The primary contribution of this study, is the compilation of a unique energy-based signature, from the attributed graph matrix, visualising changes in the operating conditions of the PCU.

Two methods are used in this study to create energy-based signatures, namely a residual-based method and an eigendecomposition-based method. Both methods produced unique signatures, specific to the operating conditions of the PCU, which was successfully used for FDI.

A third method (enthalpy-entropy error-based method) proposed by du Rand is also presented and as a secondary contribution, the methods are compared and evaluated based on the attributes an effective FDI method should exhibit. As an additional contribution, an exergy ratio is proposed, defining the exergetic conversion ratio of the components in the PCU. The exergy ratio will serve as an indication of the effect a fault has on a component's ability to transform exergy between domains.

In this study, it is concluded that an energy-based visualisation of a Brayton cycle PCU can be used for FDI.

Keywords: *Exergy, Energy, Brayton cycle, Fault signature, Fault detection and isolation, Exergy ratio, Visualisation*

Contents

List of Figures

List of Tables

List of symbols, subscripts and operators

Symbol	Description	Unit
B	Exergy	kJ
b	Specific exergy	kJ/kg
$\dot{B}$	Exergy flow	kJ/s
$\dot{b}$	Specific exergy flow	kJ/s·kg
c	Speed of light	m/s
C_p	Specific heat at constant pressure	kJ/kg·K
C_v	Specific heat at constant volume	kJ/kg·K
E	Energy	kJ
e	Specific energy	kJ/kg
$\dot{E}$	Energy flow	kJ/s
H	Enthalpy	kJ
h	Specific enthalpy	kJ/kg
$\dot{H}$	Enthalpy flow	kJ/s
$\dot{h}$	Specific enthalpy flow	kJ/s·kg
m	Mass	kg
η	Efficiency	%
N	Compressor / Turbine speed	r/min
P	Pressure	kPa
ρ	Density	kg/m^3
Q	Heat	kJ
$\dot{Q}$	Heat flow	kJ/s
R	Residual	
S	Entropy	kJ/K
s	Specific entropy	kJ/kg**.**K
$\dot{S}$	Entropy flow	kJ/s·K
$\dot{s}$	Specific entropy flow	kJ/s·kg·K
T	Temperature	K
U	Internal energy	kJ
V	Volume	m^3
W	Work	kJ
Υ	Specif heat ratio	

Subscript	Example	Description
0	T_0	Reference temperature
in	B_{in}	Exergy into a component
out	B_{out}	Exergy out of a component
ext	B_{ext}	Exergy between a component and the environment
lost	B_{lost}	Exergy lost
dest	B_{dest}	Exergy destroyed
tran	B_{tran}	Transitional exergy
cons	B_{cons}	Exergy consumed ($B_{cons} = B_{in} - B_{tran}$)
prod	B_{prod}	Exergy produced ($B_{prod} = B_{out} - B_{tran}$)
C	T_C	Temperature of cold reserviour
H	T_H	Temperature of hot reserviour
act	$\mathbf{G}_{act}$	Actual graph matrix **G**
res	$\mathbf{G}_{res}$	Residual graph matrix **G**
ref	$\mathbf{G}_{ref}$	Reference graph matrix **G**

Operator	Example	Description
˙	$\dot{m}$	flow (per second)
`	$\grave{m}$	non dimensional mass flow
Δ	ΔE	change in energy

List of acronyms

AEM	Abnormal event management
ATR	Auto thermal reformer
CBM	Condition-based maintenance
CM	Condition monitoring
COP	Coefficient of performance
CT	Compressor turbine
FD	Fault diagnosis
FDD	Fault detection and diagnosis
FDI	Fault detection and isolation
mtoe	Million tons oil equivalent
NPP	Nuclear power plant
PBMR	Pebble bed modular reactor
PCU	Power conversion unit
PGM	Process graph modelling
PT	Power turbine
RLC	Resistor, inductor and capacitor

CHAPTER 1

Introduction

In this chapter the motivation for this study is presented and the objectives listed. The chapter concludes with an overview of the thesis.

1.1 Motivation

A major challenge, in modern large scale industrial plants, is the effective and efficient operation of the plant. The operation of the plant is defined as the proactive, organised and systematic coordination of the procurement, conversion, distribution and utilisation of energy [1]. Energy efficiency is key to the efficient operation of a plant. Energy efficiency is defined as the ability to provide a higher level of service for the same energy input or the same level of service at a reduced energy input [2]. In an industrial context, this includes an effective condition monitoring system and efficient maintenance strategies to ensure the efficient utilisation of energy. Energy efficiency is also a key parameter utilised during the design phase of industrial plants to ensure an energy efficient system [3]. Before the global awareness of energy efficiency, the main design goal was cost (as cheap as possible), but since the 1970s, the design goals shifted to a "best value for money" (as energy efficient as possible) design [3, 4].

Various predictions have been made as to the future energy demand, energy supply and available energy resources. The consensus of these studies is that renewable energy and nuclear energy will become more dominant in the future [5–8]. In 2013 the total world supply of energy was 13371 million ton oil equivalent (mtoe) with 35.8% being supplied by oil and only

11.4% by renewable and nuclear sources. It is predicted that by 2030 the demand will increase to more than 17000 mtoe, with renewable and nuclear supplying 24%. In 2012, 40.4% of the total world electricity supply (22668 TWh) was generated from coal and 15.9% from nuclear and renewable sources. It is expected to see a steady increase in electricity supplied from nuclear and renewable sources over the next decade [5, 6, 9, 10]. With the predicted increase in nuclear and renewable (specifically solar) energy sources for electricity generation, the performance and efficiency of these systems are of concern. Recent advances in materials and technology and the high temperatures associated with nuclear and solar energy, make the Brayton cycle well suited in these systems. Compared to other thermodynamic cycles, the Brayton cycle is ideal in terms of efficiency, under the operating conditions associated with nuclear and renewable energy sources [11]. With an expected increase in Brayton cycle based power conversion units (PCU) and an energy efficiency mindset, the ability to monitor the condition and performance of such a system during operation is crucial.

According to Shepard and Webster [12], the operation and maintenance of a process can be improved through the optimisation of the combustion processes, incorporating performance measurements, implementing condition monitoring and maintenance strategies or adequate life cycle planning. This study will focus on the condition monitoring and performance measurement of a Brayton cycle PCU. Condition monitoring is a mature research field with its roots in vibration analysis, specifically of rotating machines. Rotating machines are common in industrial plants and therefore still an active research field [13–15]. This led to new methods and equipment being developed for condition monitoring in an industrial plant [16–18]. Condition monitoring of a system is commonly done per component, measuring component-specific parameters with minimal indication of the overall plant condition. One possible reason is the vast number of parameters and domains involved in an industrial process, leading to the "Big Data" problem [19, 20].

With modern intelligent control systems, the outputs of industrial plants are controlled to be constant (specific setpoints), thus masking any indications of a fault in the output of the plant [20]. Any changes in the operational condition, either due to a fault or a change in the operating setpoints, will, therefore, be detected by changes in the cycle (process plant condition monitoring) rather than the final output of the plant [21, 22].

In the work of du Rand, enthalpy-entropy diagrams were implemented for the purpose of condition monitoring of a Brayton cycle PCU [23–26]. In his work, faults could be uniquely identified using enthalpy and entropy, but it gave no clear indication as to the effect the fault has on the system's performance. In the work of Marais [27], the use of energy and exergy for the purpose of fault detection and isolation in an autothermal reformer (ATR) was investigated. In his work different fault conditions were simulated in an ATR and by monitoring the change

in exergy through the system, the faults were uniquely identified.

The complete Brayton cycle can be viewed as an energy transformation process involving different physical domains (hydraulic, mechanical and thermal) where ultimately, thermal energy (heat) is transformed into mechanical energy (work). Due to the different physical domains involved, a multi-domain parameter is required to effectively monitor the complete cycle. Since energy is a conserved property (first law of thermodynamics) that cannot be destroyed or created and can only be transferred between domains, it has been identified as a suitable multi-domain parameter [27, 28]. By representing each component in the system as an energy conversion node, the various components in the cycle can easily be related independent of its physical domain.

In a thermodynamic power cycle, such as the Brayton cycle, a property of energy known as exergy and defined by the second law of thermodynamics is also of significance [29]. Utilising the energy and exergy data taken at various points in the cycle, an energy-based representation or attributed graph of the cycle can be compiled [23, 27, 30, 31]. Structural information regarding the cycle is retained with the use of an attributed graph. This representation of the cycle can be seen as the energy-based visualisation of the cycle. Various techniques such as residual calculation [23, 27], eigendecomposition [31] and graph matching [31, 32] are used to create a unique signature of the cycle. Any fault in the cycle will change the signature. Comparing the signature of the cycle, under present operating conditions, with known signatures of fault conditions, allows for the detection and isolation of fault conditions. Fault detection and isolation are central to the condition monitoring of large scale industrial plants such as a Brayton cycle PCU.

1.2 Possible areas of contribution

Possible areas where contributions can be made are listed below. The contribution of this study is listed in section 1.6.

Possible areas of contribution are:

- Energy-based representation/characterisation of thermodynamic power cycles [30, 31],
- Energy-based fault diagnosis in thermodynamic power cycles [25, 27],
- Evaluation of the performance of a Brayton cycle, based on changes in energy and exergy, under various conditions [23],
- Reducing the amount of data required for fault diagnosis in a thermodynamic power cycle [19, 27].

1.3 Aim of research

This study will focus on utilising energy, as a multi-domain parameter, for the purpose of condition monitoring on a Brayton cycle PCU. Suitable methods will be used, based on energy, to visually represent the cycle either graphically or mathematically, and to detect and isolate different fault conditions in the cycle. The visual representation of the operating conditions can be seen as the energy-based signature. This signature will be used for the purpose of fault detection and isolation.

1.4 Research objectives

The **primary objectives** of this study will be to create an energy-based representation of a thermodynamic power cycle, specifically the Brayton cycle, for the purpose of characterising the energy flow and transformation through the cycle under different conditions. Suitable methods will be used, based on the energy-representation of the cycle, to detect and isolate fault conditions.

As **secondary objectives**, the methods proposed in this study for fault detection and isolation will be compared with work done by du Rand [23]. The use of the energy characteristics of the cycle to determine the effect a fault condition has on component efficiency will also be of interest.

1.5 Methodology

Following the literature provided in Chapter 2 regarding condition monitoring and fault diagnosis, Chapter 3 explains thermodynamic power cycles and the concept of energy and exergy, as applicable to this study. From this, the practicality of energy as a multi-domain parameter was highlighted. Using Flownex® simulation software, the Brayton cycle PCU that will be used in this study was simulated. The Flownex® software is a validated and verified thermohydraulic simulation environment [33, 34]. The model used in the simulation will be a representative model and will be validated against a validated Brayton cycle. The operating conditions for the simulation model are based on validated data used by du Rand [23] and data presented in the work of van Niekerk et al. [35]. From the simulation, the energy and exergy characterisation of the cycle can be determined for various operating conditions. The energy and exergy characterisation is used to create an energy-based representation of the cycle in

terms of an attributed graph matrix. Possible fault conditions (single and multiple simultaneous faults) were identified from literature. The fault conditions were simulated with different fault magnitudes, and an energy-based representation of the cycle under various fault conditions and fault magnitudes was compiled. Changes in the operational setpoint of the cycle were also simulated, as well as fault conditions at different operational setpoints.

Two different methods, based on the energy representation of the cycle, are proposed to compile unique energy-based signatures of the cycle for normal operating conditions and fault conditions. The first method for compiling a signature is based on calculating residuals between the normal operating conditions (reference conditions) and the actual operating conditions. The implementation of residuals is common in the field of fault detection [36].

The second method utilises eigendecomposition and the directional changes in the eigendecomposition to compile a signature of the cycle. Eigendecomposition was successfully used by van Graan et al. [31] for the purpose of FDI on a heat exchanger. In this study, the Brayton cycle is represented as an attributed graph matrix and therefore the possibility of using eigendecomposition for the purpose of FDI is investigated.

The signature of the cycle is a graphical representation of the difference between the energy and exergy characterisation of the cycle under current operating conditions and what is considered to be normal operating conditions. Reference fault signatures are compiled for different fault conditions by simulating the current operating condition as a fault condition. The signature of the cycle is compared to the reference fault signature to detect and isolate fault conditions. The two methods presented are compared based on the attributes an FDI method should exhibit as identified by Venkatasubramanian et al. [37], to highlight the feasibility of the methods. The methods are also compared with the enthalpy-entropy approach presented by du Rand [23]. The effect a fault condition has on the performance of each component is also determined based on the exergy transfer in the components.

1.6 Contribution

The **primary contribution** of this study is to utilise a multi-domain parameter (in this case, energy) to completely characterise a Brayton cycle PCU, for the purpose of fault detection and isolation. Included in the primary contribution, is the compilation of a unique energy-based signature for the cycle, based on the energy characteristics of different operating conditions, including fault conditions. This signature can then be used to detect and isolate faults in the cycle.

As a **secondary contribution**, the FDI methods proposed in this study will be evaluated according to the required attributes for an effective FDI method. The entropy-enthalpy method for FDI, proposed by du Rand [23], will also be compared to the methods presented in this study.

As an **additional contribution**, a method is proposed to quantify the effect that changes in the operational conditions will have on the exergetic performance of the components in the cycle.

1.7 Thesis layout

In **Chapter 2** an overview of literature relevant to condition monitoring is presented. This includes current methods being implemented and methods being researched and proposed for fault detection and isolation of a complete process, using energy as the monitoring parameter. **Chapter 3** gives a brief overview of thermodynamics and the concept of energy and exergy as applicable to a thermodynamic power cycle. A representative model of a Brayton cycle PCU is presented in **Chapter 4** with simulation results. Possible fault conditions are also listed and simulated in this chapter. In **Chapter 5** the cycle presented in Chapter 4 is characterised in terms of energy. Two methods (a residual-based and an eigendecomposition-based method) are proposed to compile an energy-based signature, that is unique to operating conditions of the cycle. The methods are implemented in **Chapter 6** to create a unique reference fault signature for each fault condition. The same methods are also used to create an operational signature of the cycle under current operating conditions (either normal or fault conditions). The operational signature is compared to the reference fault signatures to determine if a match exists, indicating a fault. The method proposed by du Rand [23] is compared in this chapter to the methods proposed in this study. A performance measurement is also introduced as an indication as to the effect a fault has on the performance of each component. **Chapter 7** concludes this study.

CHAPTER 2

Literature survey

The aim of this study is to utilise energy as a multi-domain parameter for the purpose of fault detection and isolation in a Brayton cycle power conversion unit. This chapter serves as an introduction to condition monitoring and more specifically fault detection and isolation. Various techniques and methods implemented in fault diagnosis schemes are discussed, including recent studies on energy-based fault diagnosis.

2.1 Maintenance activities

The maintenance philosophies implemented in industrial processes are influenced by numerous factors, such as plant location, operating conditions, machine availability and company policies. Maintenance activities can be categorised as either reaction-based, time-based or condition-based monitoring [38]. **Reaction-based maintenance** is based on operating the system until a component fails. Only once a failure has occurred, maintenance is carried out on the system or component. This type of maintenance has the potential of causing a chain effect of failures as a result of one component failing. This can be expensive and time-consuming in addition to the compromise of normal safety regulations.

Time-based maintenance is based on periodic maintenance of components, regardless of the condition of the components. This is somewhat of an improvement on reaction-based maintenance, but a component failure between scheduled maintenance activities will default back to reaction-based maintenance. This type of maintenance also results in the unnecessary maintenance of components that is in perfect working condition. This has the potential of

compromising the component, previously in good working condition, due to the maintenance being performed. According to Rio [39] and Anderson [40], 19% of preventative maintenance is unnecessary, 25% of preventative maintenance occur too late, 30% of preventative maintenance occur too frequently, 45% of preventative maintenance does not reduce downtime and 82% of components will have a reduced risk of failure by implementing condition monitoring.

The third type of maintenance is **condition-based maintenance** (CBM). This maintenance method is based on the continuous, non-intrusive monitoring of component-specific parameters, to assess the condition of the components in the system. This is defined as condition monitoring (CM) [39–41]. Based on changes in the parameters (conditions), the required maintenance can be scheduled and planned for in advance.

Implementing CM ensures that all maintenance relevant decisions are based on accurate and quantifiable information, making this method more economical and safer. The declining cost of sensors and increased accuracy have made CM a viable option for many systems [42].

2.2 Condition monitoring

Condition monitoring is defined by Rao [41] as a holistic multi-discipline, based on systems thinking. In the broad sense, condition monitoring includes economics, instrumentation, engineering, management, fault detection and diagnosis, maintenance strategies and legal matters. Condition monitoring is a data-driven technique implemented to optimise overall plant operations and productivity, by monitoring actual operating conditions of components [43]. Three key factors were identified by Rao [41] influencing the productivity of a plant, one being to improve the production of the plant, which can be achieved with CM.

Condition monitoring improves production by reducing maintenance cost and plant downtime. The data acquired from CM can also be utilised to achieve optimum reliability, capacity and efficiency from components [44]. Condition monitoring is commonly applied to individual components focusing on vibration monitoring, lubrication analysis, thermography and acoustic emissions [41, 45]. Vibration analysis is the most common form of condition monitoring. Transducers are installed to continuously measure vibrations in the component. A baseline is established for the normal vibrations of the component and any deviation from this baseline is indicative of a fault.

Lubrication analysis is also a common and an easily implemented form of condition monitoring. By analysing the lubricant for any foreign particles, possible fault conditions can be detected. Thermography uses thermal imaging to detect any hotspots in a component due to

a fault. A baseline image, under normal conditions, is compared with the present thermal image and any deviations in temperature will indicate a fault. Acoustic emission is based on the sound emitted by a component. A fault condition will change the sound emitted by the component or cause a sound to be emitted.

Literature on CM of individual components is abundant, especially for rotating machines. This is not surprising as condition monitoring has its roots in monitoring the vibrations in rotating machines. These methods are domain specific, monitoring a specific parameter best suited to indicate a fault in the individual component. As an example, the temperature of a bearing is monitored to determine the condition of the bearing, as an increase in temperature will indicate a fault with the bearing itself or with the lubrication of the bearing. In the case of a rotating shaft, the vibrations will be monitored and any change in the vibrations will be indicative of a fault condition.

Condition monitoring of a complete system is based on process monitoring, which involves taking measurements such as pressure, mass flow and temperature throughout the system. Any changes in these measurements can indicate a fault condition. Process monitoring results in vast amounts of data being collected, analysed and stored. Advances in technology improved the computational resources required to effectively process large amounts of data into usable information [19]. Recent work by du Rand [23] and Marais [27] focused on reducing the data required for monitoring the condition of large multi-domain systems, by monitoring multi-domain parameters in the system. The methods proposed by du Rand is based on enthalpy and entropy, while Marais used energy and exergy.

A key part for the condition monitoring of an entire plant is fault detection and diagnosis, this will be discussed next.

2.3 Fault detection and diagnosis

Abnormal event management (AEM) deals with the detection and diagnosis of abnormal conditions and suggesting possible corrective actions. This process is still mainly a manual process relying on human operators. This has proven to be problematic considering the scope of such a diagnostic process and the size and complexity of modern systems. It is no surprise that a major contributor to industrial accidents is operator error [37]. This can be attributed to the large amount of data being acquired and the need for a timeous detection and diagnosis of an abnormal event. Various techniques have been developed to automate the process of AEM. These techniques are commonly referred to as fault detection and diagnosis (FDD) [46]. The

techniques generally consist of a model to characterise the normal operating condition and a method to determine any deviations [20].

A distinction should be made between faults, failures and malfunctions. A **fault** is defined as any unintentional deviation of a parameter from that which is considered to be the standard condition [47, 48]. A **failure** is a permanent interruption in the system due to a fault, while a **malfunction** is an intermittent interruption in a system [49]. A fault can be classified according to its location or characteristics [46]. The fault classification is summarised in Table 2.1.

Table 2.1: Classification of faults

Fault classification	
Location-based	Characteristics-based
System faults	Additive/Multiplicative faults
Sensor faults	Abrupt/Incipient/Intermittent faults
Actuator faults	Permanent/Transient faults

Location-based faults are self-explanatory but characteristics-based faults require additional explanation [49]. The fault can contribute to the system as an additive or multiplicative fault. Additive faults appear as offsets on sensors, while multiplicative faults are associated with parameter changes in the system. A fault can take the form of an abrupt, incipient or intermittent fault as illustrated in Figure 2.1. The fault can either be permanent which causes a failure or transient which results in a malfunction.

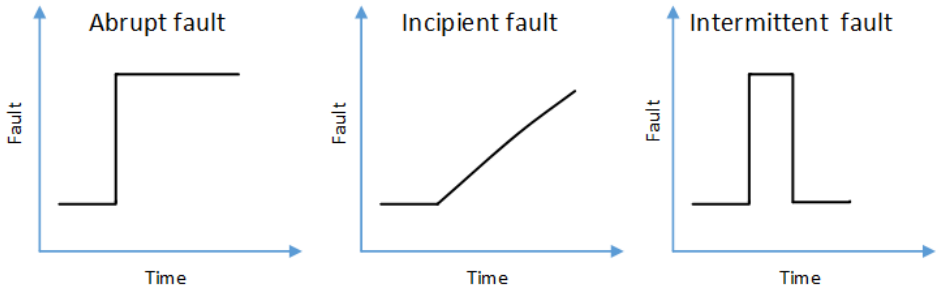

Figure 2.1: Different forms of a fault

Fault detection is defined as the discovery of an unintentional change in the component or process. **Fault diagnosis** consists of fault isolation and identification/analysis [50]. Once a fault has been detected it has to be **isolated** to a specific location or to a specific component in the system. **Fault identification** is the process of determining the type, magnitude and cause

of the fault. Fault identification is not always implemented as part of fault diagnosis (FD), due to the additional complexity and cost. In literature, it is common to see FD and FDI being used synonymously [27, 51].

2.3.1 Diagnostic methods

The various diagnostic methods used for FDI is illustrated in Figure 2.2.

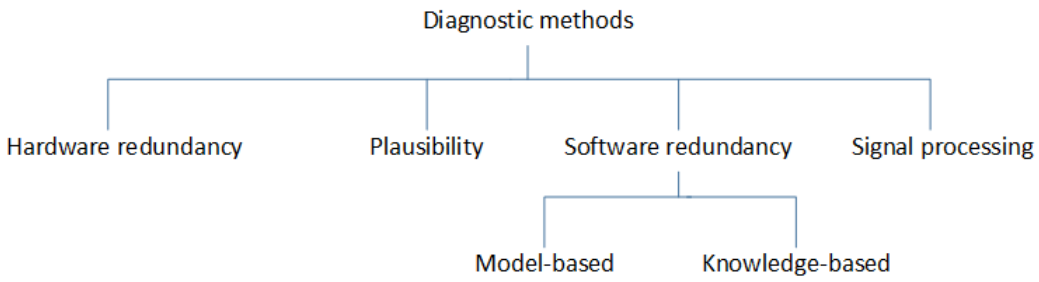

Figure 2.2: Fault diagnostic methods (Based on [37, 52, 53])

Hardware redundancy: This method relies on using an identical (redundant) component to the process component being monitored. A fault in the process component is detected when the output differs from that of the redundant component [52].

Plausibility: This method is based on the verification of the physical laws under which a component works. Based on the actual inputs to the component and the applicable physical laws, plausible outputs are determined. The assumption is that a fault condition will lead to the loss of plausibility [52].

Signal processing: This method assumes that information regarding faults is available from the process signals in the form of symptoms. Using signal processing, fault diagnostics can then be performed. Typical time domain symptoms include, but are not limited to magnitudes, mean values, trends and limit values while frequency domain symptoms include spectral power densities and frequency spectral lines to list a few. This method is limited to steady state conditions [52].

Software/analytical redundancy: This method can be divided into knowledge-based and model-based methods. Knowledge-based fault diagnosis is performed based on the evaluation of data, according to a set of rules, which the human expert has learned from past experience [54, 55]. These rules can be implemented by neural networks or fuzzy rules, for examples [56]. Model-based fault diagnosis implements a software model to replace the hardware redundancy. Model-based fault diagnosis holds several advantages over other methods [47, 57].

Some of the advantages are that models can be used to predict the impact a fault has on the system. Any assumptions and limitations are known, and models are based on first principles and not on the observed operation, that might only be valid under certain conditions.

2.3.2 Diagnostic system characteristics

Venkatasubramanian et al. [37] defined a set of desirable characteristics a fault diagnostic system should exhibit, as detailed below:

Quick detection and diagnosis: The diagnostic system should respond quickly in detecting and isolating fault conditions.

Isolability: This is the ability of the diagnostic system to distinguish between different faults and locate a faulty component among the various components in a system.

Robustness: The influence of noise, system disturbances and modelling uncertainties on the diagnostic system's ability to detect and isolate faults, are referred to as the system's robustness.

Novelty identifiability: This is the ability of the diagnostic system to determine if a process is functioning normally or not and if abnormal behaviour is exhibited, is the cause known or unknown.

Classification error estimate: This is the ability of the diagnostic system to provide an estimate on the classification error. This helps build confidence in the reliability of the diagnostic system.

Adaptability: The diagnostic systems should be able to adapt to changes, such as changing operating conditions, in the process.

Explanation facility: This is the ability of the diagnostic system not only to identify the source of a fault but also provide explanations on where the fault originated and how it propagated through the system.

Modelling requirements: The amount of modelling required to develop a fault classifier should be minimal, enabling fast and easy implementation of the diagnostic system.

Storage and computational requirements: The diagnostic system will have to balance storage and computation ability. Quick diagnosis might have large storage requirement and vice versa. Depending on the application, a compromise between these two requirements should be made.

Multiple fault diagnosis: The ability of the diagnostic system to detect and isolate multiple faults that are simultaneously present in the system.

2.4 Software redundancy

The basic principle of software redundancy for fault diagnosis is to compare the behaviour of the actual system against that of a model of the system. Software redundancy can be divided into model-based and knowledge-based fault diagnosis, as discussed in the subsequent sections.

2.4.1 Model-based fault diagnostics

Model-based FD methods require a fundamental understanding of the physics of the actual system, in order to create an accurate mathematical model of the system. This has been a limitation of a model-based approach to FD, but with advances in computational processing capabilities, ever increasingly complex systems can now be mathematically represented and simulated [53, 58].

The model will produce analytically estimated process variables, based on input data from the actual system. For a fault-free system, the actual and modelled process data will be equal. Any deviation will indicate a fault in the physical system. The difference between the actual and modelled data is called residual data. Any inconsistency expressed as a residual can be used for fault detection and isolation [37]. If the residual is zero the system is fault free, otherwise, a fault condition exists. The work of Ding [52] gives an introduction to model-based FD.

Model-based methods can further be divided into quantitative and qualitative models, as illustrated in Figure 2.3.

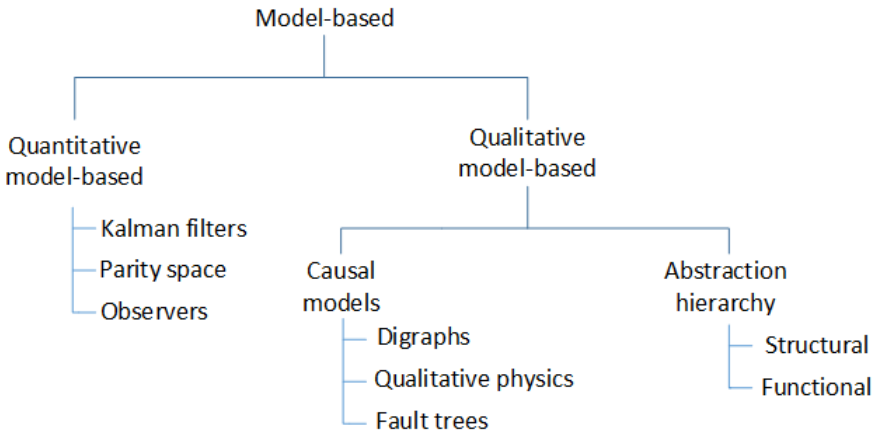

Figure 2.3: Model-based fault diagnostic methods (Based on [37, 52, 53])

Quantitative models are used to express the physics of a process as mathematical relationships between the inputs and outputs of the system. In qualitative models, the relationships between the inputs and outputs are expressed as qualitative relationships, based on expert knowledge [37, 46]. Figure 2.3 expands on quantitative and qualitative models to include the applicable techniques commonly implemented in model-based FD [59].

2.4.1.1 Quantitative model-based methods

Quantitative model-based approaches are realised with analytical redundancy. With analytical redundancy, actual process measurements (from sensors) are compared to analytically calculated values. For the purpose of FD, analytical redundancy is used to generate residuals by comparing the actual process values with the modelled values. The concept of analytical redundancy is illustrated in Figure 2.4 [60, 61].

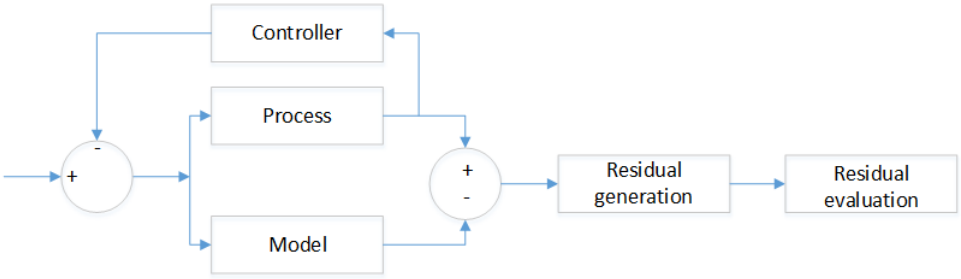

Figure 2.4: Scheme for implementing analytical redundancy (Based on [60, 61])

The output of the process and the model, for the same input, are compared and a residual calculated. The residual is then evaluated to determine if a fault condition exists. Quantitative models can be divided into detailed and simplified models. The detailed model is based on knowledge of the physical relationship and behaviour of components in the system. From this knowledge, mathematical equations, based on mass, momentum and energy balances together with heat and mass transfer relations, can be developed of the system. Simplified models are based on lumped parameters, which are computationally simpler. [37, 46, 53]

2.4.1.2 Qualitative model-based methods

Qualitative models are based on expert knowledge of the process and can either be causal models or abstraction models, as illustrated in Figure 2.3, and uses digraphs, qualitative physics, fault trees, structural and functional methods for the purpose of FD. Qualitative models are less concerned about actual values and more about an understanding of the process. As an

example, consider a tank with a single input stream and a single output stream. Without any detail information about the system, it stands to reason that an increase in the input stream above that of the output stream will result in an increase in the tank level [62, 63].

The advantages and disadvantages of quantitative and qualitative models are summarised in Table 2.2.

Table 2.2: Comparison of quantitative and qualitative models (Based on [53, 64])

Model	Advantages	Disadvantages
Quantitative models	- Based on physical principles - Most accurate estimation of outputs - Both normal and fault conditions can be modelled - Detailed models can model transients in dynamic systems	- Models are complex and computational intensive - Significant effort is required to develop a model - The model may require process data that is not readily available - The requirement for user inputs creates the possibility for erroneous inputs
Qualitative models	- Suited for data rich environments - Simple to develop - Transparent reasoning - Provide explanations	- Method is specific to a process - Difficult to define a complete set of rules describing the process - Simplicity is lost when adding new rules - Depend on the expertise of the developer

2.4.2 Knowledge-based fault diagnostics

In literature, knowledge-based FD is also referred to as process history-based or data-based FD. This method, in contrast to model-based methods, assumes no knowledge of the system and is purely based on large amounts of historical data regarding the system. A mathematical model is derived of the system, from known and measured process input-output data, which relates process inputs and outputs. This model can then be compared to the actual system to generate residuals [65]. Central to knowledge-based FD is feature extraction, which can be

either quantitative or qualitative. Figure 2.5 expands on knowledge-based methods to include applicable techniques commonly implemented [27, 65, 66].

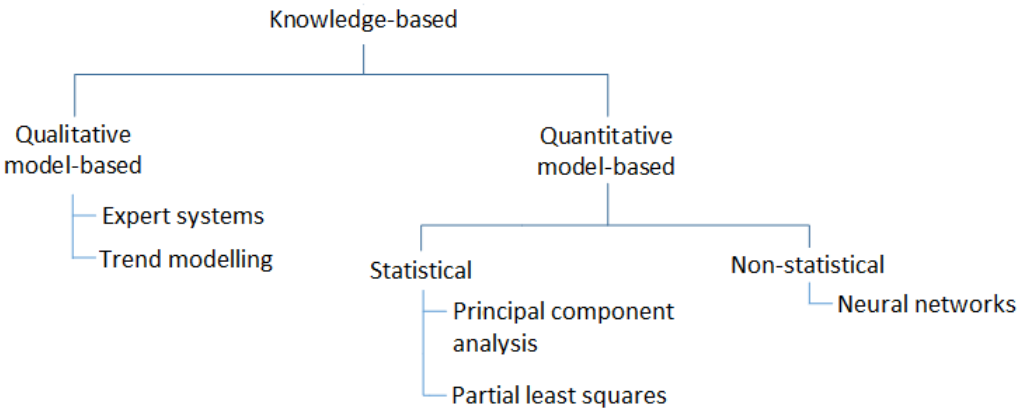

Figure 2.5: Knowledge-based fault diagnostic methods (Based on [27, 65, 66])

Quantitative knowledge-based methods are receiving considerable attention especially from chemical industries due to the amount of data available. Various data-driven algorithms have been developed, to process large quantities of data by using machine learning methods [67, 68]. Data-driven methods include principal component analysis, partial least squares and neural networks(NNs). Principle component analysis (PCA) is a multivariate statistical technique developed to reduce data dimensionality. PCA is used to transform large quantities (big data) of process variables to a smaller set of uncorrelated variables [69]. Partial least squares is an extension of PCA. NNs are a framework incorporating different machine learning algorithms to process complex data. NNs are mostly suited for FD of non-linear dynamic systems. NN can learn a relationship between an input and output, and generate the appropriate output when presented with an input. NN can also produce a generalised output when presented with unknown inputs. Programming of NNs is done using large data sets (process history) for training, rather than with explicit instructions [65].

2.5 Hybrid approach to fault diagnostics

From the work by Venkatasubramanian et al. [66], it is evident that no single FDI method can meet all the desirable characteristics (refer to section 2.3.2) of an effective FDI system. The requirements of new monitoring systems to be reliable, handle uncertainties and process large quantities of data, will require a hybrid approach. Hybrid methods overcome the limitations

posed by individual methods by integrating the complementary features of different methods [20]. Hybrid methods allow the evaluation of various kinds of knowledge, creating a powerful problem-solving platform. The combination of methods used to create a hybrid method will depend on the intended application, taking into account factors such as cost, time and computational limits.

Hybrid methods have already been created for various applications. Kim et al. [70] proposed both a hybrid hardware-based and a hybrid model-based method for FDI in unmanned aerial vehicles. The hardware-based method proposed the combination of parity equation approach and a wavelet-based technique. The model-based method is based on a Kalman filter using threshold values and confirmation time. A hybrid approach for a boiling water reactor was proposed by Hines et al. [71], combining analytical redundancy and neural network techniques. This hybrid approach addressed two problems associated with FDI of nuclear power plants (NPPs). The first being the size of an NPP, consisting of many systems, where it is impossible for a single system to detect and isolate all possible faults. Secondly, the individual systems of the NPP must be decoupled to allow FDI on the individual system (reducing the size). Analytical redundancy was used to achieve the decoupling of the various systems.

A hybrid technique based on fuzzy logic, artificial neural networks and genetic algorithms were used for FDI on a coupled-two-tank system by Khoukhi and Khalid [72]. In their work, Khoukhi and Khalid illustrated the advantages of a hybrid method over individual methods. Frank et al. [73] proposed the use of hybrid model- and data-based methods for FDI in commercial buildings. Their work showed the advantages of a hybrid method but also identified some shortcomings. More hybrid methods are available in literature, but each hybrid method is based on a specific application or process. The conclusion is that hybrid techniques, when feasible to implement, will outperform individual methods.

2.6 Energy-based fault diagnostics

Recently the use of energy-based methods has been proposed for the purpose of FDI in industrial systems. Energy-based methods focus on the energy flow and energy transformation through a system [27, 31, 47, 74, 75]. The main advantage of an energy-based method is that energy is a multi-domain parameter, in contrast with process parameters such as pressure, temperature and current that are domain specific. Another advantage is the reduction in the amount of data that has to be stored and processed. With the development and availability of smart and wireless sensors, the amount of available data has increased significantly. These large data sets are referred to as Big Data.

In this study, the use of energy reduces the amount of data by combining measurements, for example, temperature and pressure [20]. The laws governing energy is the same regardless of the domain [27, 76]. From an energy-based perspective, a system can be represented with various degrees of complexity depending on the required level of FDI. The entire system can be represented with a low level of detail, as a simple energy in, energy out system, as in Figure 2.6a or expanded to a high level of detail, including individual processes/components, to form a more detailed representation as in Figure 2.6b [27]. With a low level of detail, faults can be detected and isolated in the system. As more detail is added, to include sub-systems and eventually individual components, faults can be isolated to specific sub-systems or components.

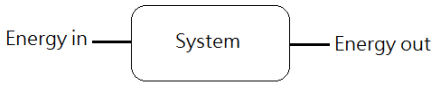

(a) Energy-based representation with a low level of detail

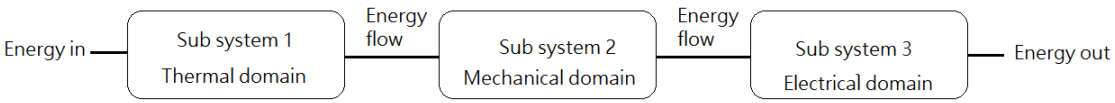

(b) Energy-based representation with a high level of detail

Figure 2.6: General energy-based representation of a system [27]

Energy-based modelling has been used for the analysis of systems, mainly during the design phase, for the purpose of optimisation in terms of energy or during its lifespan to determine the energy efficiency [11, 77, 78]. Recent studies by du Rand [23] and Marais [27] focused on using multi-domain parameters for the purpose of FDI in industrial systems. Work done by George [79] showed the use of energy and exergy analysis for FDI in the building environment specifically of chillers.

In the work of du Rand [23], enthalpy and entropy were used for FDI. The enthalpy and entropy values, at various nodes through a pebble bed modular reactor (PBMR) plant, were obtained by means of a simulation model. The values were obtained for normal operating conditions and fault conditions. Plotting these values on an h-s diagram showed that the graph transformed uniquely for the different faults.

The transformation is independent of the magnitude of the fault and only depend on the type of fault. Du Rand proposed two methods to quantify the fault. The first method is to calculate

the residual value for the enthalpy and entropy at the various nodes and plotting the values on a diagram. The second method is based on calculating the difference between the areas of the graphs. Both methods were successful in detecting and isolating the various faults that were simulated.

Marais [27] investigated the suitability of the methods proposed by du Rand for the case of an open-loop autothermal reformer. In his work, Marais showed that the methods proposed were not sufficient for fault detection and isolation in this case. The use of exergy was proposed and was shown to be able to detect and isolate various fault conditions. The physical and chemical exergy values were calculated for the various flow streams and the directions of the changes in the exergy values, due to a fault condition, were calculated. The directional changes in the exergy values of the flow streams were unique to the fault and were used to detect and isolate the faults.

In both these studies, a model of the physical system was simulated and used to generate reference fault signatures that are unique to the various fault conditions. In the same way, the real-time signature of the physical system can be determined and compared to the reference signatures, to determine the system's condition. In the work Jin and Zhou [80], Youssef [81] and Magni et al. [82] signatures were compiled, characterising or describing the condition of a system, for the purpose of fault detection and isolation. Youssef defined a signature (in the context of his work) as a graphical representation of the relationship between current and past measurements [81].

This can be seen as a hybrid approach between model-based and data-based FDI [83]. Furthermore, in the work of Chen [47] an energy balance was used for FDI in an example RLC circuit, proving the concept of using energy as a monitoring parameter.

The concept of utilising graphs was proposed by van Graan et al. [31]. Energy and its associated properties were used as the multi-domain parameter to create an energy-based attributed graph of a heat exchanger. Modelling the system using multi-domain parameters, the system can be represented as a graph, allowing the use of graph matching techniques for FDI.

2.7 Graph matching

In the work of Chandrashekar and Wong [84], a process graph model (PGM) is compiled, that defines the behaviour of a thermodynamic system. A feature of the PGM is the representation of energy flows and the transformation of energy through the system. The interactions between the different domains are modelled and presented with a single parameter. Two variable types

are used to describe the PGM, namely an across variable and a through variable. As the name implies, an across variable is used to measure a change across a component and a through variable measures the flow through a component. The power is expressed as the product of the across and through variables. Table 2.3 lists the across and through variables used in various domains. The thermal domain is the only domain where the product of the across and through variables do not result in power. In fact, the product has no physical value. Instead, the heat flow rate is used as the power equivalent in the thermal domain.

Table 2.3: Across and through variables for different physical domains (Based on [27, 84])

Domain	**Across (unit)**	**Through (unit)**	**Power (unit)**
Electrical	Voltage (V)	Current (A)	Electrical power (W)
Hydraulic	Pressure (Pa)	Flow rate (m^3/s)	Hydraulic power (W)
Mechanical (translational)	Velocity (m/s)	Force (N)	Mechanical power (W)
Mechanical (rotational)	Angular velocity (rad/s)	Torque (N·m)	Mechanical power (W)
Thermal	Temperature (K)	Heat flow (J)	-

The PGM is used to create an attributed graph of the system. Graphs are used to represent a system, consisting of interacting components, in a structured manner. The graph is a collection of nodes (components) and edges (interaction between components), representing the system [85]. An attributed graph is a specific graph where system attributes are assigned to the nodes and edges. In the context of a thermodynamic system, energy values can be assigned to the attributed graph, and graph matching techniques can be used to evaluate a change in the system. Graph matching is widely used in the field of pattern recognitioning and anomaly detection. In the work of Conte et al. [86] and Akoglu et al. [87] the techniques used for graph matching are presented and reviewed.

Graph matching is the process of comparing two graphs to establish similarities between the graphs, based on node and edge attributes. One of the methods proposed is the use of a graph distance. This method measures the similarity between graphs by calculating a cost function indicating the "cost" in transforming one graph into the other. In the work of Jouili and Tabbone [32], a cost matrix is calculated from two attributed graphs. The cost matrix represents the difference between the two graphs, based on variations in the attributes. The eigendecomposition of the cost matrix is used to characterise the difference [88]. Van Graan et al. [31] successfully implemented this method on a heat exchanger for the purpose of FDI.

2.8 Critical review and conclusion

From the literature presented it is evident that condition-based monitoring is an important aspect in modern industrial systems. At the core of an effective and efficient CBM system lies an effective and efficient FD system. Various methods have been developed for the purpose of fault detection and isolation. Recently, model-based methods have received increasing interest due to advances in computational capabilities. Model-based methods require either a quantitative or qualitative model of the system being monitored. This has been a limitation specifically for quantitative models due to the complexity of large industrial systems. For knowledge-based methods, large amounts of multi-domain data are required, measured at key-points throughout the system.

In the work of du Rand [23], an enthalpy-entropy-based approach was proposed for the condition monitoring of a Brayton cycle. Marais [27] proposed an energy-based approach to fault diagnosis for an auto-thermal reformer. This resulted in a reduction in the data required without compromising fault diagnostic capabilities. As explained by Marais, the use of a multi-domain parameter, such as energy, made it possible to reduce the complexity of large industrial systems, by simply viewing large systems as consisting of multiple energy transformation components. Based on the literature the use of a multi-domain parameter (energy) as a means of data reduction and also as a means of reducing the complexity of a large industrial system, holds merit. The literature presented supports the use of energy as a multi-domain parameter to represent a complex system for the purpose of FDI. This study will focus on utilising an energy-based representation of a Brayton cycle PCU for FDI.

CHAPTER 3

Thermodynamic concepts

The case study for this thesis is based on a thermodynamic power cycle, in this case, the Brayton cycle. Thermodynamic power cycles and the laws governing the thermodynamic processes are explained in this chapter. The concepts of energy and exergy as applicable to thermodynamic power cycles are discussed and the differences highlighted. The chapter concludes with remarks regarding the use of energy as a multi-domain parameter for the purpose of fault detection and isolation.

3.1 Background on thermodynamics

Thermal science is broadly defined as the study of the transfer, transport and conversion of energy. Thermal science can be divided into three subcategories: heat transfer, fluid mechanics and thermodynamics. Heat transfer is the exchange of thermal energy between physical systems. Fluid mechanics is the study of the interaction of fluids and the forces on them. The Industrial Revolution in the 17th century brought forth the study and development of heat engines, particularly steam engines. In 1849 Lord Kelvin introduced the term "*thermodynamics*" in his study of heat transfer. Thermodynamics is defined as the branch of physics that studies the effect temperature has on physical systems [89]. Over time specialist branches of thermodynamics developed, such as mechanical engineering- , chemical engineering- and biochemical-thermodynamics [90].The branch of thermodynamics applicable to this study is mechanical engineering thermodynamics, hereafter simply referred to as thermodynamics. Thermodynamics describes the relationship between thermal energy (heat) and mechanical

energy (work) and the laws governing an energy conversion process. In thermodynamics, a system that converts heat into work is known as a heat engine, as shown in Figure 3.1 [91]. This is achieved by taking the working fluid from a high-temperature state (T_H) to a low-temperature state (T_C). A heat source (not shown in Figure 3.1) is used to increases the temperature of the working fluid to T_H, thereby increasing its thermal energy. In a heat engine, thermal energy is transferred from the working fluid to the cold reservoir and during this process, some of the thermal energy is converted into mechanical energy.

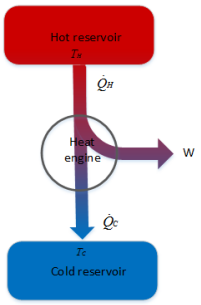

Figure 3.1: Representation of a basic heat engine [91]

This study focuses on using thermodynamic concepts for the purpose of fault detection and isolation in a thermodynamic power cycle. The study will also investigate the utilisation of component efficiencies to indicate the effect a fault has on the system. The maximum efficiency that can be obtained in a thermodynamic system is governed by both theoretical and practical constraints [92]. For a thermodynamic system the theoretical limitations are set by the laws of thermodynamics. This will set the maximum efficiency that can be achieved by the cycle. Practical considerations are factors such as available material, technology, economics and environmental impacts. These factors are not considered in this study.

All thermodynamic processes are governed by the four laws of thermodynamics as listed below and explained in more detail in the subsequent section [93, 94].

- **Zeroth law:** The zeroth law states that if two systems are in thermodynamic equilibrium with a third system, they are also in thermodynamic equilibrium with each other.
- **First law:** The first law describes the existence of energy. Energy is path independent and as such a conserved property.
- **Second law:** The second law states that energy has both quantity and quality. The quality of energy is called exergy. For all thermodynamic processes, exergy is always decreasing when considering the system and its surroundings.
- **Third law:** The third law states that the entropy of a substance approaches zero as the temperature approaches absolute zero.

3.2 Thermodynamic power cycles

A thermodynamic power cycle consists of a sequence of thermodynamic processes. These thermodynamic processes transfer heat and work to and from the system's surroundings, while varying state variables such as temperature and pressure. Examples of thermodynamic power cycles with the thermodynamic processes involved, are summarised in Table 3.1. At minimum, a thermodynamic power cycle will consist of four thermodynamic processes, namely compression, heat addition, expansion and heat rejection. The thermodynamic processes are summarised in Table 3.2. The type of thermodynamic power cycle will dictate the thermodynamic processes involved. The Carnot cycle is only a theoretical cycle that operates at the highest efficiency possible.

Table 3.1: Thermodynamic power cycles

Cycle	Compression	Heat addition	Expansion	Heat rejection
Carnot	Adiabatic	Isothermal	Adiabatic	Isothermal
Brayton	Adiabatic	Isobaric	Adiabatic	Isobaric
Diesel	Adiabatic	Isobaric	Adiabatic	Isochoric
Otto	Adiabatic	Isochoric	Adiabatic	Isochoric
Rankine	Adiabatic	Isobaric	Adiabatic	Isobaric

Table 3.2: Description of thermodynamic processes

Process	Description
Adiabatic	No energy transfer occurs as heat between the system and its surroundings
Isothermal	A change in the system without a change in the temperature
Isobaric	A change in the system without a change in the pressure
Isochoric	A change in the system without a change in the volume
Isentropic	A change in the system without a change in the entropy

3.3 The concept of energy, exergy and entropy

3.3.1 Energy

Energy is not a new concept and most people have a general understanding of energy, yet it is difficult to give a precise definition. In the simplest form, energy can be defined as the capacity

to do work or bring forth a change. Energy is a scalar quantity that can only be observed by indirect measurements [95]. Energy is also a conserved property implying that energy can not be created nor destroyed. Energy can only be transferred, transported and transformed as heat, work and mass flow. This is the conservation of energy principle and forms the basis of the first law of thermodynamics, expressed mathematically for a closed system as

$$\Delta U = Q + W, \tag{3.1}$$

with U the internal energy, Q the thermal energy and W the work. The sign convention used in this study is that of IUPAC and considers all net transfers to the system as positive and all net transfers from the system as negative.

Energy in a thermodynamic system can be divided into two groups [96]:

Macroscopic energy: This is the energy a system possesses with respect to an external reference. In a thermodynamic system, this refers to kinetic and potential energy.

Microscopic energy: This is the energy related to the molecular structure and activity of the system. Internal energy is defined as the sum of all the microscopic energy.

The internal energy depends on inherent properties (composition) and environmental variables (such as temperature and pressure). For a flowing fluid, the microscopic energy is given by the enthalpy (H). Enthalpy is defined as the total energy of a thermodynamic system and includes the internal energy, pressure(P) and volume(V) and is expressed as

$$H = U + PV. \tag{3.2}$$

In a thermodynamic system the macroscopic energy is ignored and only the microscopic energy (enthalpy) is used in an energy balance [27, 97]. An energy balance can be used to determine supply requirements of the system in terms of material, heat and work, but provides no information on how efficiently energy is being utilised. The only energy transfer that can be detected by performing an energy analysis, is the energy transfer out of the system as heat. Therefore heat transfer to the surroundings is used as a measure of energy loss in the system. This approach can be flawed since heat losses to the surroundings are unavoidable and inefficiencies mainly occur within the components, in terms of exergy destruction [97]. Exergy destruction is not accounted for with an energy balance.

An energy balance is only an indication of the quantity of energy and not the quality of energy [97–99]. The second law of thermodynamics states that energy also has a quality property

associated with it and that a process occurs in the direction of decreasing quality of energy. This quality of energy is termed exergy.

3.3.2 Exergy

Exergy is the maximum shaft work that can be done by a system as referenced to a specified environment that is assumed infinite, in equilibrium and enclose all other systems [100]. Exergy is also referred to in literature as available energy, available work, essergy or availability and has the unit of kJ. Since exergy is a measure of how much a system deviates from a state of equilibrium with its environment, it is necessary to define the environment [96, 99, 101]. The most significant environmental models proposed are natural-environment-, reference substance-, equilibrium and constrained equilibrium- and process dependent models.

A natural-environment reference model attempts to simulate subsystems of the natural environment. The reference temperature and pressure are 298.15 K and 101.3 kPa respectively and the chemical composition consists of saturated air, water, gypsum and limestone. With the reference substance model, reference substances are selected and assigned exergy values of zero. This model does not relate to the natural environment and cannot be used to evaluate efficiencies. In the equilibrium and constrained equilibrium models, all the materials present in the atmosphere, oceans and a layer of the earth's crust are used to calculate an equilibrium composition at a given temperature. The equilibrium model does not produce meaningful exergy values when analysing real processes. The constrained equilibrium model is a modified version of the equilibrium model. Process-dependent models contain only components that are part of the process under investigation. This model is dependent on the process and exergy values are only relevant to the process. For this study, the natural-environment model will be used since it is the only reference model that will provide meaningful exergy values and is not limited to a specific process. The chemical composition of the natural-environment model is ignored for this study since no chemical interactions occur in the system.

Contrary to energy, exergy is not a conserved property and can be destroyed. An irreversible (natural occurring) process leads to the destruction of exergy, and therefore exergy is an indication of thermodynamic inefficiencies. Common causes of exergy destruction include chemical reactions, heat transfer, fluid friction and flow throttling. Exergy can be seen as a measure of the quantity and quality of energy [102, 103]. The exergy consumed (energy that is not available also called anergy) during a process is proportional to the increase in entropy. Entropy represents the unavailability of thermal energy and is discussed in the subsequent section.

The entropy generation and its relation to exergy destruction is known as the Gouy-Stodola theorem [104], which states, that in an open system, the work lost due to irreversibility and the generation of entropy are related by

$$B_{dest} = T_0 \Delta S \tag{3.3}$$

where B_{dest} is the exergy destroyed with reference to the reference temperature, T_0, and ΔS is the change in entropy through the system.

The second law states that ΔS is always increasing for an irreversible process, implying that B_{dest} cannot be negative. In the case of a reversible process $\Delta S = 0$ and thus $B_{dest} = 0$. This can be expressed as

$$B_{dest} \begin{cases} > 0 & irreversible\ process \\ = 0 & reversable\ process \\ < 0 & impossible. \end{cases} \tag{3.4}$$

Exergy is based on the second law of thermodynamics and enhances the concept of an energy balance (first law of thermodynamics) by representing the thermodynamic value of energy and the inefficiencies of a system. Exergy has the advantage of being an effective method of analysing energy systems as it enables the determination of inefficiencies and the comparison of interactions that are different in the physical sense.

The use of exergy in evaluating a thermodynamic system provides more information and is more useful in improving efficiencies than an energy analysis. Exergy takes into account the thermodynamic imperfections of a thermodynamic system [96–98] due to the fact that thermal energy cannot completely be converted to work but work can completely be converted to thermal energy.

Exergy has the following characteristics:

- Exergy depends on the reference environment,
- A system in equilibrium with the environment has no exergy,
- The more a system deviates from its surroundings the more exergy it has,
- Exergy is the quality of energy. The result of exergy being destroyed is a loss in the quality of energy.

The energy associated with heat consists of exergy and anergy. Anergy is defined as the part of thermal energy that cannot be converted into work and equals the exergy destroyed [105, 106].

The exergy of thermal energy is calculated as

$$B = \left(1 - \frac{T_0}{T}\right) Q. \tag{3.5}$$

In literature, the term $\left(1 - \frac{T_0}{T}\right)$ is referred to as the exergy factor. The exergy factor implies that the exergy (B) of thermal energy (Q) decreases as T approaches T_0. In the case where $T < T_0$, the exergy factor will be negative, indicating that the exergy flow is opposite to the heat flow [95, 106, 107]. If $T = T_0$, the system is in equilibrium with its surroundings and the exergy of the thermal energy will be zero.

Table 3.3: Classification of exergy [95, 106]

Exergy					
Physical				Chemical	
Mechanical		Thermo-mechanical		Mixing and separation	Reactions
Kinetic	Potential	Temperature	Pressure		

The classification of exergy is given in Table 3.3. In this study of a closed-loop Brayton cycle, only physical exergy is present, as there is no change in the composition of the working fluid due to mixing, separation or chemical reactions taking place. The total exergy, therefore, will be the sum of the mechanical and thermo-mechanical exergy. In most cases the mechanical exergies are ignored and only thermo-mechanical exergies are of concern. As previously mentioned, exergy is dependent on the reference environment, and in this case only the reference temperature and pressure are important since no chemical exergies are present. The reference temperature (T_0) and pressure (P_0) used in this study are respectively 298.15 K and 101.3 kPa [99].

The thermo-mechanical exergy consists of temperature- and pressure-based exergy. This can be written in terms of enthalpy and entropy as

$$B^{(T)} = [H(T,P) - H(T_0,P)] - T_0[S(T,P) - S(T_0,P)] \tag{3.6}$$

for the temperature-based exergy, and as

$$B^{(P)} = [H(T_0,P) - H(T_0,P_0)] - T_0[S(T_0,P) - S(T_0,P_0)] \tag{3.7}$$

for the pressure-based exergy [108].

The total exergy is the sum of the temperature-based and pressure-based exergy, which reduces to

$$B = [H(T,P) - H(T_0,P_0)] - T_0[S(T,P) - S(T_0,P_0)]. \tag{3.8}$$

The difference between energy and exergy can be demonstrated using an uninsulated throttling device with a leak, as illustrated in Figure 3.2 [97].

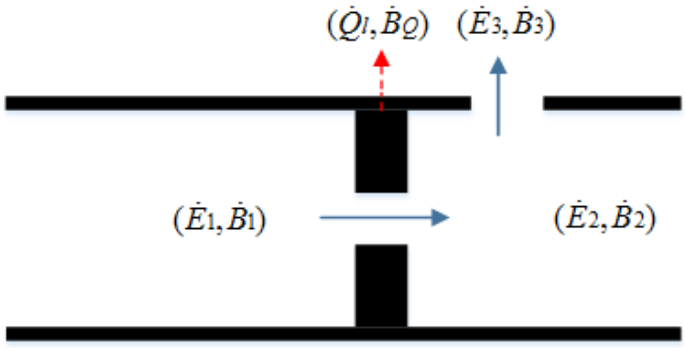

Figure 3.2: A simple throttling component with a leak

The energy balance for the throttling device is

$$\dot{E}_1 = \dot{E}_2 + \dot{E}_3 + \dot{Q}_l \tag{3.9}$$

with $\dot{Q}_l$ being the heat losses due to friction.

Assuming adiabatic conditions and no losses, (3.9) reduces to

$$\dot{E}_1 = \dot{E}_2. \tag{3.10}$$

An exergy balance of the same throttling device, including the losses, are given by

$$\dot{B}_1 = \dot{B}_2 + \dot{B}_3 + \dot{B}_Q + \dot{B}_{dest} \tag{3.11}$$

where $\dot{B}_Q$ is the exergy of the heat loss.

Without any losses (3.11) reduces to

$$\dot{B}_1 = \dot{B}_2 + \dot{B}_{dest}. \tag{3.12}$$

This implies that removing the losses in a system, an energy balance will yield a 100% efficiency, as per (3.10), while an exergy balance as per (3.12), still showed inefficiencies ($\dot{B}_{dest}$) due to irreversibility in the device. Therefore an exergy balance showed that throttling is an inefficient process in contrast with the energy balance [97].

The difference between an energy and exergy analysis of an energy system can also be illustrated with an electrical resistance heater and electric heat pump. According to Rosen [103], the energy efficiency of an electric heater is generally considered to exceed 99%, while the exergy efficiency is approximately 5%. The reason being that high-quality electrical energy is converted into low-quality heat. Exergy accounts not only for the quantity of energy but also for the quality of energy.

Using an electrical heat pump with a coefficient of performance (COP) of 7, the same space heating can be obtained with only 14% of the electricity required by an electrical resistance heater. A high exergy-efficient heater, will achieve the same results as a low exergy-efficient heater, with less energy. This is shown in Figure 3.3, comparing an electrical heater and an electric heat pump [103].

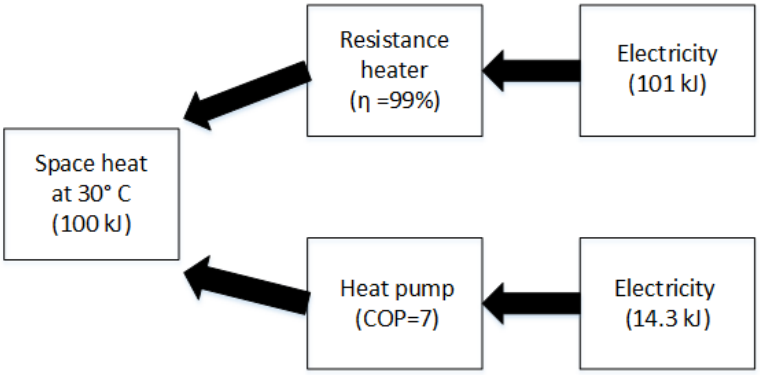

Figure 3.3: Two different space heating methods

A heat pump is a device that is used to transfer thermal energy from a low temperature area to a high temperature area and operates much like a refrigerator. If work is done on a thermodynamic power cycle thermal energy is transferred from a low temperature to high temperature [109]. In this example, the electrical heater requires 101 kJ, while the heat pump only requires 14.3 kJ to achieve the same result of heating a space to 30°C. Work done by Kumar [110], gives a critical review on the energy and exergy analysis of thermal power plants and highlights the importance and relevance of an exergy analysis on thermal systems. The differences between energy and exergy are summarised in Table 3.4.

Table 3.4: Comparison between energy and exergy [96, 100]

Energy	**Exergy**
Independent of environmental parameters, only dependent on energy flow	Dependent on environmental parameters and energy flow
Can not be zero ($E = mc^2$)	Can be zero (dead state)
Is governed only by the first law of thermodynamics	Is only governed by the first law of thermodynamics for reversible processes
Is limited by the second law of thermodynamics	Is not limited for reversible processes, due to the second law of thermodynamics
Is a conserved property	Is not a conserved property
Is a measure of quantity	Is a measure of quantity and quality

3.3.3 Entropy

The concept of entropy was first introduced in 1865 to address irreversibilities in a system. A state of maximum entropy is obtained when thermal equilibrium is reached, in the case of an isolated system. In an adiabatic system, the entropy out of the system is always larger than the entropy into the system. In simple terms, entropy is an indication of the unavailability for conversion of thermal energy into work. High-quality energy (useful energy) will have low entropy, such as mechanical and electrical energy having no entropy. Thermal energy, however, contains entropy and can therefore not completely be converted into work. The higher the entropy value of energy is, the lower the exergy value becomes, and the less useful the energy is [111, 112].

Entropy is the key concept of the second law of thermodynamics [93, 96, 113]. Entropy is defined as the measure of disorder in a system. Heat transferred to a system increases the disordered energy (entropy), while heat transferred from the system reduces the entropy. Entropy generation is a measure of the magnitude of the irreversibilities during a process. The greater the effect of irreversibilities on the system, the higher the generation of entropy will be. Entropy is not a conserved property and is always generated during an actual process, but never destroyed. The direction a process occurs in is always in the direction of increasing entropy. Although energy crossing the system boundaries can increase or decrease the entropy in the system, the total entropy (including the entropy of surroundings) is always increasing.

Considering an isolated system, consisting of the system and its surroundings, the change in the entropy of the system is equal to the sum of the change in entropy of the system and the surroundings. Since no entropy transfer occurs in an isolated system, the entropy generated can be expressed as

$$S_{gen} = \Delta S_{total} = \Delta S_{system} + \Delta S_{surrounding} \geq 0. \tag{3.13}$$

This is known as the increase in entropy principle and summarised as

$$S_{gen} = \Delta S_{total} = \begin{cases} > 0 & irreversible\ process \\ = 0 & reversable\ process \\ < 0 & impossible. \end{cases} \tag{3.14}$$

The interactions between energy, exergy and entropy are illustrated in Figure 3.4.

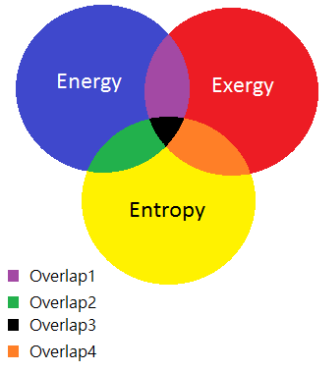

Figure 3.4: Interaction between energy, exergy and entropy (based on [95, 96])

This implies for example that a system can have only energy and exergy (no entropy), indicated by Overlap1. An example of this is shaft work. Air at atmospheric conditions, for example, has energy and entropy but no exergy, as indicated by Overlap2. A working fluid at a temperature above the reference temperature, as in the case of a thermodynamic power cycle, will have all three components present, indicated by Overlap3 [95, 96]. The terms, entropy and exergy, are not exclusive to energy systems and are commonly used in the fields of statistics and information theory. In general entropy and exergy are thus not a subset of energy and therefore the possibility exists of having entropy and exergy without energy, indicated by Overlap4 [96].

3.4 Conclusion

The basic concepts of thermodynamics were presented in this chapter by explaining the interaction between energy, exergy and entropy. In a thermodynamic power cycle, not all of the thermal energy from a high temperature source can be converted into work. Exergy is defined as the useful part of energy (that can be converted to work) and is not a conserved property. The destruction of exergy is compensated for by an increase in entropy. The difference between energy and exergy efficiency was explained and it was shown that a system can be 100% energy efficient but never 100% exergy efficient. The exergy destruction in a thermodynamic power cycle is dependent on the change in entropy, and the change in entropy is dependent on irreversibilities in the cycle. The irreversibilities in the cycle is inherent to the components and is influenced by the operational conditions of the cycle. In conclusion, exergy is an important part of energy to take into account when considering a thermodynamic power cycle. Operational conditions of the cycle will influence both the energy and exergy changes in the cycle and therefore, energy and exergy can be utilised to characterise the cycle.

CHAPTER 4

Brayton cycle model

The simulation of the Brayton cycle PCU used in this study is explained in this chapter. Different fault conditions are defined and an energy and exergy analysis are performed on the cycle for each condition. Methods for calculating exergetic efficiencies are presented and a new method, based on the ratio of exergy transfer through a component, is proposed.

4.1 Brayton cycle

A Brayton cycle can be configured as either an open-loop or a closed-loop cycle. In the case of an open-loop cycle, heat is added to the working fluid in the heat addition process, through the mixing of fuel with the working fluid and the subsequent combustion of the mixture. The working fluid, now polluted with combustion gases, is expelled to the atmosphere. In a closed-loop cycle, the working fluid is recycled back into the compression process. In this configuration, heat is added to the working fluid through heat transfer, using a heat exchanger, keeping the working fluid clean of contaminants, in contrast with an open-loop cycle. After the expansion process, the working fluid is processed to the required conditions (temperature and pressure) and introduced back into the compressor and the cycle repeats. This is illustrated in Figure 4.1, showing a Brayton cycle configured as an open-loop and closed-loop cycle. At minimum, a Brayton cycle consists of three stages. A compression (compressor) stage, heat addition stage and an expansion (turbine) stage.

An open-loop cycle can be modelled as a closed-loop cycle using air-standard assumptions [114]. The following points are collectively known as the air-standard assumptions [93]

- The working fluid is air and considered an ideal gas,
- The combustion process, commonly associated with an open-loop cycle, is modelled as a heat addition process, e.g. heat exchanger,
- A heat rejection process is used instead of the exhaust process, restoring the working fluid to its initial condition.

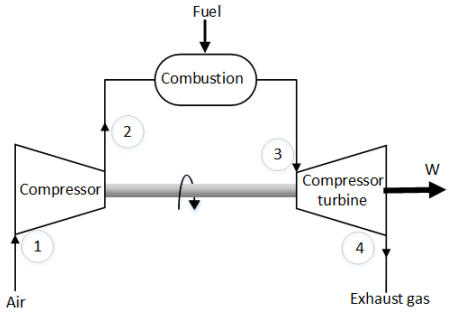

(a) Open-loop cycle

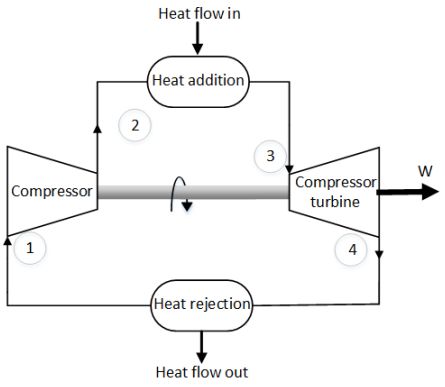

(b) Closed-loop cycle

Figure 4.1: Basic Brayton cycle configurations

In the Brayton cycle, mechanical energy is converted to hydraulic energy by means of a compressor. Thermal energy is then added to the high pressure working fluid through a heat addition process. The high temperature- high pressure working fluid is then expanded through the turbine, which converts the thermal and hydraulic energy into rotation (mechanical energy) which is used to drive the compressor and deliver a net rotational energy output. The working fluid is then converted back to its initial state, in the case of a closed-loop cycle, to complete the cycle or expelled to the surroundings in the case of an open-loop cycle.

The P-V and T-s diagrams for the basic Brayton cycle are illustrated in Figure 4.2.

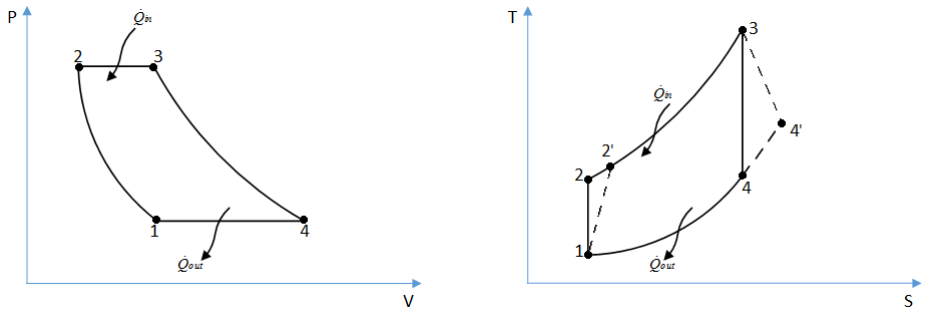

(a) P-V diagram (b) T-s diagram

Figure 4.2: P-V and T-s diagrams for basic Brayton cycle

In an ideal (reversible) cycle the compression and expansion processes are adiabatic, as indicated by the solid lines in Figure 4.2b. In an actual (irreversible) cycle the compression and expansion processes are not adiabatic, as indicated by the dashed lines in Figure 4.2b [115].

4.2 Modelling and simulation

4.2.1 Component modelling

This section briefly explains the models of the various components used in Flownex® [116, 117] and presented in research done by Pritchard [118].

Compressors and turbines

The following assumptions are made regarding turbomachinery:

- The machine has no volume. This implies any change in the input is immediately evident in the output. No energy is stored in the turbomachine.
- The machine is adiabatic. No heat transfer occurs between the turbomachine and the environment.
- Shaft dynamics are accounted for separately and not as part of the turbomachinery.
- The turbomachinery maps are valid under steady-state and transient conditions.

The following equations and steps are used to mathematically represent the compressors and turbines:

The pressure ratio for a turbomachine is calculated by

$$P_{ratio} = \begin{cases} \frac{P_{inlet}}{P_{outlet}} & Turbine \\ \frac{P_{outlet}}{P_{inlet}} & Compressor. \end{cases} \tag{4.1}$$

Using the non-dimensional speed ($\grave{N} = \frac{N}{\sqrt{T_{inlet}}}$), the non-dimensional mass flow ($\grave{m}$) are obtained from the compressor and turbine maps. Although these values are referred to as non-dimensional, they are not non-dimensional.

The mass flow can then be calculated as

$$\dot{m} = \frac{\grave{m} P_{inlet}}{\sqrt{T_{inlet}}} \tag{4.2}$$

and the isentropic efficiencies ($\eta_{compressor}$ and $\eta_{turbine}$) can then be obtained from the compressor or turbine maps.

The work input or output is calculated by

$$W = \dot{m} C_p (T_{inlet} - T_{outlet}) \tag{4.3}$$

where C_p is the specific heat of the working fluid.

The temperature difference $(T_{inlet} - T_{outlet})$ is calculated as

$$T_{inlet} - T_{outlet} = \begin{cases} \eta_{turb} T_{inlet} \left(1 - P_{ratio}^{-\left(\frac{\gamma-1}{\gamma}\right)} \right) & Turbine \\ \frac{T_{inlet}}{\eta_{comp}} \left(1 - P_{ratio}^{\left(\frac{\gamma-1}{\gamma}\right)} \right) & Compressor \end{cases} \tag{4.4}$$

where γ is the heat ratio, $\gamma = \frac{C_p}{C_v}$.

Shafts

The mechanical efficiency of the shaft takes into account the mechanical efficiency of both the compressor and turbine. The shaft power is calculated by

$$W_{shaft} = \eta W_{turbine}. \tag{4.5}$$

Heat addition and rejection

The heat transferred to or from the working fluid through the heat addition or -rejection element is calculated as

$$\dot{Q} = \dot{m} C_p (T_{outlet} - T_{inlet}). \tag{4.6}$$

4.2.2 Simulation

The Flownex® simulation environment enables the simulation and study of thermal-hydraulic systems. Flownex® was extensively validated and verified and therefore will be used as the simulation environment for this study [116, 117].

A closed-loop Brayton cycle, as in Figure 4.3, will be used for this study and was simulated in Flownex®. The simulation model constitutes a compressor-turbine pair connected through a shaft, a power turbine (PT) producing a net work output and heat exchanging elements. In this model, the heat addition and heat rejection elements are simulated as heat exchangers.

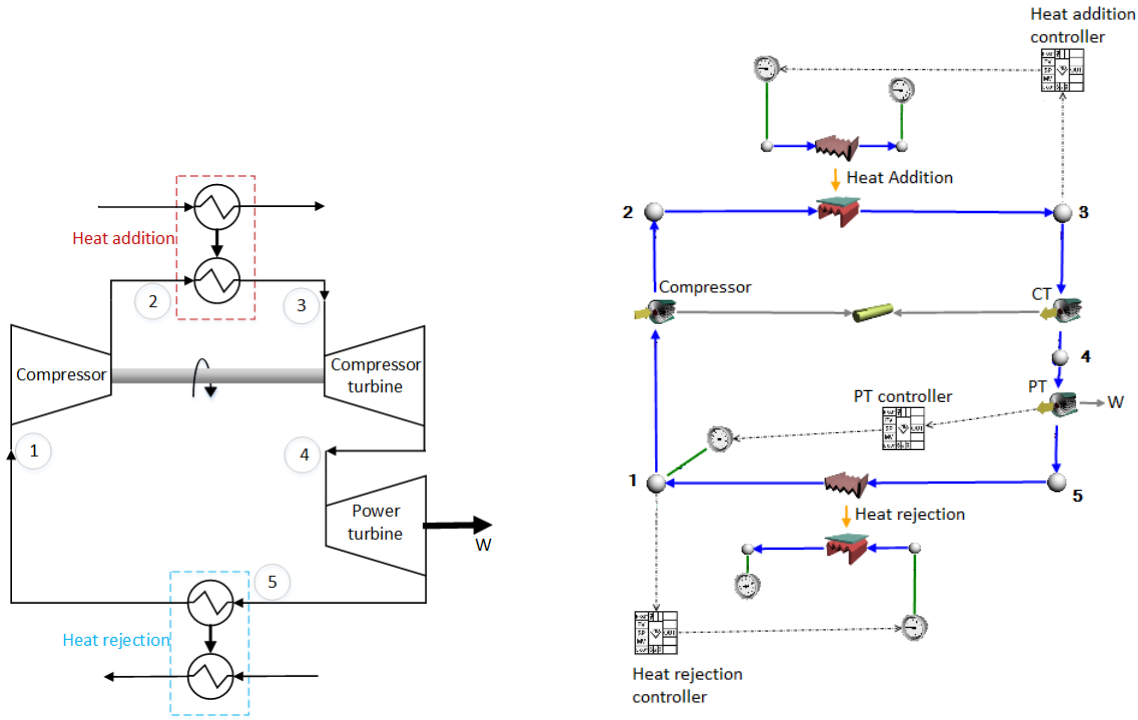

(a) Diagram of the Brayton cycle PCU used in this study

(b) The Flownex® simulation model of the Brayton cycle PCU used

Figure 4.3: The Brayton cycle PCU used in this study

In this simulation, air was selected as the working fluid and simulated as a single phase gas. Air was best suited to the compressor and turbine models used in this simulation [119]. The working fluid is controlled to a constant temperature of 298.15 K at the inlet to the compressor at Node 1, in Figure 4.3. This is achieved by controlling the heat rejection element's secondary inlet temperature. The pressure at Node 1 is controlled to maintain a constant power output at the PT as specified by the operational setpoint. This is achieved with the addition or removal of working fluid from the cycle, effectively controlling the mass flow in the cycle and influencing the pressure. The heat addition process between Node 2 and Node 3 is simulated as a heat exchanger, controlled to maintain a constant temperature of 1173.15 K at Node 3. The mass flow through the heat addition element's primary side and the heat rejection element's secondary side is fixed at 8 kg/s.

Solving the cycle with initial conditions resulted in excess power output on the shaft. The turbine power output is calculated at 67.2 kW and the power requirement of the compressor is calculated to be 50.2 kW. The difference implies that the compressor-turbine pair is still accelerating. Only when the power output of the turbine and the power requirement of the compressor are equal, has steady state been achieved. Any change in temperature, pressure or mass flow, either due to a fault or a change in operating point, will disturb this balance. The compressor-turbine pair will then either accelerate or decelerate, until the power output of the turbine and power requirements of the compressor are again equal. The power requirements of the compressor-turbine pair are influenced by the PT setpoint since the PT setpoint determines the pressure at the compressor inlet (Node 1).

The following assumptions are made:

- All processes are adiabatic.
- The effect of temperature changes is immediate.
- No energy is stored in the components.
- Potential and kinetic energy is constant and therefore ignored.
- The reference temperature (T_0) and pressure (P_0) are taken as 298.15 K and 101.1 kPa.

The assumption that all processes are adiabatic implies that no heat transfer occurs between components and the environment. In other words, no heat loss. Any change in the operational setpoint of the cycle will influence the inlet temperature to the compressor-turbine. The temperature at the inlet is controlled to be constant through changes in the heat addition component. The assumption is made that any changes in the heat addition component will immediately influence the inlet temperature of the turbine. The fact that no energy is stored in the components, implies that the effects of a change in the input variables are immediately

evident in the output. The assumption is made that there is no net change in height through the cycle and therefore the potential energy is constant and can be ignored. Since the cycle being simulated is a closed-loop cycle the net change in kinetic energy will be zero and is therefore not taken into account. No chemical interactions are present and therefore the composition of the reference environment is not important, except for the reference temperature (T_0) and pressure (P_0).

In this study, only steady state conditions are considered and the steady state simulation results are summarised in Table 4.1.

Table 4.1: Simulation results with a PT setpoint of 100 kJ/s

Node	**Enthalpy flow** (kJ/s)	**Entropy flow** (kJ/s·K)	**Temperature** (K)	**Pressure** (kPa)
1	583.63	4.97	298.15	267.76
2	811.15	5.1	461.52	874.83
3	1890.07	6.51	1173.15	872.28
4	1657.91	6.6	1027.89	397.32
5	1557.91	6.65	964.25	274.1
Heat addition$_{in}$	11110.64	38.8	1186.33	600
Heat addition$_{out}$	10031.72	38.88	1070.53	390.33
Heat rejection$_{in}$	3258.08	26.56	282.25	600
Heat rejection$_{out}$	4232.36	29.68	402.15	545.1

The operational graphs of the model are presented in Appendix A and the verification of the model is discussed in Appendix B. The steady state conditions with a PT setpoint of 100 kJ/s are tabled in Table 4.2. For the purpose of this study, the selection of setpoints are not important, as explained in the subsequent paragraphs. In this study, a setpoint of 100 kJ/s for the PT will be considered the normal operational setpoint. This setpoint was selected based on the capabilities of the components used in the model.

The model used in this study is only a representative model of a Brayton cycle. The validity of the model will be determined by comparing the behaviour of the model to that of a validated Brayton cycle. In this case, the behaviour will be compared to that of a three shaft Brayton cycle, used in the PBMR, and explained in the work of du Rand [23], Rousseau and van Ravenswaay [120] and van Niekerk et al. [35, 119].

Validation is defined as the process of determining the degree to which a model is representative of the real world from the perspective of the intended application of the model [121, 122].

Since a representative model is used, the actual cycle parameters (such as temperature and pressure) will not be compared but rather the behaviour of the model in terms of changes in the temperature and pressure. This method of validation was proposed in discussion with du Toit [123]. Several techniques exist, that are used individually or in combination to validate a model. The techniques used in this study will be a comparison to other models, face validity, internal validity and traces [124]. Comparison to other models entails comparing various results of the model being validated to other validated models. This can be either analytical models or other simulated models. Face validity is based on whether the model and its behaviour are reasonable. The model can also be simulated several times under the same conditions to determine the variations in the results. This is called internal validity. Large variations will cause the model's results to be questionable. The behaviour of certain parameters can also be traced through the model to determine if the model's logic is correct. The validation of the model is discussed in more detail in Appendix B.

The steady state conditions (Table 4.2) may not be realistically achievable values, but are used to obtain the required changes in the pressure and temperature and thus the enthalpy and entropy, to be representative of a Brayton cycle. For example, a rotational shaft speed of 100311 r/min for the compressor-turbine pair is unrealistic, but the same compressor output results, in terms of pressure and temperature, can be achieved at reduced shaft speeds, by implementing multiple compressors and intercoolers. For the purpose of this study the exact design, practical limitations and operating conditions were not as important as ensuring that the behaviour of the model is representative of a Brayton cycle.

Table 4.2: Steady state conditions with a PT setpoint of 100 kJ/s

Element	Property	Value	Unit
Heat addition - primary side	Inlet temperature	1186.33	K
	Mass flow	8	kg/s
	Inlet pressure	600	kPa
Heat rejection - secondary side	Inlet temperature	283.15	K
	Mass flow	8	kg/s
	Inlet pressure	600	kPa
Shaft	Speed	100311	r/min
Node 1	Temperature	298.15	K
	Mass flow	1.376	kg/s
	Pressure	267	kPa

4.2.3 Sensor noise and numerical noise

Sensor noise is defined as the unwanted fluctuation in the output signal of a sensor, without any change in the parameter being monitored. The sources of the noise can either be external such as changes in the ambient conditions or internal as in the case of electronic noise [125].

Various methods have been developed to reduce noise or to filter noisy signals, depending on the type of sensor and source of the noise [126–131]. Since this study is based on a simulated model, it is assumed that the measurements taken from the simulation will be noise free and time-invariant, and therefore sensor noise and drift are not taken into account.

Numerical noise, however, is part of most simulation models due to differential equations in the models. Solutions to differential equations involve the addition of noise due to adaptive methods and incomplete convergence [132]. In order to determine the numerical noise due to the simulation software, the simulation was executed multiple times under the same operating conditions and the required data acquired. The data were compared and the maximum difference in the measured data was calculated to be 1.251×10^{-12}. Since the numerical noise is small, the influence is negligible.

4.2.4 Energy and Exergy

The change in energy flow through a component is equal to the change in the enthalpy flow which is equal to the external energy flow into the component, given by

$$\Delta \dot{E} = \Delta \dot{H} = \dot{E}_{ext}. \tag{4.7}$$

This holds true since only the microscopic energy (enthalpy) is considered in this model and adiabatic conditions are assumed.

A distinction has to be made between the energy flow through a component and the energy flow into the component. The energy flow through a component is the energy contained within the working fluid. The energy into the component ($\dot{E}_{ext}$) is the energy added to or taken from the working fluid. The external energy will either be work in the case of turbomachines or heat for the heat addition and rejection elements.

Since exergy is dependent on the reference environment, the change in exergy is more commonly used. The change in exergy is independent of the reference environment, only depending on the reference temperature, T_0. This is mathematically illustrated by considering an arbitrary component with inlet, N1 and outlet, N2.

According to (3.8) the exergy is calculated as

$$B_1 = [H(T_1,P_1) - H(T_0,P_0)] - T_0[S(T_1,P_1) - S(T_0,P_0)]$$

for N1 and as

$$B_2 = [H(T_2,P_2) - H(T_0,P_0)] - T_0[S(T_2,P_2) - S(T_0,P_0)]$$

for N2.

The change in exergy will be calculated as

$$\begin{aligned}\Delta B &= B_2 - B_1 \\ &= [H(T_2,P_2) - H(T_1,P_1)] - T_0[S(T_2,P_2) - S(T_1,P_1)].\end{aligned}$$

The change in exergy across a component can now be written as

$$\Delta B = (\Delta H - T_0 \Delta S). \tag{4.8}$$

The same reasoning applies for calculating the change in exergy flow $(\Delta \dot{B})$, except the unit for exergy flow is kJ/s.

The changes in energy flow and exergy flow are summarised in Table 4.3 for the various components of the Brayton cycle in Figure 4.3, under steady state conditions, with the output of the PT maintained at 100 kJ/s. Due to irreversibilities the change in exergy will always be less than the change in energy for an energy-consuming component, as evident in Table 4.3, and the change in exergy will always be greater than the change in energy for energy-producing component. In the case of the heat rejection element, the change in energy is greater than the change in the exergy. Since it is a closed-loop cycle the working fluid has to be returned to its initial conditions at Node 1, hence the exergy destroyed by each component in the cycle from Node 1 through to Node 5 has to be replaced by the heat rejection element. Even though the energy flow is out of the system through the heat rejection component, the exergy flow is in the opposite direction. Energy and exergy flow is not necessarily in the same direction and is dependent on the chosen reference environment and the temperature of the process [100].

Table 4.3: Energy and exergy changes with a PT setpoint of 100 kJ/s

Element	**Change in energy flow** (kJ/s)	**Change in exergy flow** (kJ/s)	**Change in exergy flow external to the cycle due to the component** (kJ/s)
Compressor	227.52	188.76	227.52
Heat addition$_{sec}$	1078.92	658.53	1102.77
CT	-232.16	-258.99	-232.16
PT	-100	–114.90	-100
Heat rejection$_{pri}$	-974.28	-473.38	-44.05
Net	0	0	954.08

Energy is a conserved property and as such the net energy through the cycle has to be zero. Exergy is not a conserved property and therefore the net exergy change external to the cycle is not equal to the net exergy change in the cycle. The external change in the exergy flow, of 954.08 kJ/s, represents the exergy destroyed in the cycle. However, the exergy destroyed has to be equal to the net increase in entropy, according to (3.3).

This can be illustrated by doing an energy and exergy analysis on the heat addition element of the cycle in Figure 4.3, shown under steady state conditions in Figure 4.4. The results are summarised in Table 4.4. Although only two decimal places are shown, more decimal places were used in the calculations, therefore the results of the calculations may not match the values used in the calculations.

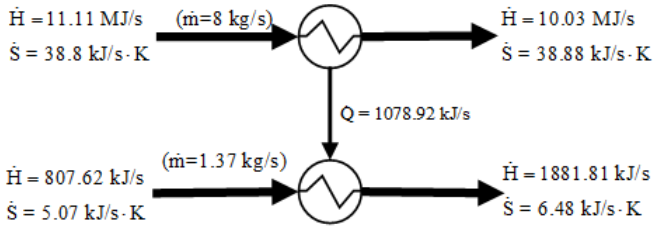

Figure 4.4: Analysis of the heat addition element

As would be expected the change in energy from the primary side is equal to the change in energy in the secondary side at 1078.92 kJ/s. The exergy is however not balanced with a change of 1102.77 kJ/s in the primary side and 658.53 kJ/s in the secondary side. The exergy destroyed in the primary and secondary side is accounted for by the change in entropy

Table 4.4: Energy and exergy analysis of the heat addition element of Figure 4.4.

Property	Primary side	Secondary side	Net
$\Delta\dot{B}$ (kJ/s)	-1102.77	658.53	-446.45
$\Delta\dot{E}$ (kJ/s)	-1078.92	1078.92	0
$\Delta\dot{S}$ (kJ/s.K)	0.08	1.41	1.49
$\dot{B}_{dest}$ (kJ/s)	23.85	420.39	444.24

as previously explained, and calculated at 23.85 kJ/s in the primary side and 420.39 kJ/s in the secondary side. The exergy flow between the primary and secondary sides from the perspective of the primary side is calculated as

$$\begin{aligned} \dot{B}_{transfer} &= \Delta\dot{B} + \dot{B}_{dest} \\ &= -1102.77 + 23.85 \\ &= -1078.92 \text{ kJ/s}. \end{aligned} \tag{4.9}$$

This is equal to the energy flow between the two sides. Doing the same calculation from the perspective of the secondary side, the exergy flow is also calculated to be equal to the energy flow between the two sides.

$$\begin{aligned} \dot{B}_{transfer} &= \Delta\dot{B} + \dot{B}_{dest} \\ &= 658.53 + 420.39 \\ &= 1078.92 \text{ kJ/s}. \end{aligned} \tag{4.10}$$

This confirms that the energy is balanced and that the exergy destroyed in the process is accounted for by the change in the entropy for both the primary and secondary side of the heat addition element. The same applies to the heat rejection element.

The above calculations were for a single component in the cycle, but the same energy and exergy analysis can be done for the complete cycle. From Table 4.1 the net increase in entropy is calculated as

$$\begin{aligned} \Delta\dot{S}_{net} &= (\Delta\dot{S}_{heataddition_{pri}}) + (\Delta\dot{S}_{heatrejection_{sec}}) \\ &= 0.08 + 3.12 \\ &= 3.2 \text{ kJ/s.K}. \end{aligned} \tag{4.11}$$

Since it is a closed-loop cycle the net change in entropy through the cycle is zero. The only change in entropy is in the primary side of the heat addition element and the secondary side of the heat rejection element.

The exergy destroyed is calculated as

$$\begin{aligned} \dot{B}_{dest} &= \Delta \dot{S}_{net} T_0 \\ &= 3.2 \times 298.15 \\ &= 954.08 \text{ kJ/s}. \end{aligned} \tag{4.12}$$

An energy balance of the system yields a net energy of 0 kJ/s, while the exergy balance yields a net exergy of 954.08 kJ/s. This shows that the energy in the system is balanced but the exergy is not. This imbalance in exergy is compensated for by an increase in the total entropy, according to the laws of thermodynamics.

4.2.5 Exergetic efficiencies

Different methods are presented in literature for the calculation of exergetic efficiencies [29, 133–136]. Some of the methods are presented below.

Conventional exergy efficiency

This is the simplest form of exergy efficiency and calculated as

$$\eta = \frac{\dot{B}_{out}}{\dot{B}_{in}} \tag{4.13}$$

where $\dot{B}_{out}$ is the outgoing exergy flow and $\dot{B}_{in}$ the incoming exergy flow.

Rational efficiency

The rational efficiency as defined by Kotas [29] is calculated as

$$\eta = \frac{\dot{B}_{desired}}{\dot{B}_{used}} = 1 - \frac{\dot{B}_{dest}}{\dot{B}_{used}}, \tag{4.14}$$

where $\dot{B}_{desired}$ is the sum of all the outgoing exergy flows and $\dot{B}_{used}$ is the required exergy consumed in order to perform the process.

Utilisable exergy coefficient

This method serves to improve on the conventional exergy efficiency by taking into account that in some processes not all of the working fluid is transformed by the process [137, 138]. For example, not all of the coal entering a boiler will burn, with some unburnt coal exiting the boiler. Although the coal has exergy associated with it, the unburnt coal did not contribute to the process. This exergy is termed transiting exergy, B_{tran}. Using the previous example, not all of the exergy produced by the coal will contribute to the process, with some of the exergy being lost to the environment, (B_{lost}), as smokestack effluents for example. The utilisable exergy coefficient takes this into account and is calculated as

$$\eta = \frac{\dot{B}_{prod}}{\dot{B}_{cons}}, \tag{4.15}$$

where $\dot{B}_{prod} = \dot{B}_{in} - \dot{B}_{dest} - \dot{B_{lost}} - \dot{B}_{tran}$ and $\dot{B}_{cons} = \dot{B}_{in} - \dot{B}_{tran}$.

Percentage exergy destruction

In the work of Satish and Dhana Raju [134] the efficiency of the components in a thermal power plant is presented as

$$\eta = \frac{\dot{B}_{dest}}{\dot{B}_{Tdest}}, \tag{4.16}$$

where $\dot{B}_{Tdest}$ is the total exergy destruction in the cycle. This method only serves as a comparison between components, to determine which component has the largest impact on the exergy being destroyed. This method was also proposed by Acar and Dincer [135] and termed the relative irreversibility of a component.

A new method called the exergy ratio (B_{ratio}) is proposed to define the efficiency of the thermodynamic conversion in a component, calculated as

$$B_{ratio} = \begin{cases} \frac{\Delta\dot{B}}{\dot{B}_{ext}} & for\ energy\ consuming\ components. \\ \\ \frac{\dot{B}_{ext}}{\Delta\dot{B}} & for\ energy\ producing\ components. \end{cases} \tag{4.17}$$

where $\dot{B}_{ext}$ is the exergy into or out of the component.

Considering the cycle in Figure 4.3, the exergy ratio for the compressor is calculated as

$$B_{ratio} = \frac{\Delta\dot{B}}{\dot{B}_{ext}},$$

where $\Delta\dot{B}$ is calculated from Table 4.1, using (4.8), as

$$\begin{aligned}\Delta\dot{B} &= (811.15 - 583.63) - 298.15(5.1 - 4.97) \\ &= 188.89\ kJ/s\end{aligned}$$

and from Table 4.3,

$$\dot{B}_{ext} = 227.52 \text{ kJ/s}.$$

The exergy ratio of the compressor is thus

$$\begin{aligned}B_{ratio} &= \frac{188.76}{227.52} \\ &= 0.829.\end{aligned}$$

In the case of the compressor-turbine the exergy ratio is calculated as

$$\begin{aligned}B_{ratio} &= \frac{\dot{B}_{ext}}{\Delta\dot{B}} \\ &= \frac{-232.16}{-258.99} \\ &= 0.896.\end{aligned}$$

In a thermodynamic reversible (ideal) system the exergy ratio will equal one, as no exergy is destroyed. This is not the case for an irreversible system. Ideally, the exergy ratio should be as close to one as possible for each component in the system. The exergy ratio for each component under normal operating conditions is shown in Figure 4.5. Under different operating conditions or fault conditions, the exergy ratios will change for each component and it may well be that some component's exergy ratio will improve, while others will deteriorate. The fact that the exergy ratio for the heat rejection element is above one is due to the fact that the energy flow is out of the heat rejection element while the exergy flow is into the element. This will not always be the case, as the exergy is dependent on the chosen reference temperature. In this case, the heat rejection element is operated at a temperature of 283.15 K, which is below the reference environment temperature of 298.15 K.

The exergy ratio and conventional exergy efficiency for each component in the cycle, under steady state conditions with a PT setpoint of 100 kJ/s, are shown in Figure 4.5. For this study,

the exergy ratio will be used to indicate the efficiency at which the component is converting exergy.

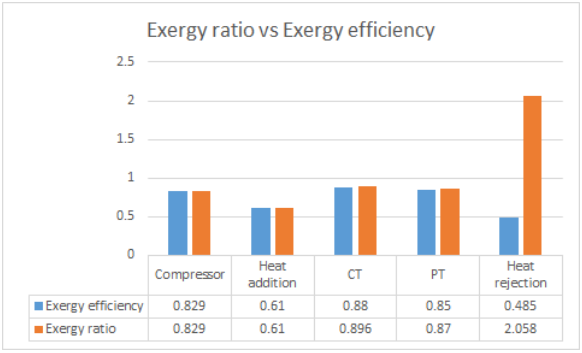

Figure 4.5: Exergy -ratio and -efficiency of the components in the cycle

4.3 Fault conditions

Changes in component parameters, due to faults, will influence the overall performance of the cycle. The implemented control logic will control the cycle to maintain specified setpoints and mask the influence a fault has on the cycle [20]. This is where an energy and exergy analysis of the cycle and individual components will determine the effect a fault has on the performance of components and the cycle. In this study, a fault is defined as the abnormal and unexpected behaviour of a component. The faults that will be investigated are summarised in Table 4.5, with the respective changes in parameters to simulate a fault in the component.

Fault-1 to Fault-6 are related to the turbomachinery (compressor and power turbine). The performance of turbomachinery is based on two performance maps, composed of the pressure ratio and the isentropic efficiency. These maps are unique to each turbomachine. Both maps express the pressure ratio and isentropic efficiency as a function of the corrected mass flow for various corrected speed curves. Using scaling factors to change the pressure ratio and isentropic efficiencies, the performance of the turbomachine can be varied to simulate a fault. The pressure ratio of the compressor and power turbine was scaled up and down by 10% and 5%. The isentropic efficiency of the compressor and power turbine was scaled down by 10% and 5%. Fault-7 represents a fault in the heat addition element. In this case, the fault is simulated as a heat loss of 100 kJ/s and 50 kJ/s. Fault-8 represents a fault in the heat rejection element, influencing the heat transfer. This is simulated as a change in the pressure drop across the element. Fault-9 and Fault-10 represent a leak at Node 2 and Node 4 respectively. The mass flow rate through the leak is simulated at 0.068 kg/s, which is 5% of the mass flow rate

Table 4.5: Description of the different fault conditions

Component	Fault ID	Effect of fault	Fault magnitude
Compressor	Fault-1	Increase in pressure ratio	10% and 5%
	Fault-2	Decrease in pressure ratio	10% and 5%
	Fault-3	Decrease in efficiency	10% and 5%
PT	Fault-4	Increase in pressure ratio	10% and 5%
	Fault-5	Decrease in pressure ratio	10% and 5%
	Fault-6	Decrease in efficiency	10% and 5%
Heat transfer elements	Fault-7	Heat loss in heat addition element	100 kJ/s and 50 kJ/s
	Fault-8	Pressure drop in heat rejection element	10% and 5%
Flow leakage	Fault-9	Change in mass flow	Leak at Node 2 of 0.068 kg/s
	Fault-10	Change in mass flow	Leak at Node 4 of 0.068 kg/s
Multiple	Fault-11	Fault-3 and Fault-5	Fault-3 at 10% Fault5 at 10%
	Fault-12	Fault-3 and Fault-5	Fault-3 at 10% Fault5 at 5%

through the cycle under normal steady state conditions [120]. The location of the leak (Node 2 or Node 4) will affect the mass flow through the cycle differently. Fault-11 and Fault-12 are a combination of two simultaneous faults with various fault magnitudes.

A fault magnitude above 10%, required the turbomachinery to operate outside of the applicable performance maps and the turbomachinery were not able to maintain the cycle at the required PT setpoint. The minimum magnitude at which all the faults could still be isolated was determined to be 5%. Therefore the fault magnitudes used are set at 10% and 5%.

4.4 Results

The energy and exergy analysis under normal steady state conditions, with a PT power output of 100 kJ/s, is shown in Figure 4.6. The exergy destroyed in the heat rejection primary side has a negative value, indicating that exergy is created. The exergy created is equal to the sum of the exergies destroyed in the rest of the cycle. The total exergy flow into the cycle is calculated as the sum of the changes in exergy in the surroundings which equals 954.08 kJ/s.

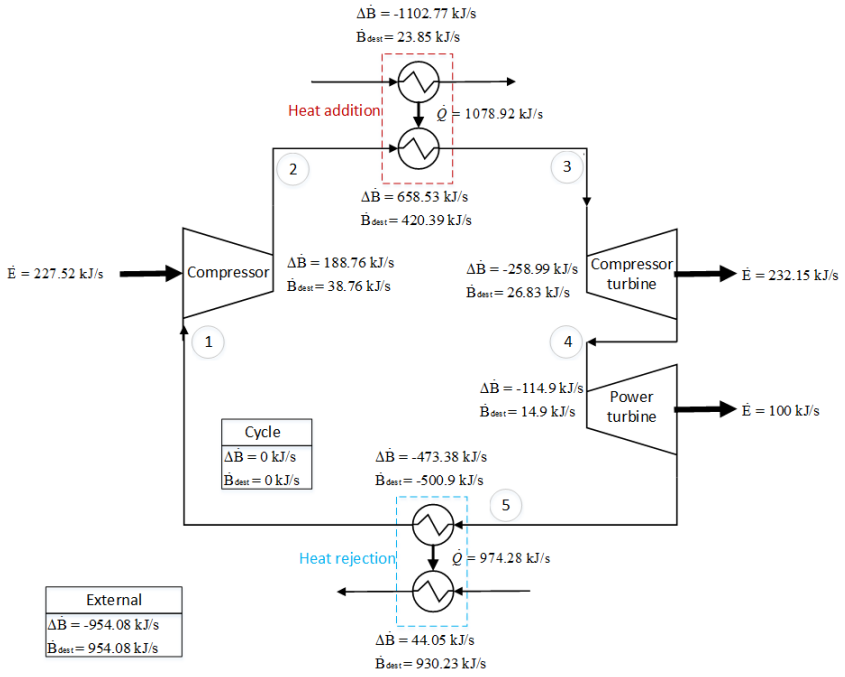

Figure 4.6: Energy and exergy analysis of the Brayton cycle PCU

Fault-1 with a fault magnitude of 5% and 10%, and a PT setpoint of 100 kJ/s, was simulated and the energy and exergy results are shown in Table 4.6. For Fault-1, the net exergy destroyed was reduced by 18.05 kJ/s from 954.08 kJ/s to 936.03 kJ/s, when the pressure ratio of the compressor was increased by 5%. In the case where the pressure ratio was increased by 10%, the net exergy destroyed was reduced by 60.16 kJ/s. In this case, the fault condition had the positive effect of reducing the exergy destroyed, implying that the overall performance can be improved by increasing the pressure ratio of the compressor. The energy and exergy analysis is a good indication as to the effect a fault condition has on the cycle. The energy and exergy analysis for Fault-2 is shown in Table 4.7.

Table 4.6: Energy and exergy results under normal conditions and Fault-1

Normal operating condition at 100 kJ/s			
Component	**ΔEnergy flow** (kJ/s)	**ΔExergy flow** (kJ/s)	**ΔExergy flow external to the cycle** (kJ/s)
Compressor	227.52	188.76	-227.52
Heat addition	1078.92	658.53	-1102.77
CT	-232.16	-258.99	232.16
PT	-100	-114.9	100
Heat rejection	-974.28	-473.38	44.05
Net	0	0	-954.08

(a)

Fault-1 with 10% fault magnitude			
Component	**ΔEnergy flow** (kJ/s)	**ΔExergy flow** (kJ/s)	**ΔExergy flow external to the cycle** (kJ/s)
Compressor	221.75	179.68	-221.75
Heat addition	1039.78	637.81	-1053.5
CT	-226.28	-253.7	226.28
PT	-100	-112.35	100
Heat rejection	-935.26	-451.44	55.05
Net	0	0	-893.92

(b)

Fault-1 with 5% fault magnitude			
Component	**ΔEnergy flow** (kJ/s)	**ΔExergy flow** (kJ/s)	**ΔExergy flow external to the cycle** (kJ/s)
Compressor	224.33	180.97	-224.33
Heat addition	1057.21	647.88	-1092.11
CT	-228.91	-257.14	228.91
PT	-100	-111.80	100
Heat rejection	-952.63	-459.9	51.5
Net	0	0	-936.03

(c)

The energy and exergy analysis for all the fault conditions are presented in Appendix C. In Chapter 5, an attributed graph matrix will be compiled from the energy and exergy analysis for the purpose of fault detection and isolation.

Table 4.7: Energy and exergy results for Fault-2

Fault-2 with 10% fault magnitude			
Component	**ΔEnergy flow** (kJ/s)	**ΔExergy flow** (kJ/s)	**ΔExergy flow external to the cycle** (kJ/s)
Compressor	235.65	187.49	-235.65
Heat addition	1133.99	694.21	-1119.32
CT	-240.46	-271.38	240.46
PT	-100	-110.58	100
Heat rejection	-1029.18	-499.73	78.3
Net	0	0	-936.21

(a)

Fault-2 with 5% fault magnitude			
Component	**ΔEnergy flow** (kJ/s)	**ΔExergy flow** (kJ/s)	**ΔExergy flow external to the cycle** (kJ/s)
Compressor	231.28	185.17	-231.28
Heat addition	1104.30	676.44	-1098.59
CT	-236.00	-265.83	236.00
PT	-100.00	-111.27	100.00
Heat rejection	-999.58	-484.51	70.74
Net	0.00	0.00	-923.13

(b)

In this case, a reduction in the pressure ratio of the compressor also improved the performance with a reduction in the exergy destroyed. The change in the net exergy destruction for the different fault types and magnitudes compared to the normal condition is shown in Figure 4.7. A positive value indicates a decrease in the exergy destruction while a negative value indicates an increase. From Figure 4.7, it is evident that both the fault type and magnitude influences the exergy being destroyed. Different magnitudes for the same fault can have different effects on the net exergy destruction, as with Fault-6. The fault magnitude determines the effect on the turbomachinery maps, which determines the temperature and pressure changes, influenc-

ing the exergy. Depending on the turbomachinery map, different fault magnitude can have different effects on the exergy.

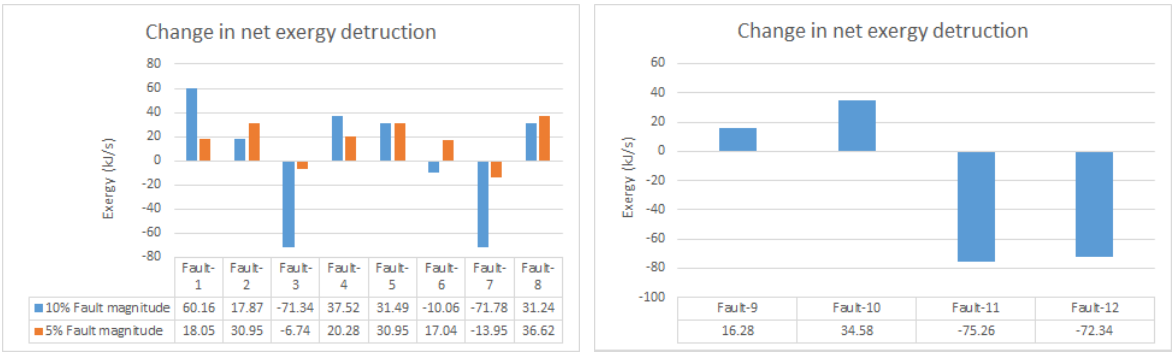

(a) Fault-1 to Fault-8

(b) Fault-9 to Fault-12

Figure 4.7: Change in net exergy destruction

From Tables 4.6 and 4.7, it is evident that both the fault type and magnitude influences the energy and exergy changes in the cycle. The reason that an increase (Fault-2), as well as a decrease (Fault-1) in the pressure ratio of the compressor, resulted in an improvement in the exergy destruction, is due to the control and the condition of the cycle under normal operating conditions. The fault conditions have an influence on both the pressure and temperature in the cycle. The temperature is however controlled to specific values at the outlet of the heat-injection and -rejection elements. The pressure at the compressor inlet is also controlled to maintain the required output at the PT. From (3.8) the exergy is based on the temperature and pressure and therefore influenced by changes in both the pressure and temperature. The changes in the pressure and temperature are based on the operating maps of the turbomachinery.

Due to the control of the cycle and the operation of the components, it is possible that both an increase and decrease in the pressure ratio of the compressor can reduce the exergy destroyed. Practical considerations will dictate the maximum and minimum pressures and temperatures, limiting the maximum exergy efficiency. The model used in this study is only a representative model and the practical considerations are not taken into account.

The pressure and temperature at the various nodes in the cycle are shown in Figure 4.8 for the normal conditions and for Fault-1 and -2, showing the influence faults have on the pressure and temperature.

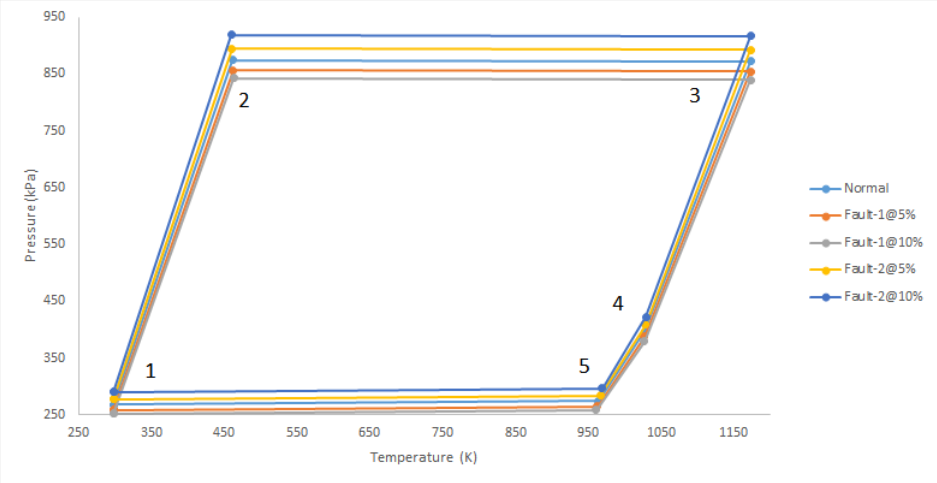

Figure 4.8: Temperature and pressure at various nodes

Considering only the PT, the output is controlled at 100 kJ/s, regardless of the pressure and temperature difference across the PT. The exergy values and therefore the exergy destroyed in the PT, is however influenced by the pressure and temperature changes due to a fault condition. For the same amount of energy output from the PT (100 kJ/s) the exergy destroyed by the PT is influenced by changes in the pressure and temperature across the PT.

The exergy ratio for the individual components under fault conditions and for the normal condition was calculated using (4.17) and the results are given in Table 4.8 for Fault-1 and Fault-2. The exergy ratios for the fault conditions were compared with the normal operating condition and the differences in the exergy ratios are shown in Figure 4.9. The faults had no effect on the exergy ratio of the heat addition component. For the heat rejection component the exergy ratio improved under Fault-1 but no change was noticed for Fault-2. The exergy ratio for the power turbine improved under the fault conditions. The compressor and CT had reduced exergy ratios under the fault conditions.

Table 4.8: Exergy ratios for fault and normal conditions

Operating condition	Compressor	Heat addition	CT	PT	Heat rejection
Normal	0.83	0.61	0.9	0.87	2.06
Fault-1 at 5%	0.81	0.61	0.89	0.89	2.07
Fault-1 at 10%	0.79	0.61	0.88	0.9	2.07
Fault-2 at 5%	0.8	0.61	0.89	0.9	2.06
Fault-2 at 10%	0.81	0.61	0.89	0.89	2.06

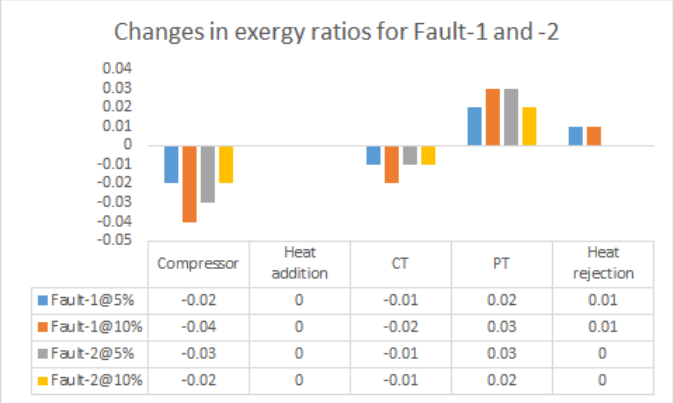

Figure 4.9: Exergy ratios under normal, Fault-1 and -2 conditions

4.5 Conclusion

In this chapter, a basic Brayton cycle was explained and the P-V and T-s diagrams presented. The calculations used in the simulation were also presented. A representative Brayton cycle model, which will be used in this study, was presented. The Flownex® simulation environment used for this study is a validated and verified environment. The representative model was validated against a model of a three-shaft Brayton cycle used in a PBMR. Based on the fact that the temperature and pressure responses of the two models are the same, it is assumed that the model proposed is valid and representative of a Brayton cycle. An energy and exergy analysis was performed on the representative model under normal and fault conditions. The

results indicated how faults influenced the exergy destruction in the cycle. This is best illustrated by the PT that is controlled to a fixed output of 100 kJ/s. The exergy output of the PT remained fixed, while the change in exergy through the PT varied, depending on the operating conditions. Both the fault type and magnitude have an influence on the energy and exergy analysis. From the energy and exergy analysis, an attributed graph matrix will be compiled for the purpose of fault detection and isolation.

Sensor noise is not considered in this study and the numerical noise introduced by the simulation software can be ignored, as its influence on the measured data is insignificant. Several methods are presented to calculate exergetic efficiency and a new method, called the exergy ratio, is presented as a performance indicator. The exergy ratio relates the exergy input or output of a component, to the change in exergy through the component. In some instances, the fault condition improved the exergetic efficiency of some components while reducing that of others.

CHAPTER 5

Energy-based visualisation for FDI

Energy and exergy data will be used to compile an attributed graph matrix, representing the Brayton cycle PCU under fault conditions and normal operating conditions. Residual-based methods were successfully implemented by du Rand [23] and Marias [27] for FDI in industrial systems and in the work of van Graan et al. [31], eigendecomposition was used for FDI on a heat exchanger. In this study, residual-based and eigendecomposition-based FDI methods will be implemented on a Brayton cycle PCU using attributed graph matrices to create unique signatures for different fault conditions. The signatures can then be used to detect and isolate faults in the Brayton cycle PCU.

5.1 Attributed graph matrix

The Brayton cycle in Figure 5.1(a) can be presented structurally as an attributed graph using nodes and edges as in Figure 5.1(b) [32]. Each component is represented as a node with attributes specific to that node. Each connection between two adjacent nodes is an edge, containing attributes specific to the connection between the nodes. The environment external to the cycle is also represented as a node. In this case, the node attributes will be the change in the specific exergy flow ($\Delta \dot{b}$) through the components and the edges will represent the specific energy flow ($\dot{e}$) between components. Specific values are used in the attributed graph matrices to eliminate the effect that changes in the operating setpoint have on the cycle. This will be explained in more detail in Chapter 6. All energy flows external to the cycle ($\dot{e}_{61}$, $\dot{e}_{62}$, $\dot{e}_{36}$, $\dot{e}_{46}$, $\dot{e}_{56}$) are assumed to be connected to a single node external to the cycle (Node 6) which

represents the environment. All energy produced by the cycle is delivered to this node and all energy consumed by the cycle is extracted from this node. The exergy change in Node 6 is calculated as the sum of the individual exergy changes brought forth in Node 6 by each component connected to Node 6.

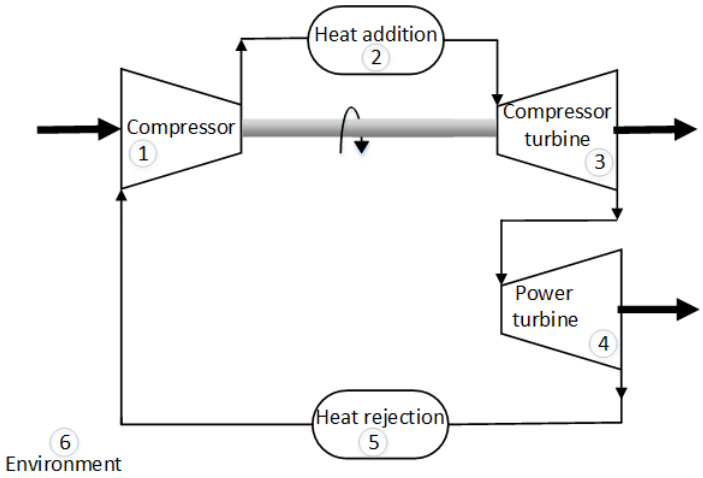

(a) Basic Brayton cycle

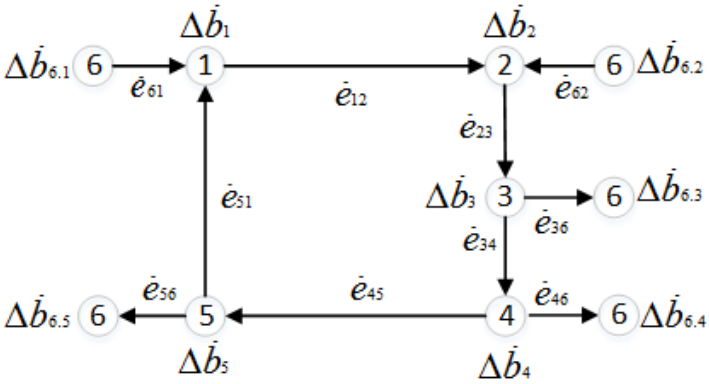

$$\Delta\dot{b}_6 = \Delta\dot{b}_{6.1} + \Delta\dot{b}_{6.2} + \Delta\dot{b}_{6.3} + \Delta\dot{b}_{6.4} + \Delta\dot{b}_{6.5}$$

(b) Attributed graph

Figure 5.1: Brayton cycle PCU and its attributed graph

From Figure 5.1(b) an attributed graph matrix (**G**) can be compiled, with each row representing attributes of a node, e.g. the first row represents Node 1 (the compressor), the second row Node 2 (the heat addition) and so forth. The matrix consists of the node attributes ($\Delta\dot{b}$) in the first column and the edge attributes ($\dot{e}$) in the remaining columns. If the edge is directed away from the node the value will be positive and if directed towards the node the value will be negative. This ensures that the edges not only indicate a connection between nodes and the magnitude

of the connection but also the direction of the connection (energy flow), retaining structural information about the cycle.

The cycle in Figure 5.1 will be visualised as an attributed graph matrix by

$$\mathbf{G} = \begin{bmatrix} \Delta\dot{b}_1 & 0 & \dot{e}_{12} & 0 & 0 & -\dot{e}_{51} & -\dot{e}_{61} \\ \Delta\dot{b}_2 & -\dot{e}_{12} & 0 & \dot{e}_{23} & 0 & 0 & -\dot{e}_{62} \\ \Delta\dot{b}_3 & 0 & -\dot{e}_{23} & 0 & \dot{e}_{34} & 0 & \dot{e}_{36} \\ \Delta\dot{b}_4 & 0 & 0 & -\dot{e}_{34} & 0 & \dot{e}_{45} & \dot{e}_{46} \\ \Delta\dot{b}_5 & \dot{e}_{51} & 0 & 0 & -\dot{e}_{45} & 0 & \dot{e}_{56} \\ \Delta\dot{b}_6 & \dot{e}_{61} & \dot{e}_{62} & -\dot{e}_{36} & -\dot{e}_{46} & -\dot{e}_{56} & 0 \end{bmatrix} \tag{5.1}$$

In the attributed graph matrix of (5.1), entry $g_{1,1}$ is the change in the specific exergy flow ($\Delta\dot{b}_1$) in Node 1. Entry $g_{1,2}$ will be the specific energy flow between Node 1 and itself. Since this connection does not exist, the entry is zero. Entry $g_{1,3}$ is the specific energy flow ($\dot{e}_{12}$) between Node 1 and Node 2. The value is positive since the flow is out of Node 1. Entry $g_{2,2}$ is the specific energy flow between Node 2 and Node 1, which is $\dot{e}_{12}$. The value is now negative since the flow is towards Node 2. The attributed graph matrix consists of specific-energy and -exergy values with the unit of kJ/kg.

The attributed graph matrix compiled under current operating conditions, can now be compared to a reference attributed graph matrix of the cycle, under normal operating conditions, to detect any changes in the cycle's operating condition. The two methods proposed for fault detection and isolation are discussed in the subsequent sections.

5.2 Residual-based method

Residual-based methods are commonly used for fault detection and consists of two main procedure; residual generation and residual evaluation. Residuals are generated by comparing the actual and expected output of a system. In a fault free case the residual will be zero, and non-zero in the case of a fault condition. The residual is then evaluated to provide additional information regarding the fault [36]. In this study the residual is based on the difference between two attributed graph matrices. The attributed graph matrix generated from the normal operating conditions ($\mathbf{G}_{ref}$) and the matrix generated from the actual operating conditions ($\mathbf{G}_{act}$) are compared and a m x n residual matrix ($\mathbf{G}_{res}$) calculated as

$$\mathbf{G}_{res} = [g_{res_{i,j}}] = \frac{g_{ref_{i,j}} - g_{act_{i,j}}}{g_{ref_{i,j}}} \text{ for } \begin{matrix} i = 1 \text{ to m} \\ j = 1 \text{ to n} \end{matrix} . \tag{5.2}$$

The values of $\mathbf{G}_{res}$ is expressed as the difference between the reference attributed graph matrix under normal operating conditions ($\mathbf{G}_{ref}$) and the actual attributed graph matrix ($\mathbf{G}_{act}$) under current operating conditions, in relation to the reference attributed graph matrix ($\mathbf{G}_{ref}$). By dividing with the reference attributed graph matrix, the residual attributed graph matrix is normalised to the specific attribute. In terms of the reference and actual attributed graph matrices for the cycle in Figure 5.1, (5.2) can be expressed as

$$\mathbf{G}_{res}^{T} = \begin{bmatrix} \frac{\Delta\dot{b}_{ref1}-\Delta\dot{b}_{act1}}{\Delta\dot{b}_{ref1}} & \frac{\Delta\dot{b}_{ref2}-\Delta\dot{b}_{act2}}{\Delta\dot{b}_{ref2}} & \frac{\Delta\dot{b}_{ref3}-\Delta\dot{b}_{act3}}{\Delta\dot{b}_{ref3}} & \frac{\Delta\dot{b}_{ref4}-\Delta\dot{b}_{act4}}{\Delta\dot{b}_{ref4}} & \frac{\Delta\dot{b}_{ref5}-\Delta\dot{b}_{act5}}{\Delta\dot{b}_{ref5}} & \frac{\Delta\dot{b}_{ref6}-\Delta\dot{b}_{act6}}{\Delta\dot{b}_{ref6}} \\ 0 & \frac{\dot{e}_{ref12}-\dot{e}_{act12}}{\dot{e}_{ref12}} & 0 & 0 & \frac{\dot{e}_{ref51}-\dot{e}_{act51}}{\dot{e}_{ref51}} & \frac{\dot{e}_{ref61}-\dot{e}_{act61}}{\dot{e}_{ref61}} \\ \frac{\dot{e}_{ref12}-\dot{e}_{act12}}{\dot{e}_{ref12}} & 0 & \frac{\dot{e}_{ref23}-\dot{e}_{act23}}{\dot{e}_{ref23}} & 0 & 0 & \frac{\dot{e}_{ref62}-\dot{e}_{act62}}{\dot{e}_{ref62}} \\ 0 & \frac{\dot{e}_{ref23}-\dot{e}_{act23}}{\dot{e}_{ref23}} & 0 & \frac{\dot{e}_{ref34}-\dot{e}_{act34}}{\dot{e}_{ref34}} & 0 & \frac{\dot{e}_{ref36}-\dot{e}_{act36}}{\dot{e}_{ref36}} \\ 0 & 0 & \frac{\dot{e}_{ref34}-\dot{e}_{act34}}{\dot{e}_{ref34}} & 0 & \frac{\dot{e}_{ref45}-\dot{e}_{act45}}{\dot{e}_{ref45}} & \frac{\dot{e}_{ref46}-\dot{e}_{act46}}{\dot{e}_{ref46}} \\ \frac{\dot{e}_{ref51}-\dot{e}_{act51}}{\dot{e}_{ref51}} & 0 & 0 & \frac{\dot{e}_{ref45}-\dot{e}_{act45}}{\dot{e}_{ref45}} & 0 & \frac{\dot{e}_{ref56}-\dot{e}_{act56}}{\dot{e}_{ref56}} \\ \frac{\dot{e}_{ref61}-\dot{e}_{act61}}{\dot{e}_{ref61}} & \frac{\dot{e}_{ref62}-\dot{e}_{act62}}{\dot{e}_{ref62}} & \frac{\dot{e}_{ref36}-\dot{e}_{act36}}{\dot{e}_{ref36}} & \frac{\dot{e}_{ref46}-\dot{e}_{act46}}{\dot{e}_{ref46}} & \frac{\dot{e}_{ref56}-\dot{e}_{act56}}{\dot{e}_{ref56}} & 0 \end{bmatrix}, \tag{5.3}$$

where the subscripts “ref” and “act” refer to the reference attributed graph matrix and the actual attributed graph matrix. Note that (5.3) is given as the transpose of (5.2).

As an example the Brayton cycle of Figure 5.1 was simulated using Flownex®, as described in Chapter 4. The reference attributed graph matrix for the cycle under normal operating conditions at steady state is given by

$$\mathbf{G}_{ref} = \begin{bmatrix} 133.03 & 0 & 589.49 & 0 & 0 & -424.15 & -165.34 \\ 480.55 & -589.49 & 0 & 1373.59 & 0 & 0 & -784.09 \\ -189.71 & 0 & -1373.59 & 0 & 1204.87 & 0 & 168.71 \\ -81.19 & 0 & 0 & -1204.87 & 0 & 1132.22 & 72.65 \\ -342.67 & 424.15 & 0 & 0 & -1132.22 & 0 & 708.07 \\ -662.57 & 165.34 & 784.09 & -168.71 & -72.65 & -708.07 & 0 \end{bmatrix}.$$

Although only two decimals are shown in the matrices, in the calculations more decimals are used. The resolution (number of decimals) of the values, determines the minimum fault magnitude that will be detectable. The higher the resolution (more decimal places), the smaller the fault magnitude that will be detectable becomes. In real life, the resolution is dependent on the sensor, while in simulation the resolution is much higher and dependent on the software used for processing.

The attributed graph matrices for an increase in the compressor pressure ratio (Fault-1) are given by $\mathbf{G}_{F1.5}$ for a fault magnitude of 5% (Fault-1.5),

$$\mathbf{G}_{F1.5} = \begin{bmatrix} 134.25 & 0 & 590.36 & 0 & 0 & -424.17 & -166.19 \\ 480.24 & -590.36 & 0 & 1373.58 & 0 & 0 & -783.21 \\ -190.38 & 0 & -1373.58 & 0 & 1204 & 0 & 169.58 \\ -83.06 & 0 & 0 & -1204 & 0 & 1129.91 & 74.08 \\ -341.05 & 424.17 & 0 & 0 & -1129.91 & 0 & 705.74 \\ -668.17 & 166.19 & 783.21 & -169.58 & -74.08 & -705.74 & 0 \end{bmatrix}$$

and $\mathbf{G}_{F1.10}$ for a fault magnitude of 10% (Fault-1.10),

$$\mathbf{G}_{F1.10} = \begin{bmatrix} 135.22 & 0 & 591.07 & 0 & 0 & -424.19 & -166.88 \\ 479.98 & -591.07 & 0 & 1373.57 & 0 & 0 & -782.49 \\ -190.92 & 0 & -1373.57 & 0 & 1203.28 & 0 & 170.28 \\ -84.54 & 0 & 0 & -1203.28 & 0 & 1128.02 & 75.25 \\ -339.73 & 424.19 & 0 & 0 & -1128.02 & 0 & 703.83 \\ -672.73 & 166.88 & 782.49 & -170.28 & -75.25 & -703.83 & 0 \end{bmatrix}.$$

The residual graph matrices ($\mathbf{G}_{resF1.5}$ and $\mathbf{G}_{resF1.10}$) for the same fault at different fault magnitudes are calculated using (5.2) resulting in

$$\mathbf{G}_{resF1.5} = \begin{bmatrix} -0.009 & 0 & -0.001 & 0 & 0 & 0 & -0.005 \\ 0 & -0.001 & 0 & 0 & 0 & 0 & 0.001 \\ -0.003 & 0 & 0 & 0 & 0 & 0 & -0.005 \\ -0.022 & 0 & 0 & 0 & 0 & 0.002 & -0.019 \\ 0.004 & 0 & 0 & 0 & 0.002 & 0 & 0.003 \\ -0.008 & -0.005 & 0.001 & -0.005 & -0.019 & 0.003 & 0 \end{bmatrix}$$

and

$$\mathbf{G}_{resF1.10} = \begin{bmatrix} -0.016 & 0 & -0.002 & 0 & 0 & 0 & -0.009 \\ 0.001 & -0.002 & 0 & 0 & 0 & 0 & 0.002 \\ -0.006 & 0 & 0 & 0 & 0.001 & 0 & -0.009 \\ -0.041 & 0 & 0 & 0.001 & 0 & 0.003 & -0.035 \\ 0.008 & 0 & 0 & 0 & 0.003 & 0 & 0.005 \\ -0.015 & -0.009 & 0.002 & -0.009 & -0.035 & 0.005 & 0 \end{bmatrix}.$$

This yielded two different residual graph matrices for the same fault, depending on the magnitude of the fault. The residual graph matrices can be graphically represented by plotting the residual specific energy flows and the residual specific exergy change for each node as in Figure 5.2 for Fault-1.5 and Figure 5.3 for Fault-1.10. In the figures, R_{Ein} and R_{Eout} represent the residuals of the energy stream respectively in and out of a node, R_{Eext} represents the residual external energy flow between a node and Node 6 and $R_{\Delta B}$ represents the residual of the change in exergy through the node. In the case of Node 1 in $\mathbf{G}_{resF1.5}$ for example, $R_{Ein} = \mathbf{G}_{resF1.5}(1,6)$, $R_{Eout} = \mathbf{G}_{resF1.5}(1,3)$, $R_{Eext} = \mathbf{G}_{resF1.5}(1,7)$ and $R_{\Delta B} = \mathbf{G}_{resF1.5}(1,1)$. Since the attributed graph matrices consist of energy and exergy data, the residual-based fault signature also consists of an energy-based and an exergy-based component. The energy-based component consists of R_{Ein}, R_{Eout} and R_{Eext} while the exergy-based component consists of $R_{\Delta B}$.

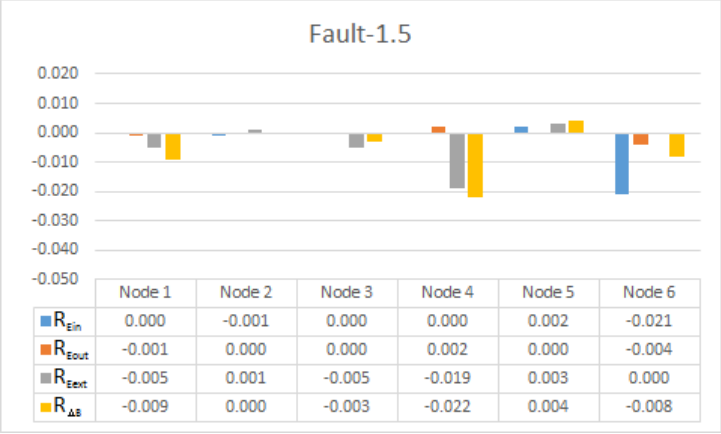

Figure 5.2: Residual-based fault signature for Fault-1.5

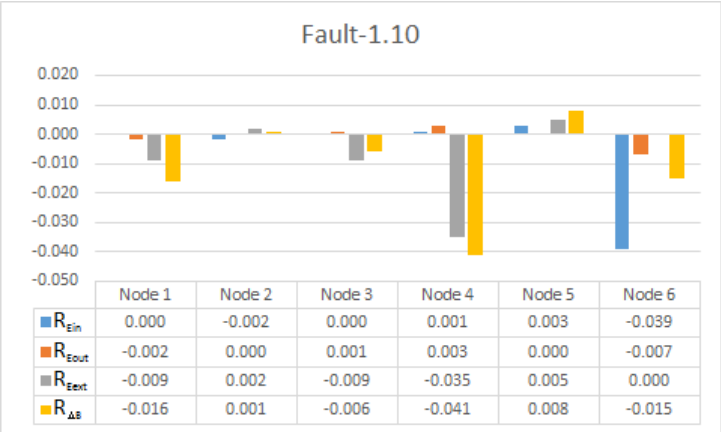

	Node 1	Node 2	Node 3	Node 4	Node 5	Node 6
R_{Ein}	0.000	-0.002	0.000	0.001	0.003	-0.039
R_{Eout}	-0.002	0.000	0.001	0.003	0.000	-0.007
R_{Eext}	-0.009	0.002	-0.009	-0.035	0.005	0.000
$R_{\Delta B}$	-0.016	0.001	-0.006	-0.041	0.008	-0.015

Figure 5.3: Residual-based fault signature for Fault-1.10

For the purpose of fault detection, the residual graph matrix should be independent of the fault magnitude and only depend on the fault condition. For this reason, the residual graph matrices have to be normalised to the maximum value of the attribute. Since the graph matrix consists of exergy values in the first column and energy values in the remaining columns, the first column is normalised to the maximum exergy value and all the energy values to the maximum energy value. The normalised residual graph matrix ($\mathbf{G}_{resn}$) is calculated by

$$g_{resn_{i,1}} = \frac{g_{res_{i,1}}}{max|g_{res_{i,1}}|} \quad \text{for } i\text{=1 to m} \tag{5.4}$$

and

$$g_{resn_{i,j}} = \frac{g_{res_{i,j}}}{max|g_{res_{i,j}}|} \text{ for } \begin{matrix} i = 1 \text{ to m} \\ j = 2 \text{ to n} \end{matrix} . \tag{5.5}$$

The normalised residual graph matrix is compiled as

$$\mathbf{G}_{resn} = \begin{bmatrix} \frac{g_{res_{1,1}}}{B_{max}} & \frac{g_{res_{1,2}}}{E_{max}} & \frac{g_{res_{1,3}}}{E_{max}} & \frac{g_{res_{1,4}}}{E_{max}} & \frac{g_{res_{1,5}}}{E_{max}} & \frac{g_{res_{1,6}}}{E_{max}} & \frac{g_{res_{1,7}}}{E_{max}} \\ \frac{g_{res_{2,1}}}{B_{max}} & \frac{g_{res_{2,2}}}{E_{max}} & \frac{g_{res_{2,3}}}{E_{max}} & \frac{g_{res_{2,4}}}{E_{max}} & \frac{g_{res_{2,5}}}{E_{max}} & \frac{g_{res_{2,6}}}{E_{max}} & \frac{g_{res_{2,7}}}{E_{max}} \\ \frac{g_{res_{3,1}}}{B_{max}} & \frac{g_{res_{3,2}}}{E_{max}} & \frac{g_{res_{3,3}}}{E_{max}} & \frac{g_{res_{3,4}}}{E_{max}} & \frac{g_{res_{3,5}}}{E_{max}} & \frac{g_{res_{3,6}}}{E_{max}} & \frac{g_{res_{3,7}}}{E_{max}} \\ \frac{g_{res_{4,1}}}{B_{max}} & \frac{g_{res_{4,2}}}{E_{max}} & \frac{g_{res_{4,3}}}{E_{max}} & \frac{g_{res_{4,4}}}{E_{max}} & \frac{g_{res_{4,5}}}{E_{max}} & \frac{g_{res_{4,6}}}{E_{max}} & \frac{g_{res_{4,7}}}{E_{max}} \\ \frac{g_{res_{5,1}}}{B_{max}} & \frac{g_{res_{5,2}}}{E_{max}} & \frac{g_{res_{5,3}}}{E_{max}} & \frac{g_{res_{5,4}}}{E_{max}} & \frac{g_{res_{5,5}}}{E_{max}} & \frac{g_{res_{5,6}}}{E_{max}} & \frac{g_{res_{5,7}}}{E_{max}} \\ \frac{g_{res_{6,1}}}{B_{max}} & \frac{g_{res_{6,2}}}{E_{max}} & \frac{g_{res_{6,3}}}{E_{max}} & \frac{g_{res_{6,4}}}{E_{max}} & \frac{g_{res_{6,5}}}{E_{max}} & \frac{g_{res_{6,6}}}{E_{max}} & \frac{g_{res_{6,7}}}{E_{max}} \end{bmatrix} \tag{5.6}$$

where

$$B_{max} = max\left|g_{res_{i,1}}\right| \text{ for } i\text{=1 to 6}$$
$$E_{max} = max\left|g_{res_{i,j}}\right| \text{ for } \begin{matrix} i = 1 \text{ to } 6 \\ j = 2 \text{ to } 7 \end{matrix}.$$

The normalised residual graph matrices for Fault-1 with two different fault magnitudes are then calculated to be

$$\mathbf{G}_{resnF1.5} = \begin{bmatrix} -0.396 & 0 & -0.074 & 0 & 0 & -0.002 & -0.259 \\ 0.028 & -0.074 & 0 & 0 & 0 & 0 & 0.057 \\ -0.153 & 0 & 0 & 0 & 0.036 & 0 & -0.259 \\ -1 & 0 & 0 & 0.036 & 0 & 0.103 & -1 \\ 0.205 & -0.002 & 0 & 0 & 0.103 & 0 & 0.166 \\ -0.368 & -0.259 & 0.057 & -0.259 & -1 & 0.166 & 0 \end{bmatrix}$$

$$\mathbf{G}_{resnF1.10} = \begin{bmatrix} -0.397 & 0 & -0.074 & 0 & 0 & -0.002 & -0.259 \\ 0.028 & -0.074 & 0 & 0 & 0 & 0 & 0.056 \\ -0.154 & 0 & 0 & 0 & 0.036 & 0 & -0.259 \\ -1 & 0 & 0 & 0.036 & 0 & 0.103 & -1 \\ 0.207 & -0.002 & 0 & 0 & 0.103 & 0 & 0.166 \\ -0.371 & -0.259 & 0.056 & -0.259 & -1 & 0.166 & 0 \end{bmatrix}$$

The residual graphs for the normalised graph matrix of Fault-1 with two different fault magnitudes, as shown in Figure 5.4 and Figure 5.5, are now independent of the fault magnitude. Using this method the residual graphs for a specific fault condition will remain the same regardless of the fault magnitude. For this reason only the normalised residual graph matrices will be used for fault detection and isolation and will be labeled with the addition of a "n" in the matrix subscript.

Due to the data processing software used and the calculations performed on the data, small variations may occur in the normalised results as evident from the small differences between $\mathbf{G}_{resnF1.5}$ and $\mathbf{G}_{resnF1.10}$ and graphically represented in Figure 5.4 and Figure 5.5.

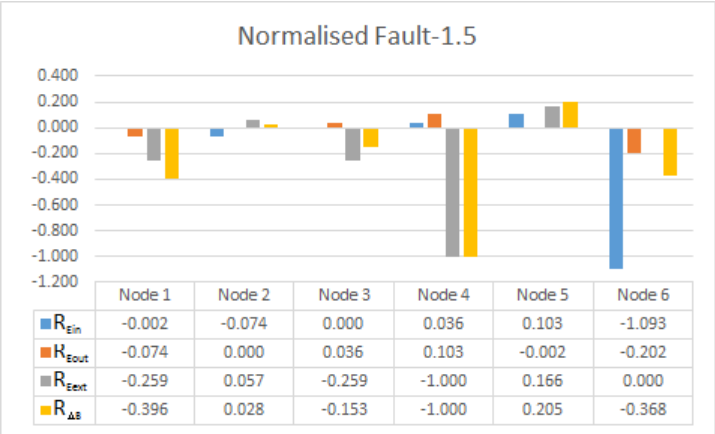

	Node 1	Node 2	Node 3	Node 4	Node 5	Node 6
R_{Ein}	-0.002	-0.074	0.000	0.036	0.103	-1.093
R_{Eout}	-0.074	0.000	0.036	0.103	-0.002	-0.202
R_{Eext}	-0.259	0.057	-0.259	-1.000	0.166	0.000
$R_{\Delta E}$	-0.396	0.028	-0.153	-1.000	0.205	-0.368

Figure 5.4: Normalised residual-based fault signature for Fault-1.5

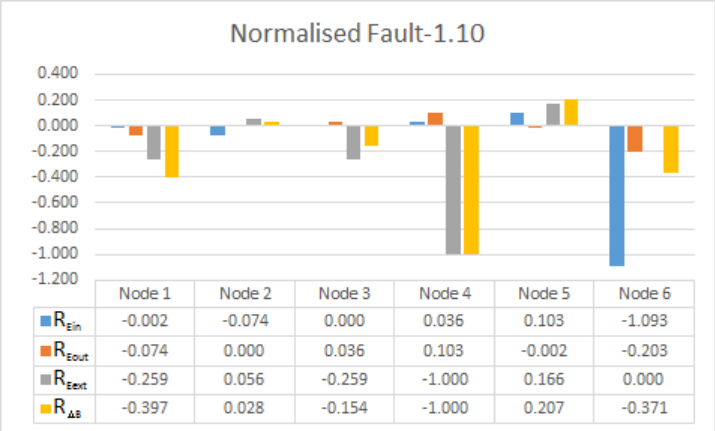

	Node 1	Node 2	Node 3	Node 4	Node 5	Node 6
R_{Ein}	-0.002	-0.074	0.000	0.036	0.103	-1.093
R_{Eout}	-0.074	0.000	0.036	0.103	-0.002	-0.203
R_{Eext}	-0.259	0.056	-0.259	-1.000	0.166	0.000
$R_{\Delta E}$	-0.397	0.028	-0.154	-1.000	0.207	-0.371

Figure 5.5: Normalised residual-based fault signature for Fault-1.10

To allow for small variations in the normalised data for the same fault condition at different magnitudes, a threshold value is implemented. In Chapter 4, numerical noise was explained and it was determined that in this case the numerical noise has little influence and is ignored. For different operating conditions or fault magnitudes, small variations may occur due to the change in the operational values being used in the calculations.

The threshold value is calculated to be large enough to include variations in data of the same fault condition at different magnitudes, but small enough not to include changes in the data due to different fault conditions. An example of the normalised fault signatures for two arbitrary

fault conditions (Fault-A and Fault-B) at a single node are shown in Figure 5.6. Although the two fault conditions changed the same data (Node 1), the magnitude of the change differ, with Fault-A having a residual value of A at Node 1 and Fault-B a residual value of B at Node 1. To allow for small variations in the data a threshold is implemented. A measured change in Node 1 of $A \pm threshold$ will be regarded as Fault-A. The same applies for Fault-B. In order to differentiate between Fault-A and Fault-B there must be no overlap in the residual values for Fault-A and Fault-B. This implies that $A + threshold$ must be smaller than $B - threshold$. The threshold will be a compromise between sensitivity (how much variations is allowed for in the value of a fault) and isolability (being able to differentiate between two fault conditions). Any residual value for Node 1 not within the range of $A \pm threshold$ or $B \pm threshold$ can not be identified as either Fault-A or Fault-B.

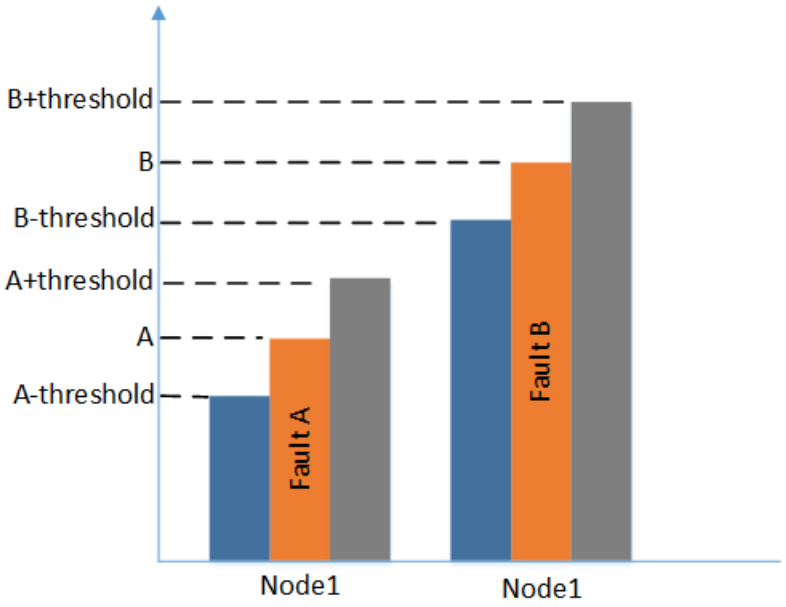

Figure 5.6: Example illustrating the use of thresholds

The normalised residual graph matrix for Fault-1 ($\mathbf{G}_{resnF1}$) will be the average between the normalised residual graph matrices of Fault-1 with fault magnitudes of 5% and 10%, given as

$$\mathbf{G}_{resnF1} = \begin{bmatrix} -0.397 & 0 & -0.074 & 0 & 0 & -0.002 & -0.259 \\ 0.028 & -0.074 & 0 & 0 & 0 & 0 & 0.057 \\ -0.153 & 0 & 0 & 0 & 0.036 & 0 & -0.259 \\ -1 & 0 & 0 & 0.036 & 0 & 0.103 & -1 \\ 0.206 & -0.002 & 0 & 0 & 0.103 & 0 & 0.166 \\ -0.369 & -0.259 & 0.057 & -0.259 & -1 & 0.166 & 0 \end{bmatrix}$$

Following the same process for Fault-4 (an increase in the pressure ratio of the power turbine) as for Fault-1, the normalised residual graph matrices for Fault-4 with fault magnitudes of 5% and 10% are given as

$$\mathbf{G}_{resnF4.5} = \begin{bmatrix} 0.96 & 0 & 0.28 & 0 & 0 & 0 & 1 \\ -0.113 & 0.28 & 0 & 0 & 0 & 0 & -0.21 \\ 1 & 0 & 0 & 0 & -0.14 & 0 & 0.993 \\ -0.157 & 0 & 0 & -0.14 & 0 & -0.139 & -0.132 \\ -0.293 & 0 & 0 & 0 & -0.139 & 0 & -0.224 \\ -0.185 & 1 & -0.21 & 0.993 & -0.132 & -0.224 & 0 \end{bmatrix}$$

and

$$\mathbf{G}_{resnF4.10} = \begin{bmatrix} 0.964 & 0 & 0.281 & 0 & 0 & 0.001 & 1 \\ -0.111 & 0.281 & 0 & 0 & 0 & 0 & -0.211 \\ 1 & 0 & 0 & 0 & -0.14 & 0 & 0.999 \\ -0.167 & 0 & 0 & -0.14 & 0 & -0.139 & -0.142 \\ -0.296 & 0.001 & 0 & 0 & -0.139 & 0 & -0.224 \\ -0.184 & 1 & -0.211 & 0.999 & -0.142 & -0.224 & 0 \end{bmatrix}$$

and the average of $\mathbf{G}_{resnF4.5}$ and $\mathbf{G}_{resnF4.10}$ results in the normalised attributed graph matrix of Fault-4, given as

$$\mathbf{G}_{resnF4} = \begin{bmatrix} 0.962 & 0 & 0.28 & 0 & 0 & 0 & 1 \\ -0.112 & 0.28 & 0 & 0 & 0 & 0 & -0.21 \\ 1 & 0 & 0 & 0 & -0.14 & 0 & 0.996 \\ -0.162 & 0 & 0 & -0.14 & 0 & -0.139 & -0.137 \\ -0.294 & 0 & 0 & 0 & -0.139 & 0 & -0.224 \\ -0.184 & 1 & -0.21 & 0.996 & -0.137 & -0.224 & 0 \end{bmatrix}.$$

In this example, considering only Fault-1 and Fault-4, the maximum difference in the normalised residual graph matrices for the same fault condition at different magnitudes are 0.003 in the case of Fault-1 and 0.006 in the case of Fault-4. A threshold value of 0.006 will thus be sufficient to compensate for small variations in the attributed graph matrices of a fault at different fault magnitudes. The minimum difference between the normalised residual graph matrices for the two different fault conditions ($\mathbf{G}_{resnF1}$ and $\mathbf{G}_{resnF4}$) is 0.14. The large difference (0.14) between the normalised residual graph matrices of Fault-1 and Fault-4 compared to the threshold range (0.006) indicates that the two fault conditions will be distinguishable

from each other, while compensating for small variations in the data.

Regardless of the fault magnitudes, the normalised residual graphs for Fault-1 and Fault-4 in this example will always be represented as in Figure 5.7 and Figure 5.8 respectively and therefore it can be used as a residual-based fault signature unique to each fault.

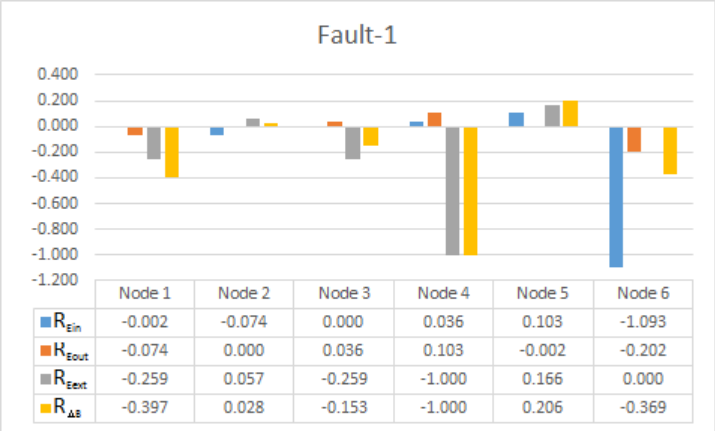

	Node 1	Node 2	Node 3	Node 4	Node 5	Node 6
R_{Ein}	-0.002	-0.074	0.000	0.036	0.103	-1.093
R_{Eout}	-0.074	0.000	0.036	0.103	-0.002	-0.202
R_{Eext}	-0.259	0.057	-0.259	-1.000	0.166	0.000
$R_{\Delta E}$	-0.397	0.028	-0.153	-1.000	0.206	-0.369

Figure 5.7: Residual-based fault signature for Fault-1

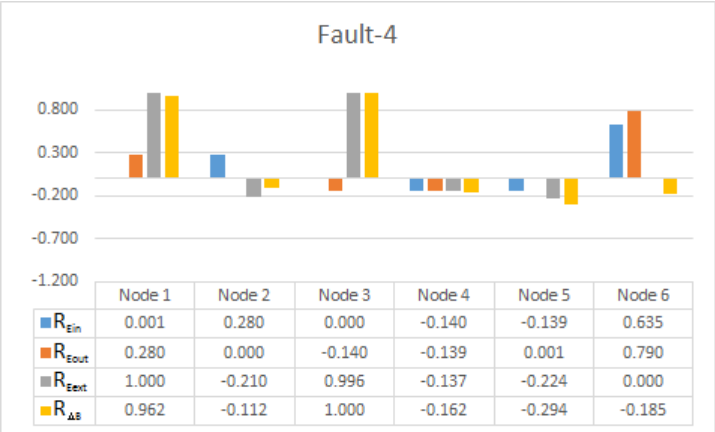

	Node 1	Node 2	Node 3	Node 4	Node 5	Node 6
R_{Ein}	0.001	0.280	0.000	-0.140	-0.139	0.635
R_{Eout}	0.280	0.000	-0.140	-0.139	0.001	0.790
R_{Eext}	1.000	-0.210	0.996	-0.137	-0.224	0.000
$R_{\Delta E}$	0.962	-0.112	1.000	-0.162	-0.294	-0.185

Figure 5.8: Residual-based fault signature for Fault-4

5.3 Eigendecomposition-based method

In this section, graph matching concepts are applied to the attributed graphs representing the normal operating conditions and a fault condition. Comparing these two graphs will highlight the differences between them. By implementing the method as described in the work of Wilson and Martinez [139] and Jouili and Tabbone [32], a cost matrix is calculated, describing the differences between the two graphs. From the cost matrix, a distance value is calculated to quantify the difference between the graphs. In the application of this method for fault detection, the distance value will not be utilised. It is recommended that the significance and application of the distance value be investigated in future work, as a possible improvement on this method for FDI. Instead of calculating the distance value, the eigendecomposition of the cost matrix is determined. The eigendecomposition of a matrix entails the calculation of the eigenvalues and eigenvectors. The eigendecomposition provides information about the structure and characteristics of the matrix [140, 141]. The eigendecomposition of a matrix is calculated so that

$$\mathbf{A}\mathbf{x} = \lambda\mathbf{x} \tag{5.7}$$

holds true, where $\mathbf{A}$ is a $n \times n$ matrix, $\mathbf{x}$ is an eigenvector and λ an eigenvalue. An eigenvector represents an orientation, while an eigenvalue represents a magnitude. A negative eigenvalue implies a reversal in the direction (eigenvector) associated with the eigenvalue. The three classes of real square matrices are symmetrical, skew and orthogonal. Matrix $\mathbf{A}$ is symmetrical if $\mathbf{A}^T = \mathbf{A}$, skew if $\mathbf{A}^T = -\mathbf{A}$ and orthogonal if $\mathbf{A}^T = \mathbf{A}^{-1}$.

The eigenvalues of a skew matrix are imaginary or zero and for an orthogonal matrix, real or complex conjugate pairs [142]. The eigenvalues of a symmetrical matrix are real and therefore the attributed graph matrices were compiled in such a way that the cost matrix will be symmetrical. Having real eigenvalues simplified the visualisation of the eigendecomposition.

In the work of van Graan [143], eigendecomposition was successfully implemented on a heat exchanger for the purpose of fault detection and warrants a study on the feasibility of this method on a thermodynamic cycle. The same attributed graph matrices, as described in the previous section will be used to illustrate the eigendecomposition-based method.

The cost matrix ($\mathbf{C}$) of two attributed graphs ($\mathbf{G}_1$and $\mathbf{G}_2$) is calculated as

$$\mathbf{C}(i,j) = \sqrt{\sum_{a=1}^{n} \left[\frac{\mathbf{G}_1(i,a) - \mathbf{G}_2(j,a)}{range_a}\right]^2} \text{ for } i,j = 1,2,...,m \tag{5.8}$$

where $\mathbf{G}_1$ and $\mathbf{G}_2$ are $m \times n$ matrices and $\mathbf{C}$ is a $m \times m$ matrix. The value, $range_a$, is used to normalise the cost matrix, and is defined as

$$range_a = max\ a - min\ a \tag{5.9}$$

where *max a* and *min a* are respectively the maximum and minimum values in the a-th column of $\mathbf{G}_1$.

A reference cost matrix, $\mathbf{C}_{ref}$ is obtained by matching the reference graph matrix $\mathbf{G}_{ref}$ with itself using (5.8), resulting in

$$\mathbf{C}_{ref} = \begin{bmatrix} 0 & 0.696 & 0.91 & 0.777 & 0.697 & 0.804 \\ 0.696 & 0 & 1.086 & 1.186 & 1.105 & 1.35 \\ 0.91 & 1.086 & 0 & 0.903 & 1.01 & 1.061 \\ 0.777 & 1.186 & 0.903 & 0 & 0.789 & 1.004 \\ 0.697 & 1.105 & 1.01 & 0.789 & 0 & 0.64 \\ 0.804 & 1.35 & 1.061 & 1.004 & 0.64 & 0 \end{bmatrix}.$$

The cost matrix for Fault-1.5 ($\mathbf{C}_{F1.5}$) obtained from $\mathbf{G}_{ref}$ and $\mathbf{G}_{F1.5}$ and the cost matrix for Fault-1.10 ($\mathbf{C}_{F1.10}$) obtained from $\mathbf{G}_{ref}$ and $\mathbf{G}_{F1.10}$ are given by

$$\mathbf{C}_{F1.5} = \begin{bmatrix} 0.001 & 1.007 & 1.129 & 1.033 & 1.024 & 0.753 \\ 1.006 & 0.001 & 1.43 & 1.512 & 1.74 & 1.574 \\ 1.13 & 1.429 & 0 & 1.13 & 1.313 & 1.29 \\ 1.034 & 1.512 & 1.131 & 0.002 & 1.112 & 1.258 \\ 1.027 & 1.742 & 1.314 & 1.112 & 0.002 & 0.926 \\ 0.749 & 1.571 & 1.288 & 1.256 & 0.925 & 0.005 \end{bmatrix}$$

and

$$\mathbf{C}_{F1.10} = \begin{bmatrix} 0.002 & 1.007 & 1.129 & 1.032 & 1.022 & 0.756 \\ 1.006 & 0.001 & 1.43 & 1.512 & 1.739 & 1.577 \\ 1.131 & 1.429 & 0.001 & 1.13 & 1.312 & 1.291 \\ 1.034 & 1.512 & 1.131 & 0.004 & 1.111 & 1.259 \\ 1.027 & 1.742 & 1.313 & 1.11 & 0.004 & 0.927 \\ 0.75 & 1.571 & 1.288 & 1.254 & 0.925 & 0.009 \end{bmatrix}.$$

The normalisation of the cost matrices ensured that the cost matrices for a fault remained the same regardless of the fault magnitude. Due to numerical noise, the cost matrices for the same fault at different magnitudes differ as evident from the small variation between $\mathbf{C}_{F1.5}$ and $\mathbf{C}_{F1.10}$. The differences are relatively small due to the large values ($range_a$) used for normalisation. The eigendecomposition of the cost matrices is tabulated in Table 5.1 and Table 5.2. The cost matrices, $\mathbf{C}_{F1.5}$ and $\mathbf{C}_{F1.10}$, are similar and therefore the eigendecomposition will be similar.

Table 5.1: Eigendecomposition for the reference condition and Fault-1 at 5%

Eigenvalues					
6.144	-1.957	-1.476	-1.137	-0.939	-0.635
Eigenvectors					
-0.339	0.040	0.336	0.015	0.394	-0.785
-0.470	0.774	0.228	-0.140	-0.255	0.209
-0.417	0.063	-0.623	0.652	-0.023	-0.082
-0.405	-0.146	-0.472	-0.667	0.360	0.134
-0.412	-0.506	0.122	-0.143	-0.717	-0.158
-0.394	-0.345	0.457	0.299	0.370	0.539

(a) Reference condition

Eigenvalues					
6.146	-1.956	-1.473	-1.134	-0.935	-0.634
Eigenvectors					
-0.339	-0.040	-0.335	0.014	0.393	-0.782
-0.470	-0.774	-0.227	-0.138	-0.253	0.209
-0.417	-0.062	0.627	0.649	-0.024	-0.084
-0.405	0.147	0.469	-0.670	0.359	0.135
-0.412	0.506	-0.124	-0.140	-0.718	-0.162
-0.394	0.344	-0.456	0.300	0.370	0.542

(b) Fault-1 at 5%

Table 5.2: Eigendecomposition of Fault-1 at 10%

Eigenvalues					
6.147	-1.954	-1.471	-1.132	-0.932	-0.634
Eigenvectors					
-0.339	-0.041	-0.334	0.013	0.392	-0.780
-0.470	-0.774	-0.226	-0.136	-0.252	0.209
-0.417	-0.061	0.629	0.647	-0.024	-0.085
-0.405	0.148	0.467	-0.673	0.358	0.135
-0.412	0.505	-0.126	-0.138	-0.719	-0.166
-0.394	0.343	-0.455	0.301	0.370	0.543

The cost matrix for Fault-1 ($\mathbf{C}_{F1}$) will be the average of $\mathbf{C}_{F1.5}$ and $\mathbf{C}_{F1.10}$, given as

$$\mathbf{C}_{F1} = \begin{bmatrix} 0.001 & 1.007 & 1.129 & 1.032 & 1.023 & 0.754 \\ 1.006 & 0.001 & 1.43 & 1.512 & 1.74 & 1.576 \\ 1.13 & 1.429 & 0.001 & 1.13 & 1.313 & 1.29 \\ 1.034 & 1.512 & 1.131 & 0.003 & 1.111 & 1.259 \\ 1.027 & 1.742 & 1.314 & 1.111 & 0.003 & 0.927 \\ 0.75 & 1.571 & 1.288 & 1.255 & 0.925 & 0.007 \end{bmatrix}.$$

The eigendecomposition of the cost matrix of Fault-1 is given in Table 5.3.

Table 5.3: Eigendecomposition of Fault-1

Eigenvalues					
6.144	-1.954	-1.470	-1.132	-0.932	-0.633
Eigenvectors					
-0.339	-0.04	-0.333	0.015	0.391	-0.779
-0.470	-0.774	-0.226	-0.136	-0.251	0.209
-0.417	-0.061	0.629	0.646	-0.023	-0.085
-0.405	0.147	0.466	-0.673	0.357	0.135
-0.412	0.505	-0.125	-0.139	-0.719	-0.165
-0.394	0.343	-0.455	0.301	0.37	0.543

Similarly the cost matrix for Fault-4 is calculated to be

$$\mathbf{C}_{F4} = \begin{bmatrix} 0.018 & 1.003 & 1.126 & 1.044 & 1.039 & 0.758 \\ 1.013 & 0.02 & 1.42 & 1.521 & 1.754 & 1.572 \\ 1.118 & 1.43 & 0.022 & 1.139 & 1.324 & 1.299 \\ 1.027 & 1.512 & 1.133 & 0.011 & 1.122 & 1.271 \\ 1.012 & 1.741 & 1.325 & 1.12 & 0.016 & 0.94 \\ 0.736 & 1.57 & 1.297 & 1.266 & 0.932 & 0.024 \end{bmatrix}$$

and the eigendecomposition of the cost matrix of Fault-4 is given in Table 5.4.

Table 5.4: Eigendecomposition of Fault-4

Eigenvalues					
6.169	-1.943	-1.466	-1.127	-0.930	-0.622
Eigenvectors					
0.339	0.044	-0.332	0.013	0.390	-0.789
0.470	0.772	-0.239	-0.156	-0.253	0.201
0.417	0.064	0.608	0.662	-0.027	-0.077
0.404	-0.144	0.490	-0.655	0.359	0.129
0.412	-0.507	-0.114	-0.140	-0.715	-0.150
0.394	-0.344	-0.456	0.294	0.375	0.538

In Figure 5.9 the eigendecomposition of the Fault-1, with different fault magnitudes, is compared to the normal condition and the directional changes in the eigendecomposition are indicated by either a “+” or a “-”.

Fault-1.5					
Eigenvalue					
+	+	+	+	+	+
Eigenvector					
-	-	-	-	-	+
-	-	-	+	+	-
+	-	+	-	-	-
-	+	+	-	-	+
+	+	-	+	-	-
-	+	-	+	+	+

(a) Fault-1.5

Fault-1.10					
Eigenvalue					
+	+	+	+	+	+
Eigenvector					
-	-	-	-	-	+
-	-	-	+	+	-
+	-	+	-	-	-
-	+	+	-	-	+
+	+	-	+	-	-
-	+	-	+	+	+

(b) Fault-1.10

Figure 5.9: Eigendecomposition-based fault signatures for Fault-1.5 and Fault-1.10

Further study is required into the significance of the magnitude of the changes, but for the purpose of fault isolation, the direction of the change is sufficient. The directional changes in the eigendecomposition are the same for the fault regardless of the fault magnitude. The changes in the eigendecomposition of Fault-1 and Fault-4 are shown in Figure 5.10.

Fault-1					
Eigenvalue					
+	+	+	+	+	+
Eigenvector					
-	-	-	-	-	+
-	-	-	+	+	-
+	-	+	-	-	-
-	+	+	-	-	+
+	+	-	+	-	-
-	+	-	+	+	+

(a) Fault-1

Fault-4					
Eigenvalue					
+	+	+	+	+	+
Eigenvector					
+	+	-	-	-	-
+	-	-	-	+	-
+	+	+	+	-	+
+	+	+	+	-	-
+	-	-	+	+	+
+	+	-	-	+	-

(b) Fault-4

Figure 5.10: Eigendecomposition-based fault signatures for Fault-1 and Fault-4

The same fault condition at different magnitudes, resulted in the same directional changes (Figure 5.9) in the eigendecomposition, while two different fault conditions, resulted in different directional changes (Figure 5.10) in the eigendecomposition of the relevant cost matrix.

5.4 Conclusion

In this chapter, a residual-based and an eigendecomposition-based method were presented to compare the graph matrices of a system under fault conditions, to that of a reference (normal) condition. Each method was used to create a signature for the fault conditions. With both methods, the signatures were shown to be unique for the specific fault condition, regardless of the fault magnitude. Due to the uniqueness of the signatures, the signatures can be used to detect faults in the cycle.

The eigendecomposition method is based solely on the directional changes in the eigendecomposition to create a signature. Further study is required regarding the significance of the magnitude of the changes in the eigendecomposition. Including the magnitude of the changes may improve this method, by quantifying the effect a specific fault has on the individual component's performance and the complete cycle.

In the following chapter, the two methods presented in this chapter will be implemented for the various fault conditions described in Chapter 4 to compile unique energy-based signatures for each fault condition. These signatures are then used to detect and isolate fault conditions.

CHAPTER 6

Fault detection and isolation

In this chapter, the reference signatures are presented for the various operating conditions including fault conditions. The fault conditions are simulated for a fault magnitude of 1% and signatures compiled of the cycle under current operating conditions. The signature of the cycle under current operating conditions are compared with the reference signatures to detect and isolate faults in the cycle. The methods and the error-based method proposed by du Rand [23] are evaluated against the required attributes of a sufficient FDI system. The exergy ratios as described in Chapter 4 are also calculated and presented to show the effect different faults have on the efficiency of the components in the cycle.

6.1 Energy-based reference fault signatures

The Brayton cycle PCU presented in Chapter 5 was simulated under fault conditions and with changes in the operating setpoint. The fault conditions are summarised in Table 6.1. The attributed graph matrices for the different operating conditions and fault conditions are presented in Appendix D. The methods as explained in Chapter 5, were implemented using the attributed graph matrices obtained from the simulation to compile energy-based reference fault signatures and operational signatures of the cycle. The reference signatures are compiled as the average between a 5% and 10% fault magnitude, as was done in Chapter 5 for Fault-1 and Fault-4.

Table 6.1: Description of the different fault conditions

Component	Fault ID	Effect of fault
Compressor	Fault-1	Increase in pressure ratio
	Fault-2	Decrease in pressure ratio
	Fault-3	Decrease in efficiency
PT	Fault-4	Increase in pressure ratio
	Fault-5	Decrease in pressure ratio
	Fault-6	Decrease in efficiency
Heat transfer elements	Fault-7	Heat loss in heat addition element
	Fault-8	Pressure drop in heat rejection element
Flow leakage	Fault-9	Change in mass flow
	Fault-10	Change in mass flow
Multiple	Fault-11	Fault-3 and Fault-5
	Fault-12	Fault-3 and Fault-5

6.1.1 Residual-based method

Single faults

The operating setpoint of the cycle was set and controlled to 100 kJ/s output from the power turbine and faults Fault-1 to Fault-10 simulated. The graphs in Figure 6.1 and Figure 6.2 shows the residual-based reference fault signatures for the different single faults conditions. The graphs are unique to the specific fault, regardless of the magnitude of the fault as previously explained in Chapter 5. Therefore the graphs represent a reference fault signature that is unique to the specific fault and can be used to detect and isolate faults during the operation of the cycle.

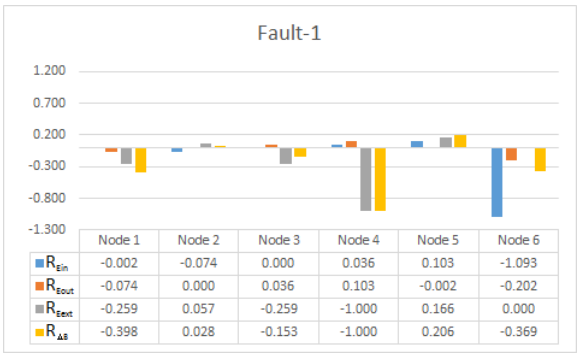

(a) Fault-1 signature

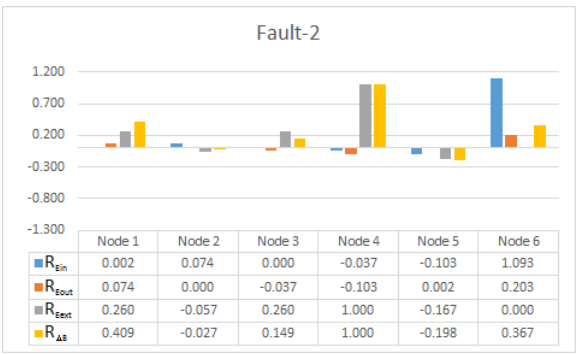

(b) Fault-2 signature

Figure 6.1: Residual-based signatures for Fault-1 and Fault-2

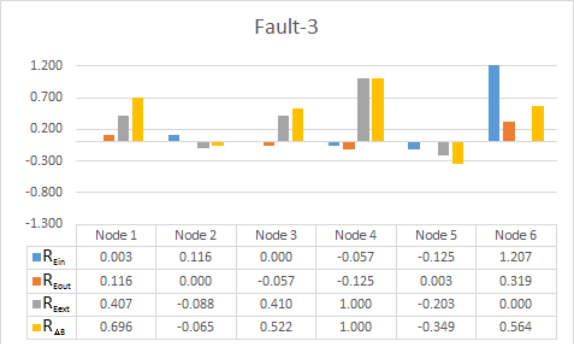

	Node 1	Node 2	Node 3	Node 4	Node 5	Node 6
R_{Ein}	0.003	0.116	0.000	-0.057	-0.125	1.207
R_{Eout}	0.116	0.000	-0.057	-0.125	0.003	0.319
R_{Eext}	0.407	-0.088	0.410	1.000	-0.203	0.000
$R_{\Delta B}$	0.696	-0.065	0.522	1.000	-0.349	0.564

(a) Fault-3 signature

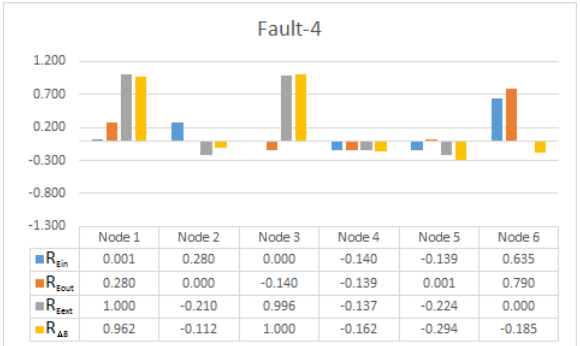

	Node 1	Node 2	Node 3	Node 4	Node 5	Node 6
R_{Ein}	0.001	0.280	0.000	-0.140	-0.139	0.635
R_{Eout}	0.280	0.000	-0.140	-0.139	0.001	0.790
R_{Eext}	1.000	-0.210	0.996	-0.137	-0.224	0.000
$R_{\Delta B}$	0.962	-0.112	1.000	-0.162	-0.294	-0.185

(b) Fault-4 signature

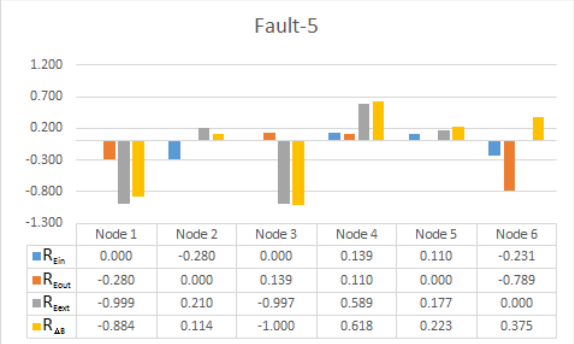

	Node 1	Node 2	Node 3	Node 4	Node 5	Node 6
R_{Ein}	0.000	-0.280	0.000	0.139	0.110	-0.231
R_{Eout}	-0.280	0.000	0.139	0.110	0.000	-0.789
R_{Eext}	-0.999	0.210	-0.997	0.589	0.177	0.000
$R_{\Delta B}$	-0.884	0.114	-1.000	0.618	0.223	0.375

(c) Fault-5 signature

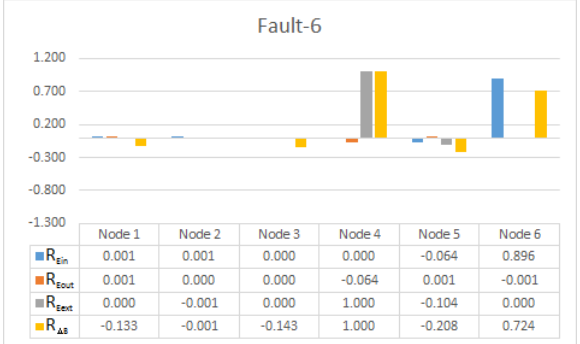

	Node 1	Node 2	Node 3	Node 4	Node 5	Node 6
R_{Ein}	0.001	0.001	0.000	0.000	-0.064	0.896
R_{Eout}	0.001	0.000	0.000	-0.064	0.001	-0.001
R_{Eext}	0.000	-0.001	0.000	1.000	-0.104	0.000
$R_{\Delta B}$	-0.133	-0.001	-0.143	1.000	-0.208	0.724

(d) Fault-6 signature

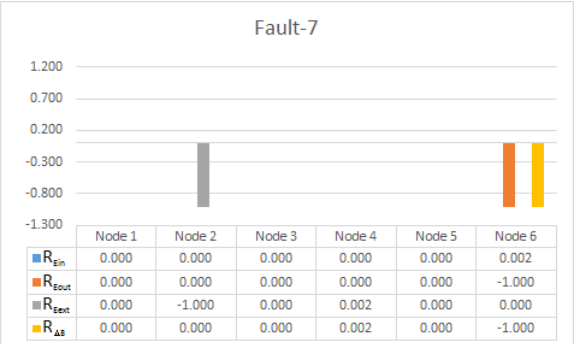

	Node 1	Node 2	Node 3	Node 4	Node 5	Node 6
R_{Ein}	0.000	0.000	0.000	0.000	0.000	0.002
R_{Eout}	0.000	0.000	0.000	0.000	0.000	-1.000
R_{Eext}	0.000	-1.000	0.000	0.002	0.000	0.000
$R_{\Delta B}$	0.000	0.000	0.000	0.002	0.000	-1.000

(e) Fault-7 signature

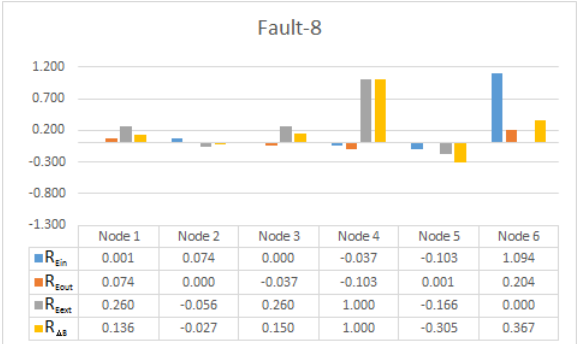

	Node 1	Node 2	Node 3	Node 4	Node 5	Node 6
R_{Ein}	0.001	0.074	0.000	-0.037	-0.103	1.094
R_{Eout}	0.074	0.000	-0.037	-0.103	0.001	0.204
R_{Eext}	0.260	-0.056	0.260	1.000	-0.166	0.000
$R_{\Delta B}$	0.136	-0.027	0.150	1.000	-0.305	0.367

(f) Fault-8 signature

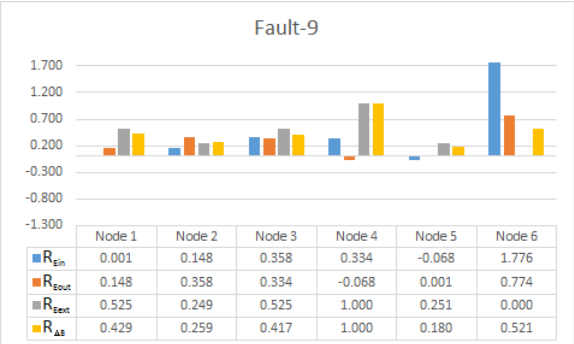

	Node 1	Node 2	Node 3	Node 4	Node 5	Node 6
R_{Ein}	0.001	0.148	0.358	0.334	-0.068	1.776
R_{Eout}	0.148	0.358	0.334	-0.068	0.001	0.774
R_{Eext}	0.525	0.249	0.525	1.000	0.251	0.000
$R_{\Delta B}$	0.429	0.259	0.417	1.000	0.180	0.521

(g) Fault-9 signature

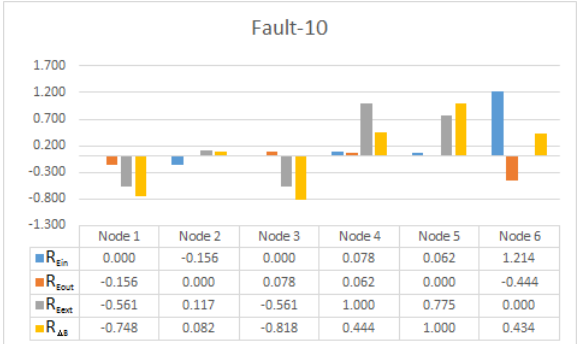

	Node 1	Node 2	Node 3	Node 4	Node 5	Node 6
R_{Ein}	0.000	-0.156	0.000	0.078	0.062	1.214
R_{Eout}	-0.156	0.000	0.078	0.062	0.000	-0.444
R_{Eext}	-0.561	0.117	-0.561	1.000	0.775	0.000
$R_{\Delta B}$	-0.748	0.082	-0.818	0.444	1.000	0.434

(h) Fault-10 signature

Figure 6.2: Residual-based signatures for Fault-3 to Fault-10

Multiple simultaneous faults

The residual fault signatures for multiple simultaneous faults are shown in Figure 6.3. In this case, Fault-3 and Fault-5 occurred simultaneously. In Figure 6.3(a), Fault-3 and Fault-5 had a fault magnitude of 10%. In Figure 6.3(b), Fault-3 had a fault magnitude of 10% and Fault-5 a fault magnitude of 5%. As evident from Figure 6.3, the magnitude of the faults influenced the signature. A unique signature that is only dependent on the fault combination is therefore not possible. Although this method can detect a multiple fault condition, it is not able to isolate the fault to the individual faults pertaining to the multiple fault.

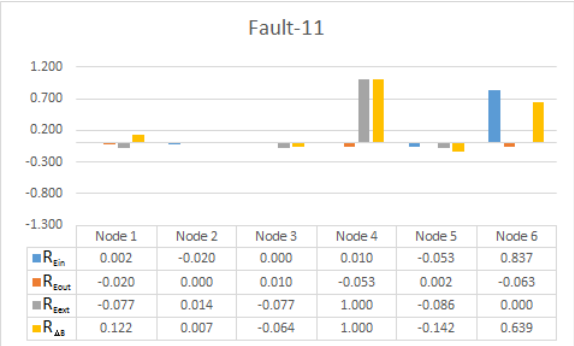

	Node 1	Node 2	Node 3	Node 4	Node 5	Node 6
R_{Ein}	0.002	-0.020	0.000	0.010	-0.053	0.837
R_{Eout}	-0.020	0.000	0.010	-0.053	0.002	-0.063
R_{Eext}	-0.077	0.014	-0.077	1.000	-0.086	0.000
$R_{\Delta E}$	0.122	0.007	-0.064	1.000	-0.142	0.639

(a) Fault-11 signature

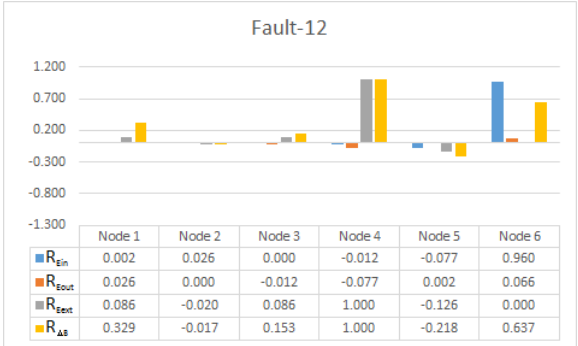

	Node 1	Node 2	Node 3	Node 4	Node 5	Node 6
R_{Ein}	0.002	0.026	0.000	-0.012	-0.077	0.960
R_{Eout}	0.026	0.000	-0.012	-0.077	0.002	0.066
R_{Eext}	0.086	-0.020	0.086	1.000	-0.126	0.000
$R_{\Delta E}$	0.329	-0.017	0.153	1.000	-0.218	0.637

(b) Fault-12 signature

Figure 6.3: Residual-based signatures for Fault-11 and Fault-12

Changes in the operating setpoint of the power turbine

The operating setpoint of the PT was changed and the residual-based signatures are shown in Figure 6.4, with no faults. The energy-based components of the signature are not unique to the specific setpoint. The signature is only dependent on the change (increased or decreased) in the setpoint and not the magnitude of the change. The energy-based components of the signature for an increase of 20 kJ/s (Figure 6.4(a)) and 50 kJ/s (Figure 6.4(b)) are identical, but differ from the energy-based components of the signature for a decrease of 10 kJ/s in the setpoint (Figure 6.4(c)). The exergy-based component of the signature, however, depends on the magnitude and whether the setpoint was increased or decreased. The exergy-based component of the signature for 120 kJ/s is different from the exergy-based component of the signature for 150 kJ/s. This is to be expected since exergy is not a conserved property and the change in exergy through a component depends on the operational conditions of the component. This enables the detection of a change in the operating setpoint using the energy-based components of the signature while the exergy-based component will indicate the value of the new operating setpoint, by matching the signature to known reference signatures.

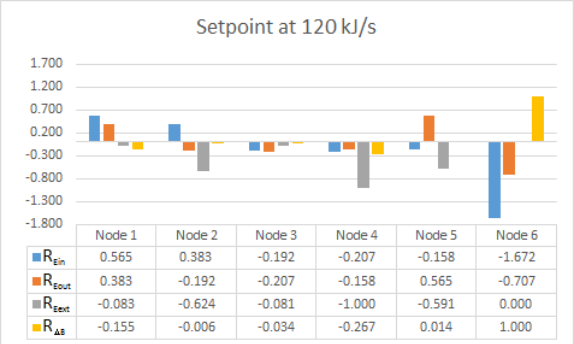

	Node 1	Node 2	Node 3	Node 4	Node 5	Node 6
R_{Ein}	0.565	0.383	-0.192	-0.207	-0.158	-1.672
R_{Eout}	0.383	-0.192	-0.207	-0.158	0.565	-0.707
R_{Eext}	-0.083	-0.624	-0.081	-1.000	-0.591	0.000
$R_{\Delta B}$	-0.155	-0.006	-0.034	-0.267	0.014	1.000

(a) Residual-based signature for an increase in operating setpoint from 100 kJ/s to 120 kJ/s

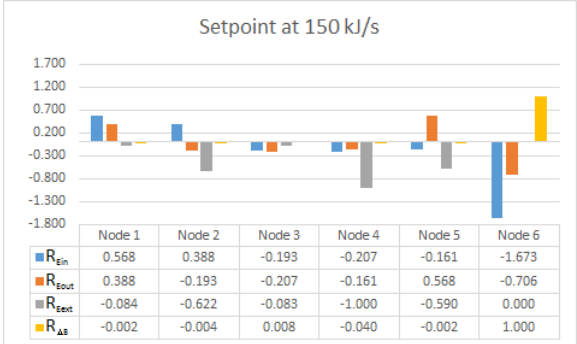

	Node 1	Node 2	Node 3	Node 4	Node 5	Node 6
R_{Ein}	0.568	0.388	-0.193	-0.207	-0.161	-1.673
R_{Eout}	0.388	-0.193	-0.207	-0.161	0.568	-0.706
R_{Eext}	-0.084	-0.622	-0.083	-1.000	-0.590	0.000
$R_{\Delta B}$	-0.002	-0.004	0.008	-0.040	-0.002	1.000

(b) Residual-based signature for an increase in operating setpoint from 100 kJ/s to 150 kJ/s

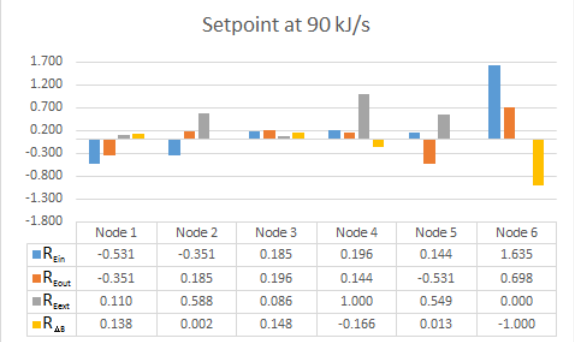

	Node 1	Node 2	Node 3	Node 4	Node 5	Node 6
R_{Ein}	-0.531	-0.351	0.185	0.196	0.144	1.635
R_{Eout}	-0.351	0.185	0.196	0.144	-0.531	0.698
R_{Eext}	0.110	0.588	0.086	1.000	0.549	0.000
$R_{\Delta B}$	0.138	0.002	0.148	-0.166	0.013	-1.000

(c) Residual-based signature for a decrease in operating setpoint from 100 kJ/s to 90 kJ/s

Figure 6.4: Residual-based signatures for changes in operating setpoints

Changes in the operating setpoint of the power turbine with a fault

In the case of Figure 6.5, the reference attributed graph matrix used in (5.2) to calculate the residual graph matrix, was changed to reflect an operating setpoint of 120 kJ/s for the PT output and Fault-1 was introduced.

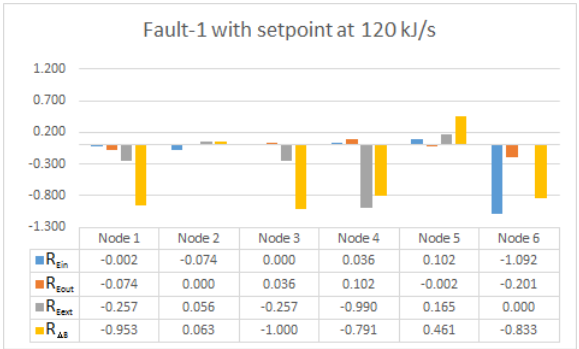

	Node 1	Node 2	Node 3	Node 4	Node 5	Node 6
R_{Ein}	-0.002	-0.074	0.000	0.036	0.102	-1.092
R_{Eout}	-0.074	0.000	0.036	0.102	-0.002	-0.201
R_{Eext}	-0.257	0.056	-0.257	-0.990	0.165	0.000
$R_{\Delta B}$	-0.953	0.063	-1.000	-0.791	0.461	-0.833

Figure 6.5: Residual-based signature for Fault-1 at an operating setpoint of 120 kJ/s

The energy-based components of the signature are the same (within the specified threshold value) as that of Fault-1 with a PT setpoint of 100 kJ/s (Figure 6.1(a)) and is unique to the fault condition. The exergy-based component of the signature is however different reflecting the change in the operating setpoint. The exergy-based component of the signature is thus dependent on the fault condition and the operating setpoint.

Summary

Using the residual method, unique signatures were determined for each fault, regardless of the fault magnitude. The signatures for changes in the operating setpoint of the PT were also unique depending on the direction (increase or decrease) as well as the magnitude of the change. This method can distinguish between a fault and a change in the operating setpoint of the PT. In the case of a fault condition at a different operating setpoint , the energy-based component of the signature remained the same regardless of the setpoint. The exergy-based component of the signature was however different depending on the operating setpoint. A unique residual-based signature could not be compiled for multiple simultaneous faults. Multiple faults can be detected but not isolated.

6.1.2 Eigendecomposition-based method

Single faults

The operating setpoint of the PT was set and controlled to 100 kJ/s and faults Fault-1 to Fault-10 simulated. The directional changes in the eigendecomposition of the cost matrices are shown in Figure 6.6 and Figure 6.7 for the different single fault conditions. The directional changes are shown to be unique for each fault type, regardless of the fault magnitude and can be regarded as the eigendecomposition-based reference fault signatures, representing the different single fault conditions. These reference fault signatures can be used to detect and isolate faults in the cycle.

Fault-1					
Eigenvalue					
+	+	+	+	+	+
Eigenvector					
-	-	-	-	-	+
-	-	-	+	+	-
+	-	+	-	-	-
-	+	+	-	-	+
+	+	-	+	-	-
-	+	-	+	+	+

(a) Fault-1 signature

Fault-2					
Eigenvalue					
+	+	+	+	+	+
Eigenvector					
+	-	-	+	+	+
+	+	-	-	-	-
+	-	+	-	+	+
+	-	+	-	-	-
+	-	-	+	+	+
+	+	-	-	-	+

(b) Fault-2 signature

Fault-3					
Eigenvalue					
+	+	+	+	+	+
Eigenvector					
+	-	-	+	+	+
+	+	-	-	-	-
+	-	+	+	+	+
+	-	+	+	-	-
+	-	-	+	+	+
+	+	-	-	-	+

(c) Fault-3 signature

from

Fault-4					
Eigenvalue					
+	+	+	+	+	+
Eigenvector					
+	+	-	-	-	-
+	-	-	-	+	-
+	+	+	+	-	+
+	+	+	+	-	-
+	-	-	+	+	+
+	+	-	-	+	-

(d) Fault-4 signature

Fault-5					
Eigenvalue					
+	+	+	+	+	+
Eigenvector					
+	-	-	-	+	+
-	-	-	+	-	+
-	-	+	-	+	-
+	+	+	-	-	-
+	+	-	+	+	-
-	+	-	-	-	+

(e) Fault-5 signature

Fault-6					
Eigenvalue					
+	+	+	+	+	+
Eigenvector					
+	-	-	+	+	+
+	+	-	-	-	-
+	-	+	-	+	+
+	-	+	-	-	-
+	-	-	+	+	-
+	+	-	-	-	+

(f) Fault-6 signature

Fault-7					
Eigenvalue					
+	+	+	+	+	-
Eigenvector					
-	-	-	-	-	+
-	-	-	+	-	-
+	-	+	-	+	-
+	+	+	-	-	-
+	+	-	+	-	-
-	+	-	-	+	+

(g) Fault-7 signature

Fault-8					
Eigenvalue					
+	+	+	+	+	+
Eigenvector					
+	-	-	+	+	+
+	+	-	-	-	-
+	-	+	-	+	+
+	-	+	-	-	-
+	-	-	+	-	+
+	+	-	-	-	+

(h) Fault-8 signature

Figure 6.6: Eigendecomposition-based signatures for Fault-1 to Fault-8

Fault-9					
Eigenvalue					
-	+	+	+	+	+
Eigenvector					
+	-	-	+	+	+
+	-	-	-	-	-
+	+	+	+	+	+
+	-	+	-	-	-
+	-	-	+	+	+
+	+	-	-	-	+

(a) Fault-9 signature

Fault-10					
Eigenvalue					
+	+	+	+	+	+
Eigenvector					
+	-	-	-	+	+
+	-	-	+	+	+
+	-	+	-	+	+
+	+	+	-	-	-
-	+	-	+	-	-
-	+	-	-	-	+

(b) Fault-10 signature

Figure 6.7: Eigendecomposition-based signatures for Fault-9 and Fault-10

Multiple simultaneous faults

The fault signatures for multiple simultaneous faults are shown in Figure 6.8. In this case, Fault-3 and Fault-5 occurred simultaneously. In the case of Fault-11, Fault-3 and Fault-5 had a magnitude of 10%. The directional changes in the eigendecomposition for Fault-11 are shown in Figure 6.8(a). The directional changes in the eigendecomposition of Fault-12 are shown in Figure 6.8(b), in this case, Fault-3 had a fault magnitude of 10% and Fault-5 a fault magnitude of 5%. As evident from Figure 6.8, the magnitude of the faults influenced the signature. A unique signature that is only dependent on the fault combination is therefore not possible. Although this method can detect a multiple fault condition, it cannot isolate the fault to the individual faults pertaining to the multiple fault.

Fault-11					
Eigenvalue					
+	+	+	+	+	+
Eigenvector					
-	-	-	+	+	+
-	-	+	+	-	-
-	-	+	-	+	+
-	+	-	-	-	-
-	+	-	+	+	-
-	+	+	-	-	+

(a) Fault-11 signature

Fault-12					
Eigenvalue					
+	+	+	+	+	+
Eigenvector					
-	-	-	+	+	+
-	+	+	-	-	-
-	-	+	-	+	+
+	-	-	-	-	-
+	-	-	+	+	-
+	+	+	-	-	+

(b) Fault-12 signature

Figure 6.8: Eigendecomposition-based signature for Fault-11 and Fault-12

Changes in the operating setpoint of the power turbine

The directional changes of the eigendecomposition of the cost matrices for a change in the operating setpoint of the PT are shown in Figure 6.9. The signatures differ depending on whether the setpoint was increased (Figure 6.4(a&b)) or decreased (Figure 6.4(c)). The signature is,

however, the same regardless of the magnitude of the change, as evident from Figure 6.9(a) and Figure 6.9(b). Based on these signatures a distinction cannot be made between different setpoint values. This is in contrast with the residual-based method, where the energy-based components of the signatures indicated a change in the operating setpoint and the exergy-based component of the signature was used to identify the new setpoint.

Setpoint of 120 kJ/s					
Eigenvalue					
-	+	+	+	+	+
Eigenvector					
+	-	-	+	+	+
+	+	-	-	-	-
+	-	+	-	+	+
+	-	+	-	-	-
+	-	-	+	+	-
+	+	-	-	-	+

(a) Eigendecomposition-based signature for an increase in operating setpoint from 100 kJ/s to 120 kJ/s

Setpoint of 150 kJ/s					
Eigenvalue					
-	+	+	+	+	+
Eigenvector					
+	-	-	+	+	+
+	+	-	-	-	-
+	-	+	-	+	+
+	-	+	-	-	-
+	-	-	+	+	-
+	+	-	-	-	+

(b) Eigendecomposition-based signature for an increase in operating setpoint from 100 kJ/s to 150 kJ/s

Setpoint of 90 kJ/s					
Eigenvalue					
+	+	+	+	+	-
Eigenvector					
-	-	-	-	-	+
+	-	-	+	+	-
+	-	+	-	-	-
+	+	+	-	-	+
+	+	-	+	-	-
-	+	-	-	+	+

(c) Eigendecomposition-based signature for a decrease in operating setpoint from 100 kJ/s to 90 kJ/s

Figure 6.9: Eigendecomposition-based signatures for changes in operating setpoints

Changes in the operating setpoint of the power turbine with a fault

The signature for fault Fault-1 at a PT setpoint of 120 kJ/s is shown in Figure 6.10. Using only the directional changes of the eigendecomposition is not sufficient for detecting and isolating faults at different operating setpoints. The signature is unique to the fault type and PT setpoint and will differ for the different faults at different operating setpoints, as evident from comparing Fault-1 at 100 kJ/s (Figure 6.6(a)) and Fault-1 at 120 kJ/s (Figure 6.10). This is in contrast with the residual-based method, where the energy-based components of the signature of the fault remained the same regardless of the operating setpoint. Only the exergy-based component of the signature changed, indicating a change in the operating setpoint.

Fault-1 at 120 kJ/s					
Eigenvalue					
-	+	-	+	-	+
Eigenvector					
-	-	+	-	+	+
-	-	-	+	+	-
-	-	+	+	-	+
-	+	+	+	+	-
-	+	-	-	-	+
-	+	-	+	+	-

Figure 6.10: Eigendecomposition-based signature for Fault-1 at an operating setpoint of 120 kJ/s

Summary

Using the eigendecomposition method, unique signatures were calculated for each single fault, regardless of the fault magnitude. The signature for a change in the operating setpoint of the PT was, however, not unique. The signature could only detect a change in the operating setpoints and distinguish between an increase and decrease in the setpoint (Figure 6.9). The magnitude of the change could not be determined, as the signatures were the same regardless of the magnitude of the change (Figure 6.9(a) and Figure 6.9(b)). In the case of a fault condition at a different PT setpoint, the signature is unique to the fault and the operating setpoint. This method could not detect the same fault at different operating setpoints. Multiple faults could also not be isolated and only detected.

6.2 Enthalpy and Entropy-based reference signatures

The error-based method proposed by du Rand [23] was implemented on the Brayton cycle PCU under normal operating conditions and with fault conditions. The specific enthalpy and entropy values were obtained at Nodes 1 through 5 (see Figure 4.3) and plotted on an h-s diagram. In his study, du Rand concluded that the shape of the h-s diagram will change under fault conditions and that the change is unique to each fault. For a change in the operating setpoint, the shape of the h-s diagram remained constant and only shifted on the horizontal axis.

Single faults

The h-s diagrams and error signatures are illustrated in Figure 6.11 for faults Fault-1 and -3, Figure 6.12 illustrates the results for faults Fault-5, -7, and -8. In the results, Fx.10 represents Fault-x with a 10% fault magnitude and Fx.5 representing Fault-x with a 5% fault magnitude. Figure 6.13 illustrates the results for Fault-9 with a leak of 0.068 kg/s. The method proposed

by Du Rand was able to uniquely detect and isolate the faults and changes in operating set-points. The h-s diagrams show the different fault conditions at different fault magnitudes compared to the normal operating conditions. The h-s diagrams and the error signatures (showing the normalised error for each fault with respect to the normal operating conditions) show that the magnitude of the fault had little influence on the error values and the error values are mainly influenced by the fault type. The reference error signature of a fault will be taken as the average between a fault magnitude of 5% and 10%. A threshold value is implemented to compensate for the small variations for the same fault type at different fault magnitudes. In applying this method to the Brayton cycle PCU used in this study, unique signatures were compiled for the different fault conditions. This method was however not used by Du Rand as a performance measurement to indicate the effect a fault has on the components. Although specific entropy and specific enthalpy were used to detect and isolate faults, the interpretation of entropy [144] is more difficult compared to the use of energy and exergy. By using energy and exergy it is possible to calculate an exergy ratio as a performance indicator as explained in Chapter 4.

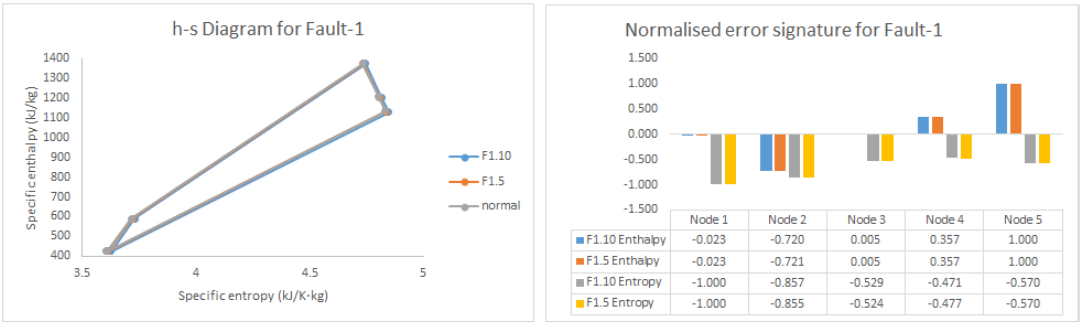

	Node 1	Node 2	Node 3	Node 4	Node 5
F1.10 Enthalpy	-0.023	-0.720	0.005	0.357	1.000
F1.5 Enthalpy	-0.023	-0.721	0.005	0.357	1.000
F1.10 Entropy	-1.000	-0.857	-0.529	-0.471	-0.570
F1.5 Entropy	-1.000	-0.855	-0.524	-0.477	-0.570

(a) Fault-1 signature

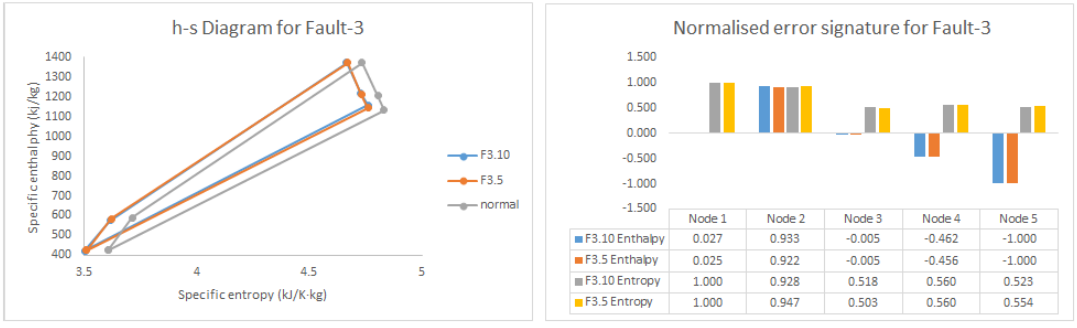

	Node 1	Node 2	Node 3	Node 4	Node 5
F3.10 Enthalpy	0.027	0.933	-0.005	-0.462	-1.000
F3.5 Enthalpy	0.025	0.922	-0.005	-0.456	-1.000
F3.10 Entropy	1.000	0.928	0.518	0.560	0.523
F3.5 Entropy	1.000	0.947	0.503	0.560	0.554

(b) Fault-3 signature

Figure 6.11: Enthalpy and entropy-based fault signatures for Fault-1 and Fault-3

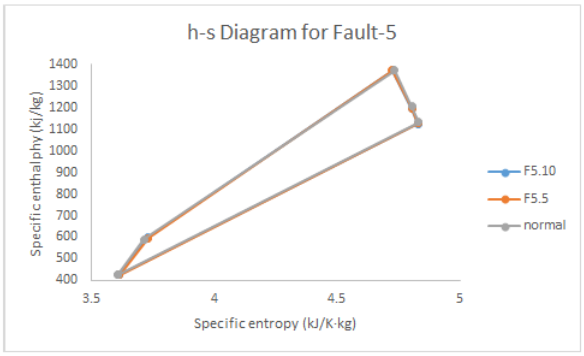

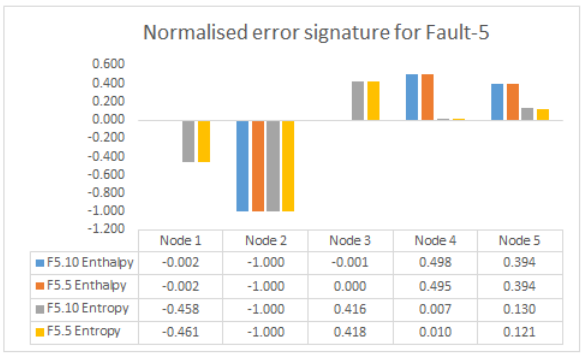

	Node 1	Node 2	Node 3	Node 4	Node 5
F5.10 Enthalpy	-0.002	-1.000	-0.001	0.498	0.394
F5.5 Enthalpy	-0.002	-1.000	0.000	0.495	0.394
F5.10 Entropy	-0.458	-1.000	0.416	0.007	0.130
F5.5 Entropy	-0.461	-1.000	0.418	0.010	0.121

(a) Fault-5 signature

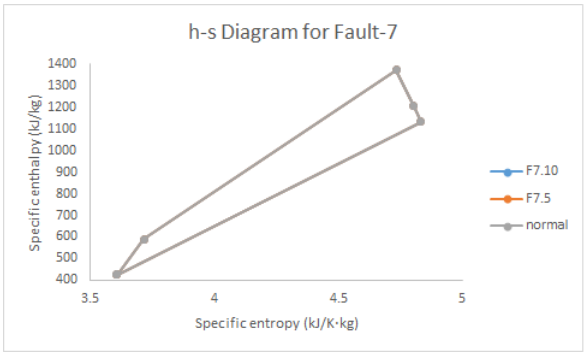

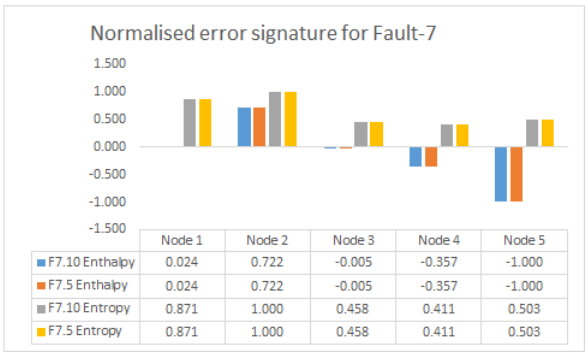

	Node 1	Node 2	Node 3	Node 4	Node 5
F7.10 Enthalpy	0.024	0.722	-0.005	-0.357	-1.000
F7.5 Enthalpy	0.024	0.722	-0.005	-0.357	-1.000
F7.10 Entropy	0.871	1.000	0.458	0.411	0.503
F7.5 Entropy	0.871	1.000	0.458	0.411	0.503

(b) Fault-7 signature

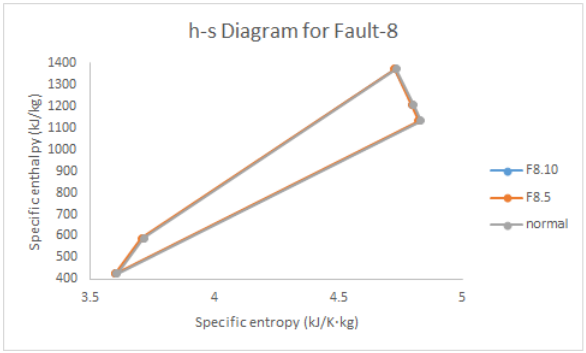

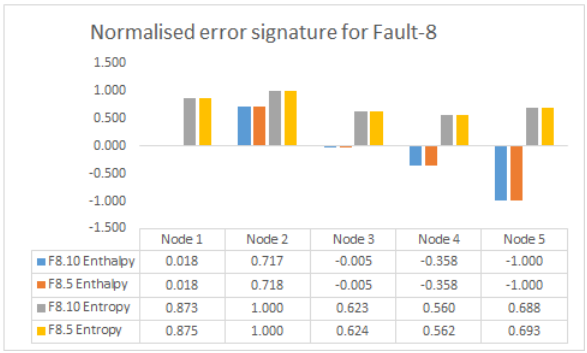

	Node 1	Node 2	Node 3	Node 4	Node 5
F8.10 Enthalpy	0.018	0.717	-0.005	-0.358	-1.000
F8.5 Enthalpy	0.018	0.718	-0.005	-0.358	-1.000
F8.10 Entropy	0.873	1.000	0.623	0.560	0.688
F8.5 Entropy	0.875	1.000	0.624	0.562	0.693

(c) Fault-8 signature

Figure 6.12: Enthalpy and entropy-based fault signature for Fault-5, Fault-7 and Fault-8

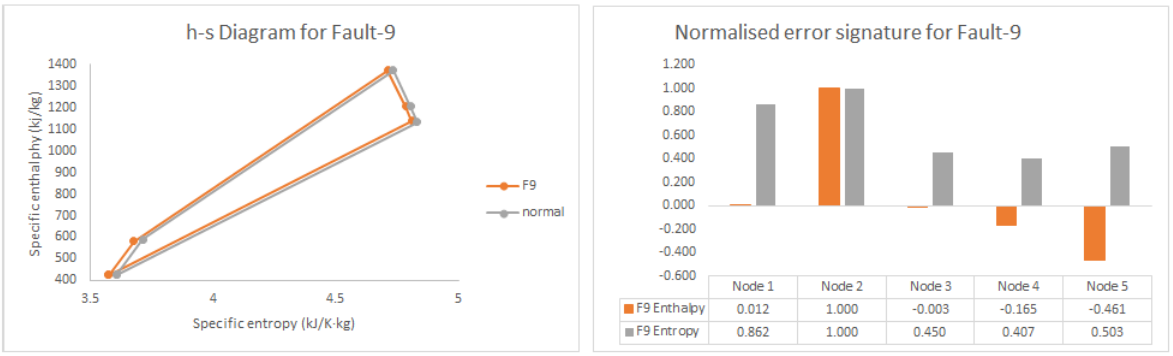

Figure 6.13: Enthalpy and entropy-based fault signature for Fault-9

Multiple simultaneous faults

Figure 6.14 shows the h-s diagram and error signature for multiple simultaneous faults. As evident from the error signature the same fault combination with different fault magnitudes, resulted in different error signatures. Multiple simultaneous faults can be detected but not isolated. In his work, du Rand proposed a method called the fault isolation index (FII) that indicated the possibility of a single fault being present in the multiple simultaneous fault. This is only an indication and not an exact isolation of the single faults pertaining to the multiple simultaneous faults.

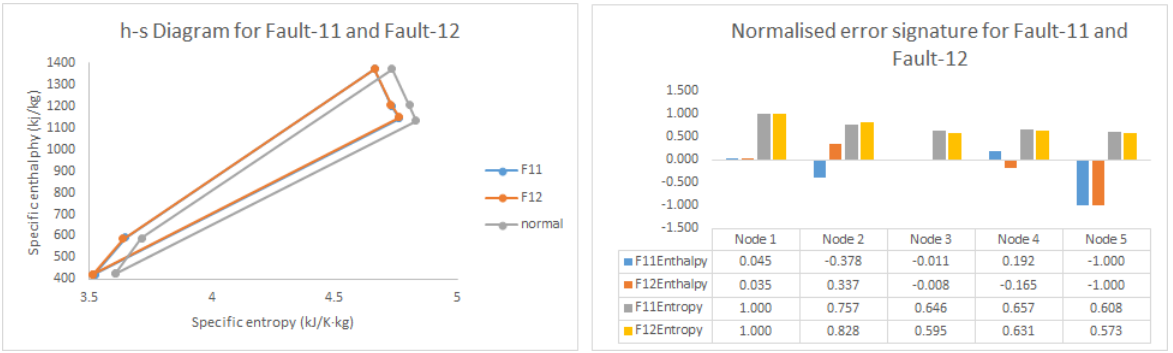

Figure 6.14: Enthalpy and entropy-based fault signature for Fault-11 and Fault-12

Changes in the operating setpoint of the power turbine

In Figure 6.15, the h-s diagram and error signature for a change in the PT operating setpoint is illustrated. A change in the setpoint only influenced the specific entropy resulting in the h-s diagram shifting on the x-axis but retaining its shape. An increase in the setpoint resulted in a shift to the left, while a decrease resulted in a shift to the right. The magnitude of the change determines how much the diagram will shift. The accompanying chart indicates that

the specific enthalpy values remained constant (within a specified threshold) while the specific entropy values varied. Based on this, a distinction can be made between a fault condition and a change in operating setpoint. The specific setpoint can also be identified since the signature is unique depending on the magnitude of the change in the operating setpoint.

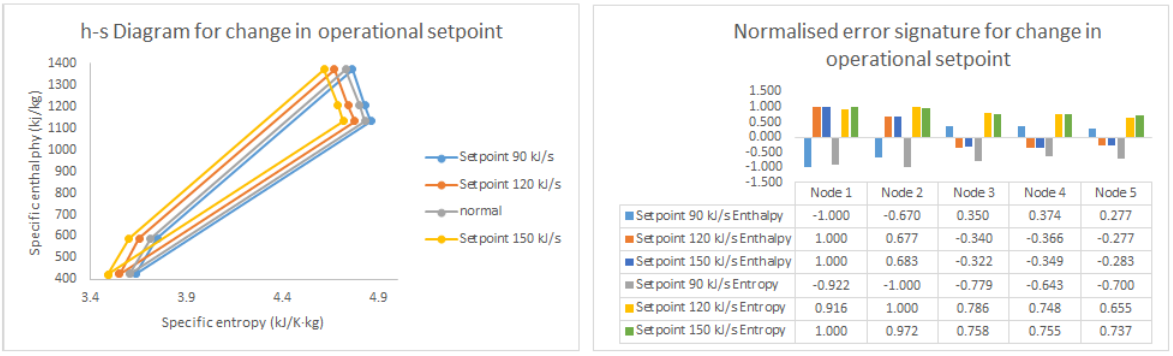

Figure 6.15: Enthalpy and entropy-based signatures for changes in operating setpoints

Changes in the operating setpoint of the power turbine with a fault

The h-s diagram for Fault-1, at an operating setpoint of 120 kJ/s, is shown in Figure 6.16. By comparing Figure 6.16 with Figure 6.11(a) it is evident that the enthalpy values are similar but the entropy values differ. From this, the same fault, at different operating setpoints, can be detected using enthalpy. The entropy values of the signatures being different, indicates a change in the PT setpoint.

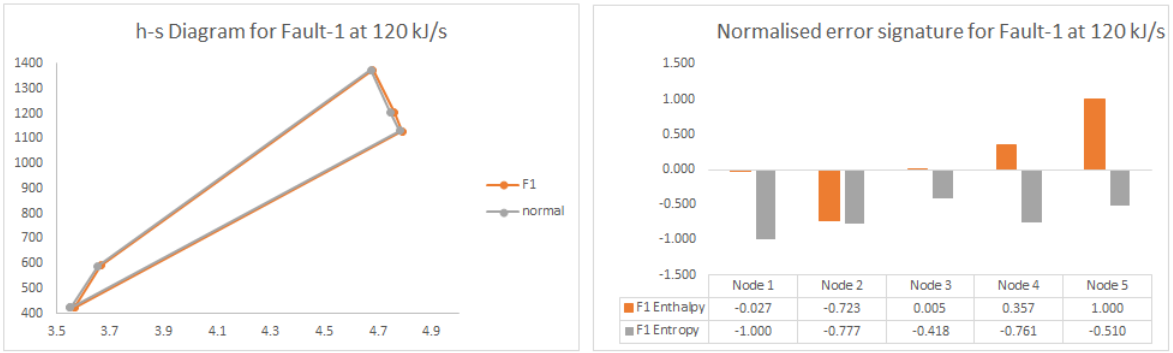

Figure 6.16: Enthalpy and entropy-based signature for Fault-1 at an operating setpoint of 120 kJ/s

Summary

Using the error-based method, unique signatures were compiled for each fault, regardless of the fault magnitude. The signatures for changes in the operating setpoint of the PT were also unique depending on the direction (increase or decrease) as well as the magnitude of the change. This method can distinguish between a fault and a change in the operating setpoint of the PT. In the case of a fault, at a different operating setpoint, the shape of the graph remained the same for the specific fault condition but shifted on the x-axis due to the change in the operating setpoint. From comparing Figure 6.11(a) with Figure 6.16 it is evident that the enthalpy values are the same regardless of the change in the operating setpoint. The entropy value did, however, change, causing the shift of the graph on the x-axis. A unique error-based signature could not be compiled for multiple simultaneous faults. Multiple faults can be detected but not isolated.

6.3 Fault detection and isolation

The minimum fault magnitude is determined by the accuracy (resolution) of the data used, as explained in Chapter 5. For this study, the minimum fault magnitude will be set at 1%. The fault conditions were simulated with a fault magnitude of 1% and the operational signatures compiled. The operational signatures and the reference fault signatures are shown in the following sections for the different methods used. For the purpose of illustrating the fault detection and isolation capabilities of the methods, Faults-1, -3, -5, -7, -8, -9 will be simulated.

6.3.1 Energy-based method

6.3.1.1 Residual-based

In Figure 6.17 and Figure 6.18, the reference fault signature and the actual signature obtained with a fault magnitude of 1% is shown, using the residual-based FDI method. This method was able to detect and isolate all the fault conditions simulated with a fault magnitude of 1%. The small differences between the reference and actual signatures are compensated for by implementing a threshold value.

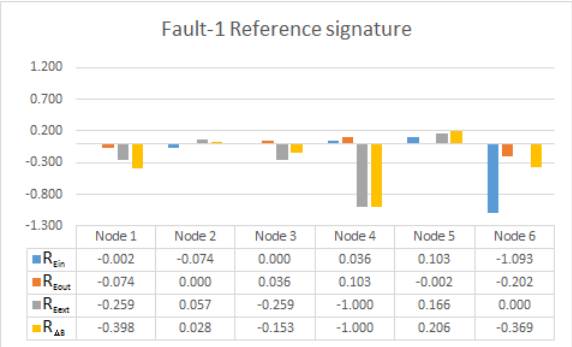

	Node 1	Node 2	Node 3	Node 4	Node 5	Node 6
R_{Ein}	-0.002	-0.074	0.000	0.036	0.103	-1.093
R_{Eout}	-0.074	0.000	0.036	0.103	-0.002	-0.202
R_{Eext}	-0.259	0.057	-0.259	-1.000	0.166	0.000
R_{AB}	-0.398	0.028	-0.153	-1.000	0.206	-0.369

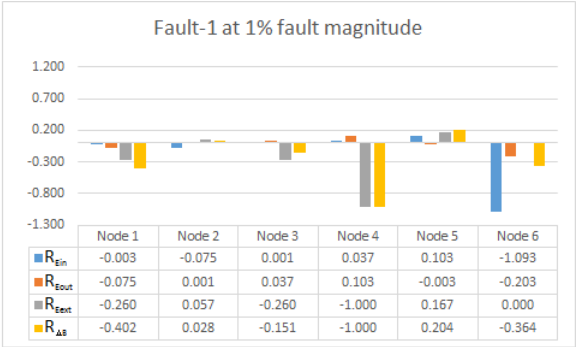

	Node 1	Node 2	Node 3	Node 4	Node 5	Node 6
R_{Ein}	-0.003	-0.075	0.001	0.037	0.103	-1.093
R_{Eout}	-0.075	0.001	0.037	0.103	-0.003	-0.203
R_{Eext}	-0.260	0.057	-0.260	-1.000	0.167	0.000
R_{AB}	-0.402	0.028	-0.151	-1.000	0.204	-0.364

(a) Fault-1

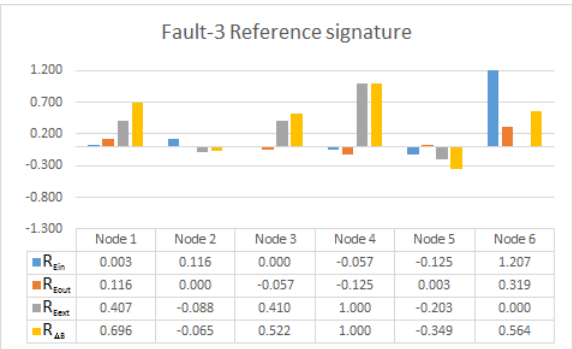

	Node 1	Node 2	Node 3	Node 4	Node 5	Node 6
R_{Ein}	0.003	0.116	0.000	-0.057	-0.125	1.207
R_{Eout}	0.116	0.000	-0.057	-0.125	0.003	0.319
R_{Eext}	0.407	-0.088	0.410	1.000	-0.203	0.000
R_{AB}	0.696	-0.065	0.522	1.000	-0.349	0.564

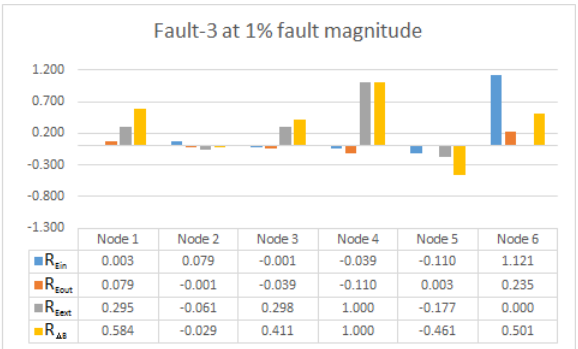

	Node 1	Node 2	Node 3	Node 4	Node 5	Node 6
R_{Ein}	0.003	0.079	-0.001	-0.039	-0.110	1.121
R_{Eout}	0.079	-0.001	-0.039	-0.110	0.003	0.235
R_{Eext}	0.295	-0.061	0.298	1.000	-0.177	0.000
R_{AB}	0.584	-0.029	0.411	1.000	-0.461	0.501

(b) Fault-3

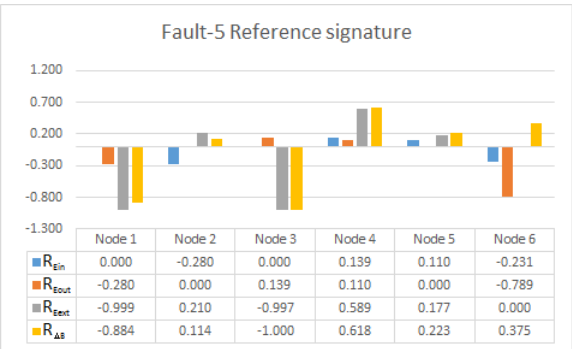

	Node 1	Node 2	Node 3	Node 4	Node 5	Node 6
R_{Ein}	0.000	-0.280	0.000	0.139	0.110	-0.231
R_{Eout}	-0.280	0.000	0.139	0.110	0.000	-0.789
R_{Eext}	-0.999	0.210	-0.997	0.589	0.177	0.000
R_{AB}	-0.884	0.114	-1.000	0.618	0.223	0.375

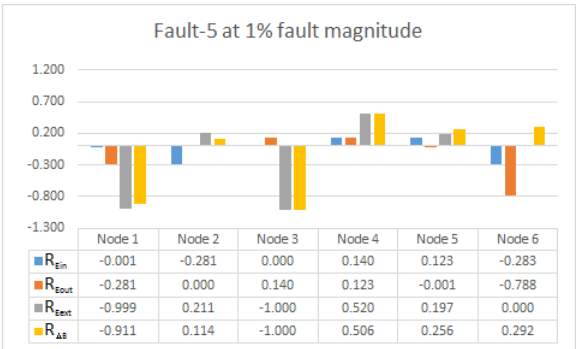

	Node 1	Node 2	Node 3	Node 4	Node 5	Node 6
R_{Ein}	-0.001	-0.281	0.000	0.140	0.123	-0.283
R_{Eout}	-0.281	0.000	0.140	0.123	-0.001	-0.788
R_{Eext}	-0.999	0.211	-1.000	0.520	0.197	0.000
R_{AB}	-0.911	0.114	-1.000	0.506	0.256	0.292

(c) Fault-5

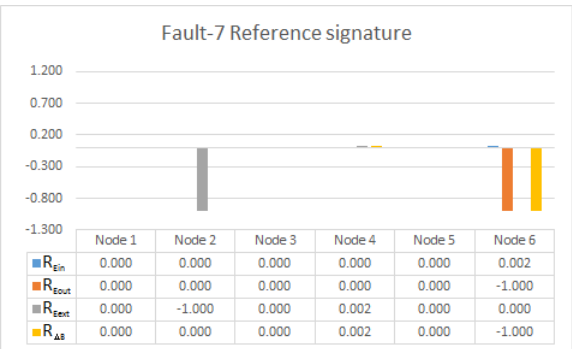

	Node 1	Node 2	Node 3	Node 4	Node 5	Node 6
R_{Ein}	0.000	0.000	0.000	0.000	0.000	0.002
R_{Eout}	0.000	0.000	0.000	0.000	0.000	-1.000
R_{Eext}	0.000	-1.000	0.000	0.002	0.000	0.000
R_{AB}	0.000	0.000	0.000	0.002	0.000	-1.000

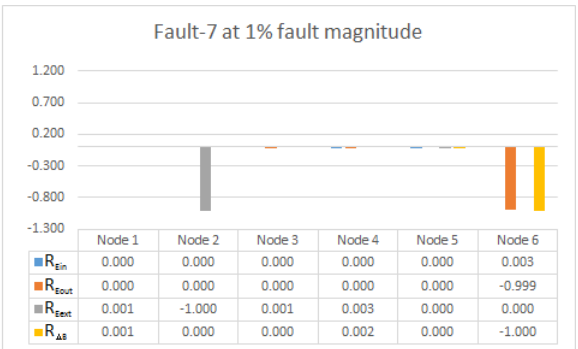

	Node 1	Node 2	Node 3	Node 4	Node 5	Node 6
R_{Ein}	0.000	0.000	0.000	0.000	0.000	0.003
R_{Eout}	0.000	0.000	0.000	0.000	0.000	-0.999
R_{Eext}	0.001	-1.000	0.001	0.003	0.000	0.000
R_{AB}	0.001	0.000	0.000	0.002	0.000	-1.000

(d) Fault-7

Figure 6.17: Reference vs Actual residual-based fault signatures for Fault-1,-3, -5 and -7

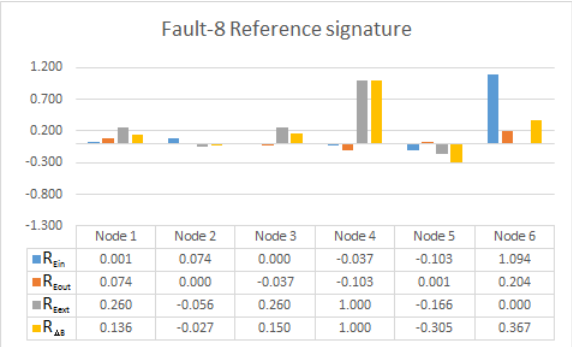

	Node 1	Node 2	Node 3	Node 4	Node 5	Node 6
R_{Ein}	0.001	0.074	0.000	-0.037	-0.103	1.094
R_{Eout}	0.074	0.000	-0.037	-0.103	0.001	0.204
R_{Eext}	0.260	-0.056	0.260	1.000	-0.166	0.000
R_{AB}	0.136	-0.027	0.150	1.000	-0.305	0.367

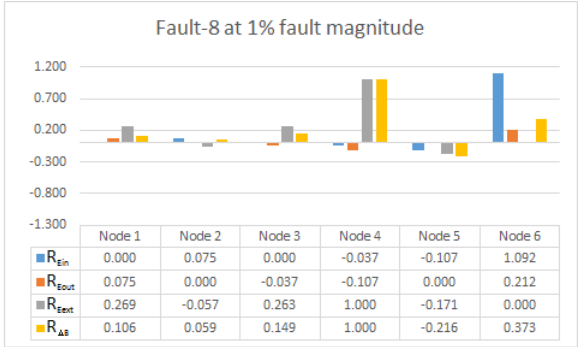

	Node 1	Node 2	Node 3	Node 4	Node 5	Node 6
R_{Ein}	0.000	0.075	0.000	-0.037	-0.107	1.092
R_{Eout}	0.075	0.000	-0.037	-0.107	0.000	0.212
R_{Eext}	0.269	-0.057	0.263	1.000	-0.171	0.000
R_{AB}	0.106	0.059	0.149	1.000	-0.216	0.373

(a) Fault-8

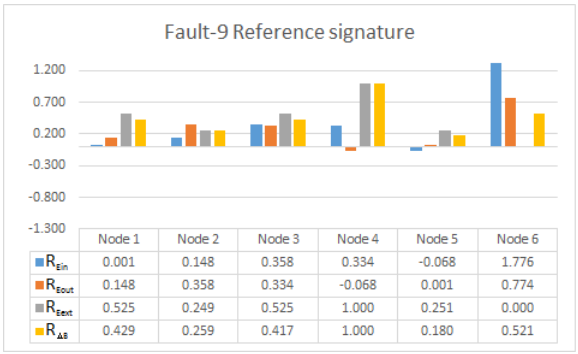

	Node 1	Node 2	Node 3	Node 4	Node 5	Node 6
R_{Ein}	0.001	0.148	0.358	0.334	-0.068	1.776
R_{Eout}	0.148	0.358	0.334	-0.068	0.001	0.774
R_{Eext}	0.525	0.249	0.525	1.000	0.251	0.000
R_{AB}	0.429	0.259	0.417	1.000	0.180	0.521

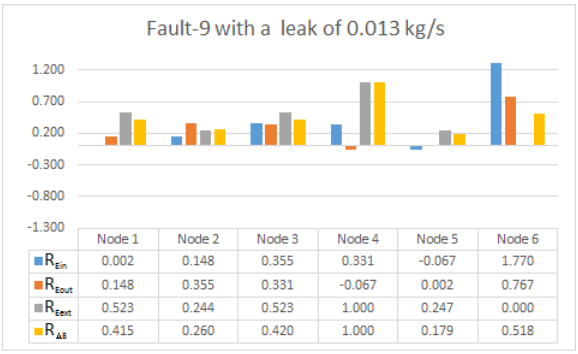

	Node 1	Node 2	Node 3	Node 4	Node 5	Node 6
R_{Ein}	0.002	0.148	0.355	0.331	-0.067	1.770
R_{Eout}	0.148	0.355	0.331	-0.067	0.002	0.767
R_{Eext}	0.523	0.244	0.523	1.000	0.247	0.000
R_{AB}	0.415	0.260	0.420	1.000	0.179	0.518

(b) Fault-9

Figure 6.18: Reference vs Actual residual-based fault signatures for Fault-8 and Fault-9

6.3.1.2 Eigendecomposition-based

In Figure 6.19 and Figure 6.20, the reference fault signature and the actual signature obtained with a fault magnitude of 1% is shown, using the eigendecomposition-based FDI method. This method was not able to detect and isolate all the fault conditions simulated with a fault magnitude of 1%. In some instance the effect a fault, with a magnitude of 1%, had on the cost matrix was minimal, which led to different eigenvalues and eigenvectors. This method was only able to detect and isolate Fault-5 and Fault-8 at a fault magnitude of 1%.

Fault-1 at 1% fault magnitude					
Eigenvalue					
+	+	+	+	+	+
Eigenvector					
+	+	-	-	-	+
+	+	-	+	+	-
+	-	+	-	-	-
+	-	+	-	-	+
+	+	-	+	-	-
+	+	-	+	+	+

Fault-1 Reference signature					
Eigenvalue					
+	+	+	+	+	+
Eigenvector					
-	-	-	-	-	+
-	-	-	+	+	-
+	-	+	-	-	-
-	+	+	-	-	+
+	+	-	+	-	-
-	+	-	+	+	+

(a) Fault-1

Fault-3 at 1% fault magnitude					
Eigenvalue					
+	+	+	+	+	+
Eigenvector					
+	-	-	+	+	+
+	+	-	-	-	-
+	-	+	+	+	+
+	-	+	-	-	-
+	-	-	+	+	+
+	+	-	-	-	+

Fault-3 Reference signature					
Eigenvalue					
+	+	+	+	+	+
Eigenvector					
+	-	-	+	+	-
+	+	-	-	-	-
+	-	+	+	+	+
+	-	+	+	-	-
+	-	-	+	+	+
+	+	-	-	-	+

(b) Fault-3

Fault-5 at 1% fault magnitude					
Eigenvalue					
+	+	+	+	+	+
Eigenvector					
+	-	-	-	+	+
-	-	-	+	-	+
-	-	+	-	+	-
+	+	+	-	-	-
+	+	-	+	+	-
-	+	-	-	-	+

Fault-5 Reference signature					
Eigenvalue					
+	+	+	+	+	+
Eigenvector					
+	-	-	-	+	+
-	-	-	+	-	+
-	-	+	-	+	-
+	+	+	-	-	-
+	+	-	+	+	-
-	+	-	-	-	+

(c) Fault-5

Fault-7 at 1% fault magnitude					
Eigenvalue					
+	+	+	+	+	-
Eigenvector					
+	+	-	-	-	+
+	-	-	+	-	-
+	+	+	-	+	-
+	-	+	-	-	-
+	-	-	+	-	-
+	+	-	-	+	+

Fault-7 Reference signature					
Eigenvalue					
+	+	+	+	+	-
Eigenvector					
-	-	-	-	-	+
-	-	-	+	-	-
+	-	+	-	+	-
+	+	+	-	-	-
+	+	-	+	-	-
-	+	-	-	+	+

(d) Fault-7

Figure 6.19: Reference vs Actual eigendecomposition-based fault signatures for Fault-1, -3, -5 and -7

Fault-8 at 1% fault magnitude					
Eigenvalue					
+	+	+	+	+	+
Eigenvector					
+	-	-	+	+	+
+	+	-	-	-	-
+	-	+	-	+	+
+	-	+	-	-	-
+	-	-	+	-	+
+	+	-	-	-	+

Fault-8 Reference signature					
Eigenvalue					
+	+	+	+	+	+
Eigenvector					
+	-	-	+	+	+
+	+	-	-	-	-
+	-	+	-	+	+
+	-	+	-	-	-
+	-	-	+	-	+
+	+	-	-	-	+

(a) Fault-8

Fault-9 with a leak of 0.013 kg/s					
Eigenvalue					
-	+	+	+	+	+
Eigenvector					
+	-	-	+	+	+
-	-	-	-	-	-
-	-	+	+	+	+
+	+	+	+	-	-
+	+	-	-	+	+
-	+	-	-	-	+

Fault-9 Reference signature					
Eigenvalue					
-	+	+	+	+	+
Eigenvector					
+	-	-	+	+	+
+	-	-	-	-	-
+	+	+	+	+	+
+	-	+	-	-	-
+	-	-	+	+	+
+	+	-	-	-	+

(b) Fault-9

Figure 6.20: Reference vs Actual eigendecomposition-based fault signatures for Fault-8 and Fault-9

6.3.2 Enthalpy and Entropy-based method

Figure 6.21 and Figure 6.22 show the reference fault signatures and the actual signatures obtained, with a fault magnitude of 1%, using the error method based on enthalpy and entropy. This method was able to detect and isolate all the fault conditions simulated with a fault magnitude of 1%. As previously explained a fault condition will change the shape of the h-s diagram and the change only depends on the fault condition and not on the magnitude. Small variations are compensated for with the implementation of a threshold. For all the fault conditions, except for Fault-3, the variations were small. In the case of Fault-3, the variations caused a shift in the diagram for a fault magnitude of 1%. This can be compensated for with a larger threshold value but will reduce the isolability of this method.

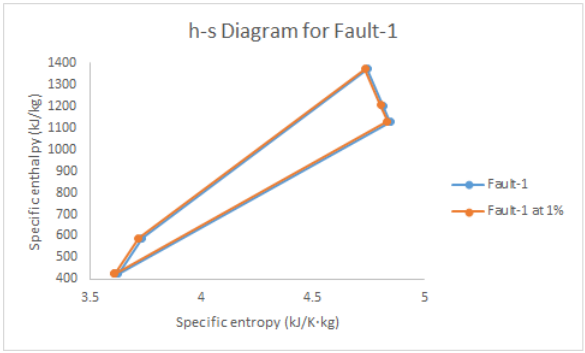

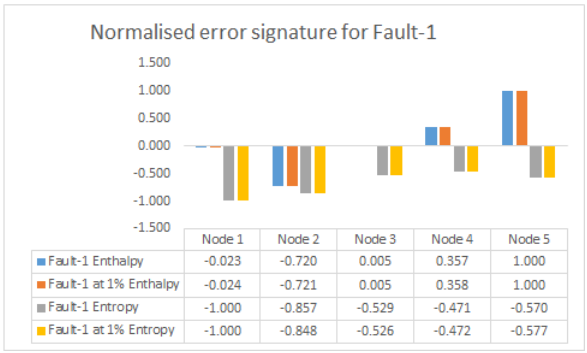

	Node 1	Node 2	Node 3	Node 4	Node 5
Fault-1 Enthalpy	-0.023	-0.720	0.005	0.357	1.000
Fault-1 at 1% Enthalpy	-0.024	-0.721	0.005	0.358	1.000
Fault-1 Entropy	-1.000	-0.857	-0.529	-0.471	-0.570
Fault-1 at 1% Entropy	-1.000	-0.848	-0.526	-0.472	-0.577

(a) Fault-1

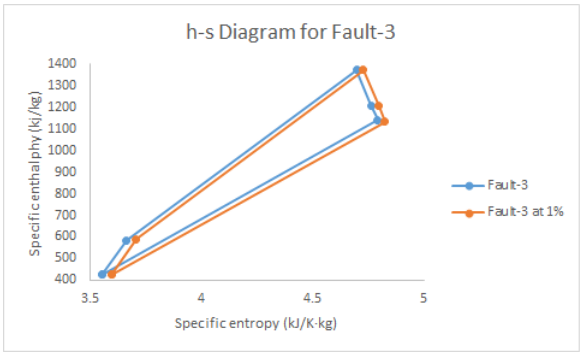

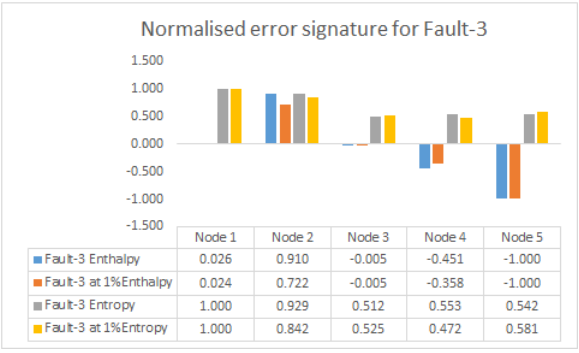

	Node 1	Node 2	Node 3	Node 4	Node 5
Fault-3 Enthalpy	0.026	0.910	-0.005	-0.451	-1.000
Fault-3 at 1%Enthalpy	0.024	0.722	-0.005	-0.358	-1.000
Fault-3 Entropy	1.000	0.929	0.512	0.553	0.542
Fault-3 at 1%Entropy	1.000	0.842	0.525	0.472	0.581

(b) Fault-3

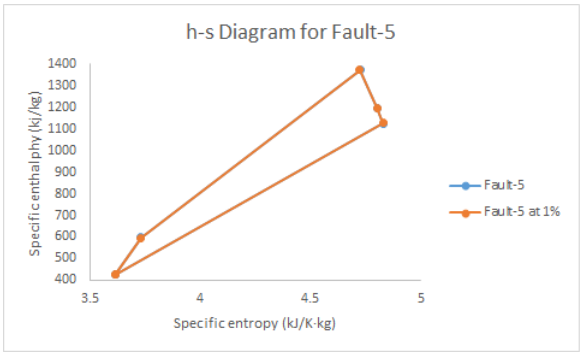

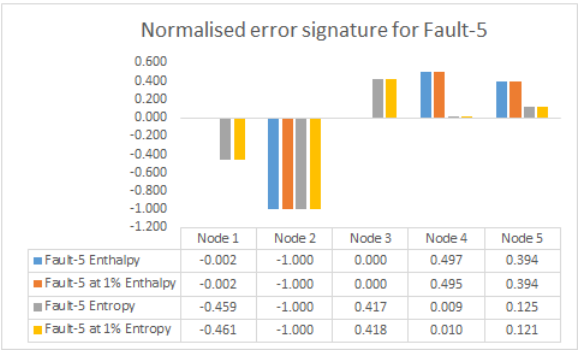

	Node 1	Node 2	Node 3	Node 4	Node 5
Fault-5 Enthalpy	-0.002	-1.000	0.000	0.497	0.394
Fault-5 at 1% Enthalpy	-0.002	-1.000	0.000	0.495	0.394
Fault-5 Entropy	-0.459	-1.000	0.417	0.009	0.125
Fault-5 at 1% Entropy	-0.461	-1.000	0.418	0.010	0.121

(c) Fault-5

Figure 6.21: Reference vs Actual error-based fault signatures for Fault-1, -3 and -5

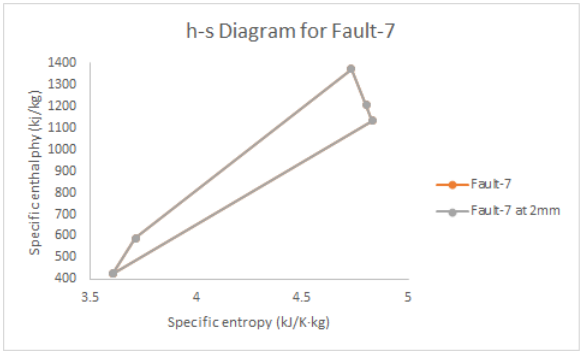

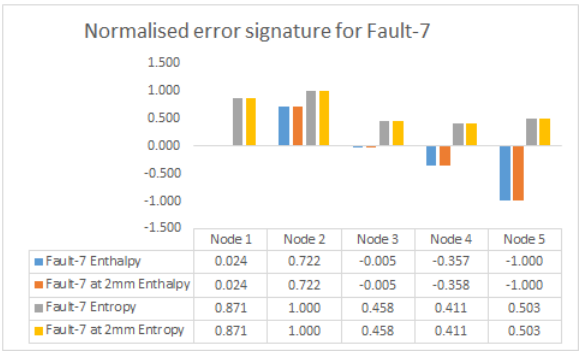

	Node 1	Node 2	Node 3	Node 4	Node 5
Fault-7 Enthalpy	0.024	0.722	-0.005	-0.357	-1.000
Fault-7 at 2mm Enthalpy	0.024	0.722	-0.005	-0.358	-1.000
Fault-7 Entropy	0.871	1.000	0.458	0.411	0.503
Fault-7 at 2mm Entropy	0.871	1.000	0.458	0.411	0.503

(a) Fault-7

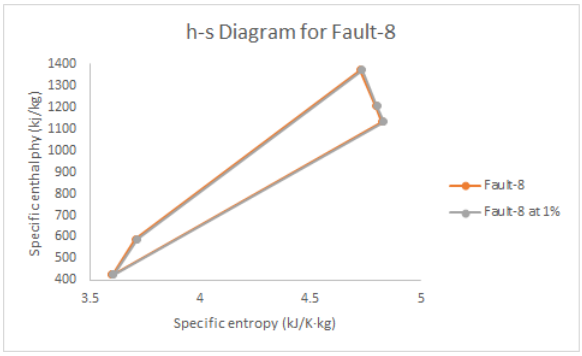

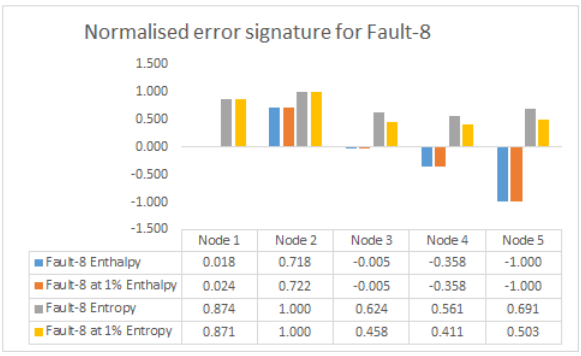

	Node 1	Node 2	Node 3	Node 4	Node 5
Fault-8 Enthalpy	0.018	0.718	-0.005	-0.358	-1.000
Fault-8 at 1% Enthalpy	0.024	0.722	-0.005	-0.358	-1.000
Fault-8 Entropy	0.874	1.000	0.624	0.561	0.691
Fault-8 at 1% Entropy	0.871	1.000	0.458	0.411	0.503

(b) Fault-8

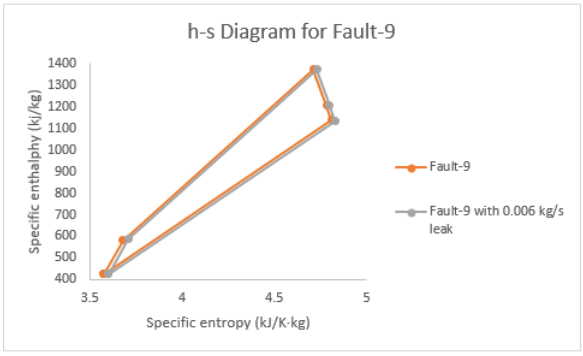

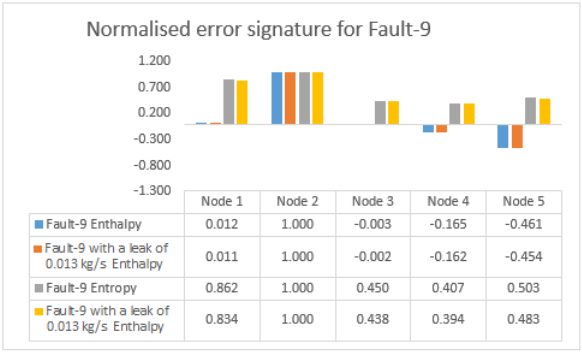

	Node 1	Node 2	Node 3	Node 4	Node 5
Fault-9 Enthalpy	0.012	1.000	-0.003	-0.165	-0.461
Fault-9 with a leak of 0.013 kg/s Enthalpy	0.011	1.000	-0.002	-0.162	-0.454
Fault-9 Entropy	0.862	1.000	0.450	0.407	0.503
Fault-9 with a leak of 0.013 kg/s Enthalpy	0.834	1.000	0.438	0.394	0.483

(c) Fault-9

Figure 6.22: Reference vs Actual error-based fault signatures for Fault-7, -8 and -9

6.4 Result evaluation

In Chapter 2, ten attributes that an FDI system should exhibit were listed as identified by Venkatasubramanian et al. [37]. The two energy-based methods and the enthalpy-entropy method presented in this study are evaluated against these attributes and listed in Table 6.2.

Table 6.2: Comparison of FDI methods based on the attributes of an effective FDI method

Attribute	**Energy-based FDI methods**		**Enthalpy-Entropy FDI method**
	Residual-based	**Eigen decomposition-based**	**Error-based**
Quick detection	✔	✔	✔
Isolability	✔	✔	✔
Robustness	✔	✗	✔
Novelty identifiability	✔	✗	✔
Classification error estimate	✗	✔	✗
Adaptability	✔	✗	✔
Explanation facility	✗	✗	✗
Modelling requirements	✗	✗	✗
Storage and processing requirements	✔	✔	✔
Multiple fault detection	✗	✗	✗

Both energy-based methods and the enthalpy-entropy method were able to generate a signature of the cycle under current operating conditions. This signature can then be compared to the reference signatures of the faults to detect and isolate possible faults. The use of tolerances improves the **robustness** of the methods, by limiting the effect numerical noise (in the form of data processing) has on the method's ability to detect a fault condition. The use of tolerances are however a compromise between **quick detection** (sensitivity) and **isolability**.

Novelty identifiability and **adaptability** were only achieved with the residual-based and error-based methods. The methods could distinguish between fault conditions and a change in the operating setpoint and identify the new operating setpoint (**adaptability**), while the eigendecomposition-based method could detect a change in the operating setpoint, but not identify the new setpoint. The residual-based and error-based methods were able to detect all fault conditions regardless of the fault magnitude. It is therefore concluded that any unknown (**novel**) fault will be detected regardless of the magnitude. The eigendecomposition-based method was only able to detect some fault conditions depending on the fault magnitude. This method will therefore not be able to detect all unknown fault conditions as the fault magnitude has an influence on the ability to detect the fault.

Although not implemented in this study, a distance value could be calculated from the cost matrices used in the eigendecomposition-based method. This distance value could be used as a measure of how accurately (**classification error estimate**) the current operating signature matches a reference signature. The residual-based and error-based methods do not have this attribute.

Since the energy-based method is solely based on energy and exergy values in the cycle, this can be seen as a form of data reduction, reducing **storage and processing** requirements. This is also true for the enthalpy-entropy method relying only on enthalpy and entropy measurements.

None of the methods was able to detect and isolate **multiple faults** occurring simultaneously. In the case of the energy-based methods, the signature of the multiple fault was not solely dependent on the fault combination but also on the magnitude of the individual faults. Therefore a unique signature for the fault combination was not possible. The detection of a multiple fault is possible, as the signature will differ from that of the normal operating condition. The isolation of the multiple fault to a specific combination of single faults was not possible. In the case of the enthalpy-entropy method, du Rand proposed a method to determine if a single fault pertains to the multiple fault. This method was only able to indicate the possibility that a specific single fault is part of the multiple fault. Therefore this method could not isolate a multiple simultaneous fault.

The **modelling requirements** are based on the complexity of the system and the amount of modelling required for the FD system to be effective. This study is based on a basic Brayton cycle and the modelling requirements were minimal. The evaluation of the modelling requirements is, however, unrealistic in this case since a basic representative model is used. Furthermore, the same model was used in all three methods and a comparison cannot be made.

The methods proposed only detect and isolate faults and do not identify the faults. Fault identification forms part of the **explanation facility**, and therefore none of the methods proposed, possesses this attribute.

6.5 Exergetic efficiency

In Chapter 4, the concept of an exergy ratio was introduced as a method to determine the exergetic efficiency of components in the cycle. In this section, the exergy ratio for each component, under different fault conditions and magnitudes, are compared to the normal operating conditions. The exergy ratios for the different fault conditions at different fault magnitudes are given in Appendix E. The difference between the exergy ratio of the normal operating condition and the different fault conditions are shown in Figure 6.23 and Figure 6.24.

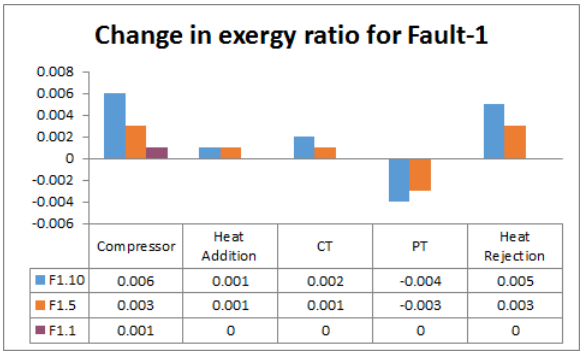

	Compressor	Heat Addition	CT	PT	Heat Rejection
F1.10	0.006	0.001	0.002	-0.004	0.005
F1.5	0.003	0.001	0.001	-0.003	0.003
F1.1	0.001	0	0	0	0

(a) Exergy ratio for Fault-1

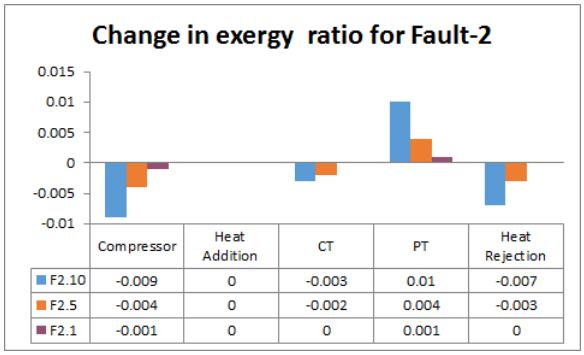

	Compressor	Heat Addition	CT	PT	Heat Rejection
F2.10	-0.009	0	-0.003	0.01	-0.007
F2.5	-0.004	0	-0.002	0.004	-0.003
F2.1	-0.001	0	0	0.001	0

(b) Exergy ratio for Fault-2

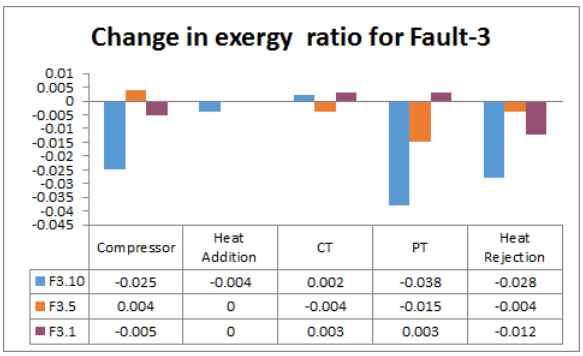

	Compressor	Heat Addition	CT	PT	Heat Rejection
F3.10	-0.025	-0.004	0.002	-0.038	-0.028
F3.5	0.004	0	-0.004	-0.015	-0.004
F3.1	-0.005	0	0.003	0.003	-0.012

(c) Exergy ratio for Fault-3

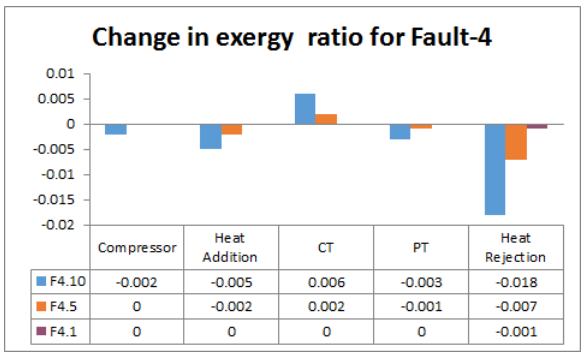

	Compressor	Heat Addition	CT	PT	Heat Rejection
F4.10	-0.002	-0.005	0.006	-0.003	-0.018
F4.5	0	-0.002	0.002	-0.001	-0.007
F4.1	0	0	0	0	-0.001

(d) Exergy ratio for Fault-4

Figure 6.23: Exergy ratios for Fault-1 to Fault-4

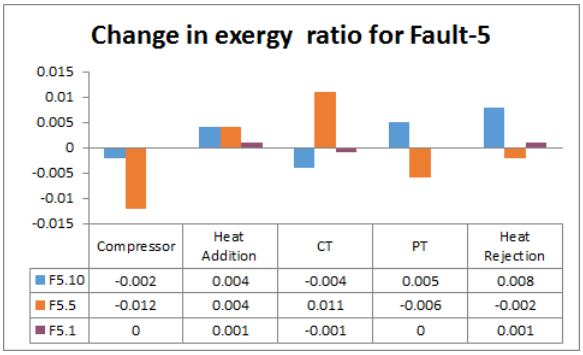

(a) Exergy ratio for Fault-5

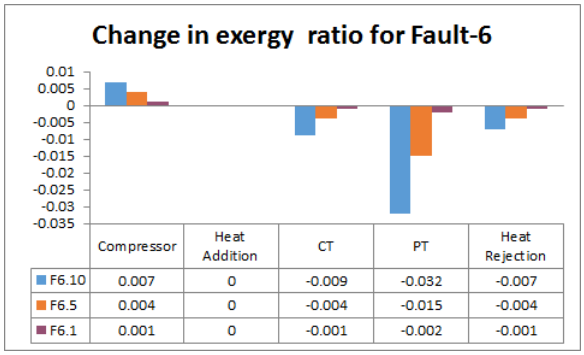

(b) Exergy ratio for Fault-6

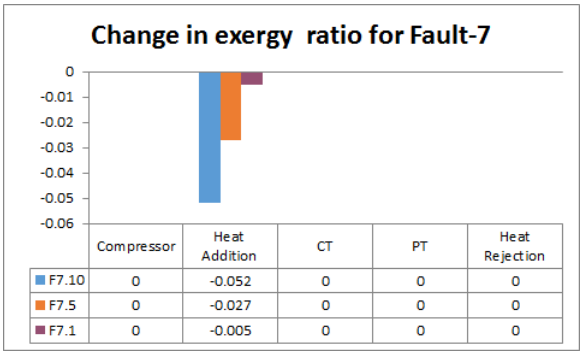

(c) Exergy ratio for Fault-7

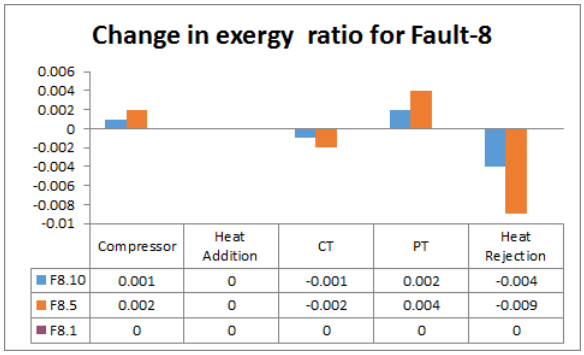

(d) Exergy ratio for Fault-8

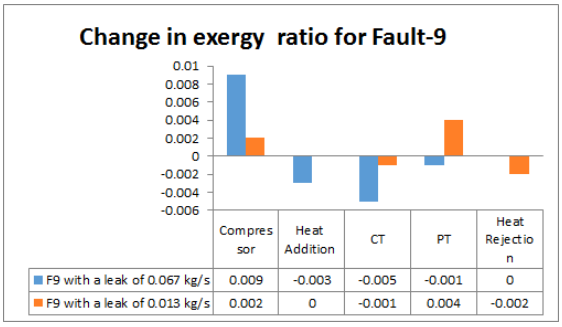

(e) Exergy ratio for Fault-9

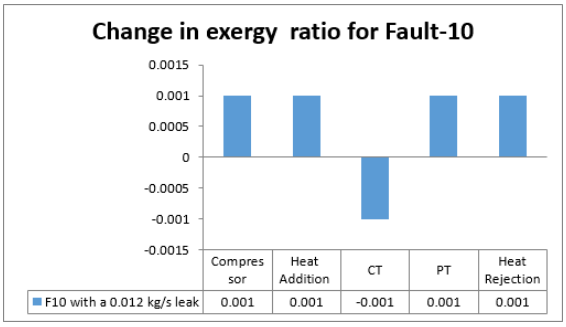

(f) Exergy ratio for Fault-10

Figure 6.24: Exergy ratios for Fault-5 to Fault-10

In the results, F*x*.*y* represents Fault-*x* with a magnitude of *y* %. The exergy ratios are influenced by both the fault type and fault magnitude. As evident from the exergy ratios, different fault types and fault magnitudes will influence the components differently. In some instances, the fault improved the exergy ratio of a component while reducing that of another component. The magnitude of a fault is not always an indication as to the effect the fault will have on the cycle. Depending on the fault type, it is possible for a small magnitude fault to have a more significant effect than a larger magnitude fault. The change in the exergy ratio indicates the effect the

fault type and magnitude have on each component. This can be used in conjunction with FDI to assess the significance of the effect a fault condition has on the exergetic performance of individual components.

In Figure 6.25 the change in the exergy ratio for the different components are shown at various operating setpoints and Figure 6.26 shows the change in the exergy ratios for Fault-1 at an operating setpoint of 120 kJ/s. Comparing Figure 6.23(a) with Figure 6.26, it is evident that the change in the exergy ratio of the components, under a fault condition, will change depending on the operating setpoint. It will thus be possible to determine the most suitable operating setpoint for a given fault condition based on the exergy ratios of the components.

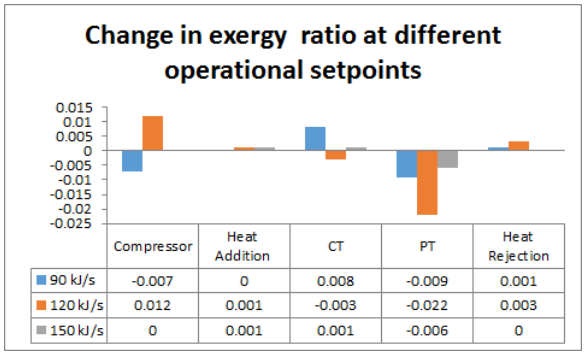

	Compressor	Heat Addition	CT	PT	Heat Rejection
90 kJ/s	-0.007	0	0.008	-0.009	0.001
120 kJ/s	0.012	0.001	-0.003	-0.022	0.003
150 kJ/s	0	0.001	0.001	-0.006	0

Figure 6.25: Exergy ratios at different operating setpoints

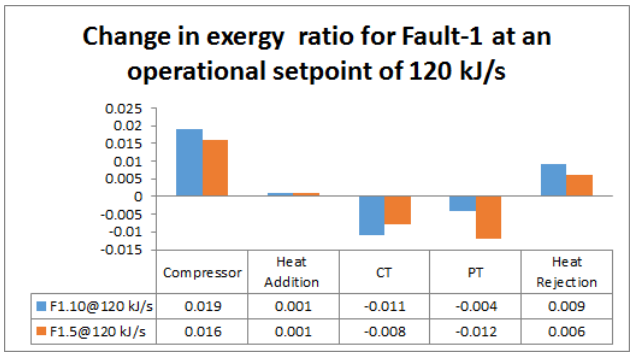

	Compressor	Heat Addition	CT	PT	Heat Rejection
F1.10@120 kJ/s	0.019	0.001	-0.011	-0.004	0.009
F1.5@120 kJ/s	0.016	0.001	-0.008	-0.012	0.006

Figure 6.26: Exergy ratio for Fault-1 at an operating setpoint of 120 kJ/s

6.6 Conclusion

In this chapter, the results for the two FDI methods proposed in Chapter 4 were presented. Both methods were successful in detecting and isolating fault conditions. The residual-based method was able to identify changes in the operating setpoints while the eigendecomposition-based method was only able to detect the change.

Further study is required into the application of eigendecomposition to improve this method by including the magnitude of the changes in the eigendecomposition. The possible advantages of using a distance value to indicate the estimated accuracy/confidence by which faults are detected and isolated will also be of interest.

The error-based method proposed by Du Rand [23] was also applied to this cycle and the results presented. Similar results were obtained using the enthalpy and entropy error-based method as was obtained using the energy and exergy residual-based method.

The exergy ratios for each fault condition were presented, showing the influence various faults at different magnitudes had on the performance of each component. Being able to detect and isolate faults, using energy and exergy, and using exergy as a performance measure for each component in the cycle, will be of great value for condition monitoring and maintenance planning.

CHAPTER 7

Conclusion

This chapter concludes this study by summarising the conclusions reached throughout this study. The contributions made are highlighted, limitations are identified and possible future studies are proposed.

7.1 Conclusion

7.1.1 Energy characterisation for FDI

A Brayton cycle PCU was represented as an attributed graph in terms of energy flow and exergy changes. From the attributed graph an attributed graph matrix was composed in such a manner as to retain structural information regarding the cycle.

The attributed graph matrix completely represents the cycle and FDI methods were successfully applied to detect and isolate faults.

7.1.2 Energy and exergy-based FDI

7.1.2.1 Residual-based method

This method calculated the residual values between two attributed graph matrices. The various fault conditions, presented in Chapter 4, were used to derive unique residual-based fault

signatures for each fault condition. It was determined that the signatures are unique to each fault condition regardless of the magnitude of the fault. A change in the operational setpoint of the cycle could also be detected and the exergy-based residual signature could differentiate between different setpoints e.g. between a change from 100 kJ/s to 120 kJ/s or from 100 kJ/s to 150 kJ/s. The energy-based residual signature for the various fault types remained the same regardless of the operational setpoint. The exergy-based residual signature did change in this case and was unique to the fault condition based on the operational setpoint. Multiple simultaneous fault detection and isolation were not possible. Multiple simultaneous faults could be detected, but not isolated to the individual faults contributing to the multiple fault.

7.1.2.2 Eigendecomposition-based method

In the work done by Van Graan [31], eigenvalues and eigenvectors were used to detect and identify faults in a heat exchanger. The same approach was followed in this study to determine if this method is also effective in detecting and isolating faults in a complete thermodynamic cycle. The attributed graph matrices were compared using the heterogeneous euclidean overlap metric method to obtain a cost matrix. To determine the properties of the cost matrix, the eigenvalues and eigenvectors were calculated. The eigenvalues and eigenvectors were compared to that of a fault-free cycle and the changes noted. For this study only the directional changes were important, that is whether the values increased or decreased. The directional changes in the eigenvalues and eigenvectors were unique to each fault type, regardless of the magnitude, resulting in a unique signature for each fault. This method could however not differentiate between different changes in the operational setpoint e.g. the signatures for a change from 100 kJ/s to 120 kJ/s and from 100 kJ/s to 150 kJ/s are the same. This method was not as sensitive as the residual-based method since not all the faults could be detected and isolated at a fault magnitude of 1%. Multiple simultaneous faults could be detected, but not isolated to the individual faults contributing to the multiple fault.

7.1.3 Enthalpy and entropy-based FDI

The method proposed by Du Rand [23] was implemented on the Brayton cycle used in this study. The fault conditions were simulated and the enthalpy and entropy values determined at the required nodes. The values were plotted on an h-s diagram and the difference between a normal condition and fault condition calculated. This resulted in error-based signatures that were unique to each fault type regardless of the fault magnitude. Faults at different operational setpoints caused the entropy of the fault signature to change but the enthalpy remained

unchanged. This implies that the shape of the h-s diagram remained the same for the fault condition, but a change in the operational setpoint caused a shift in the graph along the x-axis. Multiple faults could be detected, but not isolated to the individual faults.

7.2 Contribution

This study contributed by:

- Completely characterising a Brayton cycle PCU in terms of a multi-domain parameter (energy) for the purpose of FDI,
- Enabling the compilation of a unique energy-based signature, from the energy characterisation of the cycle, for various operating conditions, enabling the detection and isolation of fault conditions in the cycle,
- Comparing and evaluating the methods proposed in this study, together with the error-based method proposed by du Rand [23], according to the attributes exhibited by an effective FDI method,
- Defining an exergy ratio parameter as a performance indicator to indicate the effect a fault has on the components in the cycle.

7.3 Future work/recommendation

7.3.1 Complexity

The Brayton cycle used in this study is a basic cycle with the minimum components required. The effect a more complex system will have on the uniqueness of the signature has to be investigated. The exergy ratios of the various components might be more evident in a more complex system.

7.3.2 Transient conditions

This study was conducted considering only steady state conditions. The effect transient conditions will have on the signatures requires further study.

7.3.3 Multiple simultaneous faults

Further study is required to improve the method's ability not only to detect multiple faults but also to isolate the individual faults pertaining to the multiple fault.

7.3.4 Explanation facility

This study only focused on fault detection and isolation as fault identification was not included. Future work should include methods to uniquely identify the faults, once the fault has been detected and isolated.

7.3.5 Magnitude of eigendecomposition

Only the directional changes in the eigenvalues and eigenvectors were used to create a unique signature for the fault conditions. Future studies should include the magnitude of the changes in the eigenvalues and eigenvectors to determine if additional information can be obtained, regarding the fault detected, such as the effect the fault has on the cycle. This method also lends itself to quantify how confident the FDI system is that the fault has been correctly isolated, but requires further study.

7.4 Closure

In closing, this study aimed to use a multi-domain parameter to completely characterise a Brayton cycle PCU for the purpose of FDI. Energy was identified as a suitable multi-domain parameter. The Brayton cycle PCU was characterised in terms of energy in the form of an attributed graph matrix. Two methods were proposed, utilising the attributed graph matrix, to compile a unique signature of the cycle. Unique energy-based reference signatures were compiled for different operating conditions. These signatures are used to detect and isolate fault conditions in the cycle by matching the reference signature to the actual operating signature of the cycle.

The methods proposed were also compared to the error-based method proposed by du Rand and similar results were obtained. Using the energy characterisation of the cycle, an exergy ratio was defined as a performance indicator. The exergy ratios indicated how different faults and fault magnitudes influenced the exergetic efficiency of the components in the cycle.

Bibliography

[1] O.M. Rouhani and A. Beheshtian. *Energy management, Chapter 1*, pages 1–25. Energy, Science and Technology. Studium Press LLC, 1 edition, 2015.

[2] S. Thomas, S. Böhler, M. Spitzner, and I. Wolfgang. Defining energy efficiency. *Wuppertal Institut für Klima, Umwelt, Energie*, 2008.

[3] P.M. Petersen and J. O'Sullivan. Energy efficient design - a methodology applied in major international projects. *ECEEE: Summer study on energy efficiency in industry*, pages 181–192, 2012.

[4] The alliance to save energy. The history of energy efficiency. *Alliance commission on national energy efficiency policy*, 2013.

[5] International Atomic Energy Agency. *Energy, electricity and nuclear power estimates for the period up to 2050*. 2010.

[6] International Energy Agency. *Key world energy statistics*. 2014.

[7] G. Aydin. The modeling and projection of primary energy consumption by the sources. *Energy Sources, Part B: Economics, planning and policy*, 10:67–74, 2014.

[8] J.M. Harris and B. Roach. *Environmental and natural resource economics: A contemporary approach.* Fourth edition, 2017.

[9] International Energy Agency. *Energy and climate change: World energy outlook special report*. 2015.

[10] International Energy Agency. *Technology roadmap: Nuclear energy*. 2015.

[11] W.G. Le Roux, T. Bello-Ochende, and J.P. Meyer. A review on the thermodynamic optimisation and modelling of the solar thermal brayton cycle. *Renewable and Sustainable Energy Reviews*, 28:677–690, 2013.

[12] R. Shepard and P. Webster. How to increase plant efficiency through positive O&M. *Electric light & power*, 81(1), 2003.

[13] M. Vishwakarma, R. Purohit, V. Harshlata, and P. Rajput. Vibration analysis & condition monitoring for rotating machines: A review. *Materials Today: Proceedings*, 4:2659–2664, 2017.

[14] K.H. Hui, L.M. Hee, M.S. Leong, and A.M. Abdelrhman. Vibration condition monitoring: Latest trend and review. *Applied Mechanics and Materials*, 779-774:139–143, 2014.

[15] D. Miljkovic. Brief review of vibration based machine condition monitoring. *CrSNDT Journal*, 5:14–23, 2015.

[16] R. Bogue. Sensors for condition monitoring: A review of technologies and applications. *Sensor Review*, 33:295–299, 2013.

[17] S.A. Mortazavizadeh and S.M.G. Mousavi. A review on condition monitoring and diagnostic techniques of rotating electrical machines. *Physical Science International Journal*, 4:310–338, 2014.

[18] S. Goel, R. Ghosh, S. Kumar, and A. Akula. A methodical review of condition monitoring techniques for electrical equipment. *The e-Journal of Nondestructive Testing*, 20, 2014.

[19] M.S. Reis and G. Gins. Industrial process monitoring in the big data/industry 4.0 era: From detection, to diagnosis, to prognosis. *Processes*, 5:35–51, 2017.

[20] K. Severson, P. Chaiwatanodom, and R.D. Braatz. Perspective on process monitoring of industrial systems. *Annual reviews in control*, 42:190–200, 2016.

[21] M.A. Sharif and R.I. Grosvenor. Process plant condition monitoring and fault diagnostics. *Proceedings of the Institution of Mechanical Engineers, Part E: Journal of Process Mechanical Engineering*, 212:13–30, 1998.

[22] P. Zhang, T. Jeinsch, S.X. Ding, and P. Liu. Process monitoring and fault diagnosis-status and application. *18th IFAC world congress*, 2011.

[23] C.P. du Rand. *Health monitoring of a Brayton cycle-based power conversion unit.* PhD thesis, Computer and Electronic Engineering. North West University, 2007.

[24] C.P. du Rand and G. van Schoor. Fault diagnosis of generation IV nuclear HTGR components–Part II: The area error enthalpy–entropy graph approach. *Annals of Nuclear Energy*, 41:79–86, 2012.

[25] C.P. du Rand, G. van Schoor, and C. Nieuwoudt. Enthalpy–entropy graph approach for the classification of faults in the main power system of a closed Brayton cycle HTGR. *Annals of Nuclear Energy*, 36(6):703–711, 2009.

[26] C.P. du Rand and G. van Schoor. Fault diagnosis of generation IV nuclear HTGR components–Part I: The error enthalpy–entropy graph approach. *Annals of Nuclear Energy*, 40(1):14–24, 2012.

[27] H. Marais. *An energy-based approuch to condition monitoring of an auto-thermal reformer*. PhD thesis, Computer and Electronic Engineering. North West University, 2015.

[28] Y. Demirel. *Energy: production, conversion, storage, conservation and coupling*. Springer Science & Business Media, 2012.

[29] T. J. Kotas. *The exergy method of thermal plant analysis*. Butterworth-Heinemann, 1985.

[30] L.B. Fouche, K.R. Uren, and G. van Schoor. Energy-based visualisation of an axial-flow compressor system for the purpose of fault detection and diagnosis. *11th IFAC Symposium on Dynamics and Control of Process Systems Including Biosystems DYCOPS-CAB*, 49(7):314–319, 2016.

[31] S. van Graan, G. van Schoor, and K.R. Uren. Graph matching as a means to energy-visualisation of a counter-flow heat exchanger for the purpose of fault diagnosis. *20th IFAC world congress*, 50(1):2842–2847, 2017.

[32] S. Jouili and S. Tabbone. Attributed graph matching using local descriptions. *11th International Conference on Advanced Concepts for Intelligent Vision Systems*, pages 89–99, 2009.

[33] F. Botha and G.P. Greyvenstein. Verification and validation of a thermal hydraulics code used to model the PBMR. In *The 4th South African Conference on Applied Mechanics.*, 2004.

[34] W.A. Landman, E. van Heerden, J.P. van Ravenswaay, and G.P. Greyvenstein. Flownet nuclear architecture, implementation and verification & validation. *International Congress on Advances in Nuclear Power Plants*, 2003.

[35] W.M.K. van Niekerk, P.G. Rousseau, and G.P. Greyvenstein. Operation and simulation of a three-shaft, closed-loop, Brayton cycle model of the PBMR power plant. In *Proceedings of International Congress on Advances in Nuclear Power Plants*, 2003.

[36] M.H. Sobhani and J. Poshtan. Fault detection and isolation using unknown input observers with structured residual generation. *International journal of instrumentation and control systems*, 2(2), 2012.

[37] V. Venkatasubramanian, R. Rengaswamy, K. Yin, and S.N. Kavuri. A review of process fault detection and diagnosis Part I: Quantitative model-based methods. *Computers and Chemical Engineering*, 27:293–311, 2003.

[38] R.C.(Jr) Eisenmann and R.C.(Sr) Eisenmann. *Machinery malfunction, diagnosis and correction*. Prentice Hall, 1998.

[39] R. Rio. Optimize asset performance with industrial IoT and analytics. ARC Advisory Group, 2015.

[40] D. Anderson. Reducing the cost of preventive maintenance. Oniqua Enterprise Analytics, 2002.

[41] B.K.N. Rao. *Handbook of condition monitoring*. Elsevier Advanced Technolgy, 1996.

[42] N. Dyess. Maximizing motor life through condition monitoring. Technical report, Motors@work, 2017.

[43] A. Davies. *Handbook of condition monitoring: Techniques and methodology*. Chapman & Hall, 1998.

[44] H.R. Patel and V.A. Shah. Fault detection and diagnosis methods in power generation plants- the Indian power generation sector perspective: An introductory review. *PDPU Journal of Energy & Management*, pages 31–47, 2017.

[45] S. Dunn. Condition monitoring in the 21st century. *The plant maintenance resource centre*, 2015.

[46] M.D. Shah. Fault detection and diagnosis in nuclear power plant - a brief introduction. *Nirma University International Conference on Engineering*, 2011.

[47] W. Chen. *Fault detection and isolation in nonlinear systems: observer and energy-balance based approaches*. PhD thesis, University of Duisburg-Essen, 2011.

[48] D.M. Himmelblau. *Fault detection and diagnosis in chemical and petrochemical processes*, volume 8 of *Chemical engineering monographs*. Elsevier Scientific Publishing Company, 1978.

[49] D. Miljkovic. Fault detection methods: A literature survey. In *Proceedings of the 34th International Convention MIPRO*, pages 110–115, 2011.

[50] Z. Gao, C Cecati, and S.X. Ding. A survey of fault diagnosis and fault-tolerant techniques part i: Fault diagnosis with model-based and signal-based approaches. *IEEE transactions on industrial electronics*, 62(6):3757–3767, 2015.

[51] J. Gertler. *Fault detection and diagnosis in engineering systems.* CRC press, 1998.

[52] S.X. Ding. *Model-based fault diagnosis techniques*. Springer, 2013.

[53] S. Katipamula and M.R. Brambley. Methods for fault detection, diagnostics, and prognostics for building systems- A review, Part I. *HVAC&R Research*, 11:3–25, 2005.

[54] R. Isermann. *Fault-diagnosis systems: An introduction from fault detection to fault tolerance*. Springer Science & Business Media, 2005.

[55] C. Nan, F. Khan, and M.T. Iqbal. Real-time fault diagnosis using knowledge-based expert system. *Process safety and environmental protection*, 86:55–71, 2008.

[56] P.M. Frank. Real-time fault diagnosis using knowledge-based expert system. *European Journal of Control*, 2:6–28, 1996.

[57] K. van der Merwe. Model-based condition monitoring. *EngineerIT*, 2018.

[58] Q. Yang. *Model-based and data driven fault diagnosis methods with applications to process monitoring*. PhD thesis, Electrical Engineering and Computer Scienecs. Case Western Reserve University, 2004.

[59] J. Ma. *Methods and systems for fault diagnosis in nuclear power plants*. PhD thesis, The University of Western Ontario, 2015.

[60] M.J. de la Fuente. Fault detection and isolation: An overview. *Ingenieria de Sistemas y automatica. Universidad de Valladolid*.

[61] P. Herrero, J. Vehi, R. Calm, and J. Armengol. Robust fault detection system for insulin pump therapy using continuous glucose monitoring. *Journal of diabetes science and technology*, 6:1131–1142, 2012.

[62] V. Venkatasubramanian, R. Rengaswamy, and S.N. Kavuri. A review of process fault detection and diagnosis Part II: Qualitative models and search strategies. *Computers and Chemical Engineering*, 27:313–326, 2003.

[63] K.D. Forbus. *Handbook of knowledge representation*. Elsevier, 2008. Chapter 9: Qualitative modeling.

[64] T. Muller, N. Rehault, and T. Rist. A qualitative modeling approach for fault detection and diagnosis on HVAC systems. *Proceeding of the 13th international conference for enhanced building operations*, 2013.

[65] A. Mouzakitis. Classification of fault diagnosis methods for control systems. *Measurement and Control*, 46:303–308, 2013.

[66] V. Venkatasubramanian, R. Rengaswamy, K. Yin, and S.N. Kavuri. A review of process fault detection and diagnosis Part III: Process history based methods. *Computers and Chemical Engineering*, 27:327–346, 2003.

[67] M. El Koujok and M. Amazouz. Data-driven algorithms for fault detection and diagnosis in industrial process. *International conference on advances in big data analytics*, 2016.

[68] M. Amini and S. Chang. A review of machine learning approaches for high dimensional process monitoring. *Proceedings of the 2018 Industrial and Systems Engineering Research Conference*, 2018.

[69] T. Villegas, M.J. Fuente, and M. Rodriguez. Principal component analysis for fault detection and diagnosis. experience with a pilot plant. In *Proceedings of the 9th WSEAS International Conference on Computational Intelligence, Man-machine Systems and Cybernetics*, pages 147–152. World Scientific and Engineering Academy and Society, 2010.

[70] S. Kim, Y. Kim, C. Park, and I. Jung. Hybrid fault detection and isolation techniques for aircraft inertial measurement sensors. *AIAA Guidance, Navigation, and Control Conference and Exhibit*, 2004.

[71] J.W. Hines, D.W. Miller, and B.K. Hajek. Fault detection and isolation: A hybrid approach. In *Proceedings: Topical meeting on computer-based human support systems: Technology, methods and future*, pages 25–29, 1995.

[72] A. Khoukhi and M.H. Khalid. Hybrid computing techniques for fault detection and isolation, a review. *Computer and Electrical Engineering*, 43:17–32, 2015.

[73] S. Frank, M. Heaney, X. Jin, J. Robertson, H. Cheung, R. Elmore, and G. Henze. Hybrid model-based and data-driven fault detection and diagnostics for commercial buildings. ACEEE Summer study on energy efficicency in buildings, 2016.

[74] A. Berton and D. Hodouin. Linear and bilinear fault detection and diagnosis based on mass and energy balance equations. *Control Engineering Practice*, 11:103–113, 2003.

[75] D. Theilliol, H. Noura, D. Sauter, and F. Hamelin. Sensor fault diagnosis based on energy balance evaluation: Application to a metal processing. *ISA Transactions*, 45(4):603–610, 2006.

[76] G. van Schoor, K.R. Uren, M.A. van Wyk, P.A. van Vuuren, and C.P. du Rand. An energy perspective on modelling, supervision, and control of large-scale industrial systems: Survey and framework. *IFAC Proceedings*, 47(3):6692–6703, 2014.

[77] R. Arango-Miranda, R. Hausler, R. Romero-Lopez, M. Glaus, and S.P. Ibarra-Zavaleta. An overview of energy and exergy analysis in the industrial sector, a contribution to sustainability. *Sustainability*, 10:153–171, 2018.

[78] V. Reddy, S. Kaushik, S. Tyagi, and N. Panwar. An approach to analyse energy and exergy analysis of thermal power plants: A review. *Smart Grid and Renewable Energy*, 1:143–152, 2010.

[79] E.N. George. Advanced thermodynamic analysis of energy intensive building mechanical system. Master's thesis, Rochester Institute of Technology: Department of Mechanical Engineering, 2006.

[80] N. Jin and S. Zhou. Signature construction and matching for fault diagnosis in manufacturing processes through fault space analysis. *IIE Transactions*, 38:341–354, 2006.

[81] B. Youssef. A graphical signature generation tool for diagnosis and parametric estimation of industrial systems: Application to induction motors. *Control, Signal Processing and Real-Time Computing Department. IFP Energies nouvelles, France. Available at: https://www.iconceptpress.com/book/...diagnosis...industrial-systems/.../1107000188.pdf.*

[82] L. Magni, R. Scattolini, and C. Rossi. A fault detection and isolation method for complex industrial systems. *IEEE Transactions on systems, man, and cybernetics-Part A: Systems and humans*, 30(6):860–865, 2000.

[83] K.S. Raj. Performance/condition monitoring & optimization for fossil power plant. *ASME Proceedings*, 1, 2014.

[84] M. Chandrashekar and F.C. Wong. Thermodynamic system analysis: A graph-theoretic approach. *Energy*, 7:539–566, 1981.

[85] C. Christensen and R. Albert. Using graph concepts to understand the organization of complex systems. *International Journal of Bifurcation and Chaos*, 17(7):2201–2214, 2007.

[86] D. Conte, P. Foggia, C. Sansone, and M. Vento. Graph matching applications in pattern recognition and image processing. *IEEE International Conference on Image Processing*, 2:21–24, 2003.

[87] L. Akoglu, H. Tong, and D. Koutra. Graph-based anomaly detection and description: A survey. *Data Mining and Knowledge Discovery*, 29, 2014.

[88] Y. Koren. Drawing graphs by eigenvectors: Theory and practice. *Computers and Mathematics with applications*, 49:1867–1888, 2005.

[89] J.M. Powers. Lecture notes on thermodynamics. Department of Aerospace and Mechanical Engineering: University of Notre Dame, 2018.

[90] W Muschik. Survey of some branches of thermodynamics. *Journal of Non-equilibrium Thermodynamics*, 33:165–198, 2008.

[91] J.C. Weatley, G.W. Swift, and A. Migliori. The natural heat engine. *Los Alamos Science*, 1986.

[92] M. A. Rosen. *Limits to efficiency for energy utilization*. John Wiley & Sons, Ltd, 2015.

[93] Y.A. Cengel and M.A. Boles. *Thermodynamics: An engineering approach*. McGraw-Hill, 4 edition, 2002.

[94] R.D. Robinett III and D.G. Wilson. *Nonlinear power flow control design: Utilizing exergy, entropy, static and dynamic stability, and lyapunov analysis*. Springer-Verlag London, 2011.

[95] T. Tadese and G. Tesema. Energy, entropy and exergy concepts: Thermodynamic approach, a critical review. *Abhinav-National Monthly Refereed Journal Of Research In Science & Technology*, 3(5):4–17, 2014.

[96] I. Dincer and Y.A. Cengel. Energy, entropy and exergy concepts and their roles in thermal engineering. *Entropy*, 3(3):116–149, 2001.

[97] G. Tsatsaronis and F. Cziesla. Basic exergy concepts. *Exergy, energy system analysis and optimization*, 1, 2004.

[98] A. Ghannadzadeh. *Exergetic balances and analysis in a process simulator: A way to enhance process energy integration*. PhD thesis, Hamedan University of Technology, 2013.

[99] S.H. Khattak, R. Greenough, and N. Brown. Suitability of exergy analysis for industrial energy efficiency, manufacturing and energy management. *ECEEE: Industry Summer Study*, pages 237–245, 2012.

[100] M. A. Rosen and I. Dincer. *Exergy: Energy, environment and sustainable development*. Elsevier, 2 edition, 2012.

[101] K. Gaudreau, R.A. Fraser, and S. Murphy. The characteristics of the exergy reference environment and its implications for sustainability-based decision-making. *Energies*, 5(7):2197–2213, 2012.

[102] M. Shukuya. *Exergy: Theory and application in the built environment*. Springer, 2013.

[103] M.A. Rosen. Exergy analysis of energy systems. *Encyclopedia of Energy*, 2:607–621, 2004.

[104] U. Lucia. Gouy-stodola theorem as a variational principle for open systems, 2012.

[105] J. Honerkamp. *Statistical physics: An advanced approach with applications.* Springer Science & Business Media, 2002.

[106] T. Gundersen. An introduction to the concept of exergy and energy quality. *Department of Energy and Process Engineering, Norwegian University of Science and Technology, Trondheim, Norway, Version*, 2009.

[107] S. Jansen and N. Woudstra. Understanding the exergy of cold: theory and practical examples. *International Journal of Exergy*, 7(6):693–713, 2010.

[108] D. Marmolejo-Correa and T. Gundersen. A new graphical representation of exergy applied to low temperature process design. *Computer aided chemical engineering*, pages 1180–1184, 2012.

[109] J. Bundschuh and G. Chen. *Sustainable energy solutions in agriculture*. Sustainable Energy Developments. CRC Press, 2014.

[110] R. Kumar. A critical review on energy, exergy, exergoeconomic and economic (4-E) analysis of thermal power plants. *Engineering Science and Technology*, pages 283–292, 2017.

[111] R. Wolfson. *Energy, Environment and Climate*. NY: W.W. Norton & company, 2nd edition, 2012.

[112] W.M. Haddad. Thermodynamics: The unique universal science. *Entropy*, 19(11):621–690, 2017.

[113] Y.A. Cengel, R.H. Turner, and J.M. Cimbala. *Fundamentals of thermal-fluid sciences*. McGraw-Hill, 2008.

[114] T.K. Ghosh and M.A. Prelas. *Energy resources and systems: Volume 1: Fundamentals and non-renewable resources*. Springer.

[115] S. Abed and K. Tahar. Thermodynamic and energy study of a regenerator in gas turbine cycle and optimization of performance. *International journal of energy optimization and engineering*, 5(2), 2016.

[116] Flownex. *Flownex: General user manual*. M-Tech Industrial (Pty.) Ltd, Potchefstroom, South Africa, 2013.

[117] Flownex. *Flownex: Library theory manual*. M-Tech Industrial (Pty.) Ltd, Potchefstroom, South Africa, 2013.

[118] J.F. Pritchard. Development of a linear model of the Brayton cycle. *Plant control, Doc. 013202-318, PBMR (Pty.) Ltd.*, 2002.

[119] P.G. Rousseau, G.P. Greyvenstein, and W.M.K. van Niekerk. Start-up of the three-shaft closed loop Brayton cycle model of the PBMR power plant. School of mechanical and materials engineering. Potchefstroom university for CHE. South Africa.

[120] P.G. Rousseau and J.P. Van Ravenswaay. Thermal-fluid comparison of three- and single-shaft closed loop Brayton cycle configurations for HTGR power conversion. *Proceedings of International Congress on Advances in Nuclear Power Plants*, 2003.

[121] T.L. Paez. Introduction to model validation. *Proceedings of the International Modal Analysis Conference*, 2009.

[122] M.S. Martis. Validation of simulation based models: A theoretical outlook. *The electronic journal of business research methods*, 4:39–46, 2006.

[123] Meeting with Prof. C.G. du Toit. *Verification and validation of simulation model*. North-West University: School of Mechanical and Nuclear Engineering, March 2019.

[124] R.G. Sargent. Verification and validation of simulation models. *Proceedings of the 2001 winter simulation conference*, pages 183–198, 2001.

[125] K. Kalantar-Zadeh. *Sensors: An introductory course*. Springer, 2013.

[126] F. Bordoni and A. D'Amico. Noise in sensors. *Sensors and Actuators A: Physical*, 21(1-3):17–24, 1990.

[127] K.H. Eom, S.J. Lee, Y.S. Kyung, C.W. Lee, M.C. Kim, and K.K. Jung. Improved Kalman filter method for measurement noise reduction in multi sensor RFID systems. *Sensors*, 11:10266–10282, 2011.

[128] V. Barat, Y. Borodin, and A. Kuzmin. Intelligent ae signal filter methods. *Journal of Acoustic Emission*, 28:109–119, 2010.

[129] R. Moghimi. Low noise signal conditioning for sensor-based circuits. Technical report, Analog Devices, 2010.

[130] S.M. LaValle. Sensing and filtering: A fresh perspective based on preimages and information spaces. *Foundations and Trends in Robotics*, 1:253–372, 2012.

[131] D.C. Stone. Application of median filtering to noisy data. *Canadian Journal of Chemistry*, 73:1573–1581, 1995.

[132] K.E. Vugrin. On the effect of numerical noise in simulation-based optimization. Master's thesis, Virginia Polytechnic Institute and State University, 2003.

[133] M. Shukuya and A. Hammache. Introduction to the concept of exergy- for a better understanding of low-temperature-heating and high-temperature-cooling systems. *VTT Tiedotteita - Valtion Teknillinen Tutkimuskeskus*, 2158:3–41, 2002.

[134] V. Satish and V. Dhana Raju. Energy and exergy analysis of thermal power plant. *International journal of engineering science and computing*, 6(8):2636–2644, 2016.

[135] C. Acar and I. Dincer. Energy and exergy analysis of a residential cold thermal energy storage system. *International journal of exergy*, 19:441–458, 2016.

[136] E. Sciubba and G. Wall. A brief commented history of exergy from the beginnings to 2004. *International journal of thermodynamics*, 10(1):1–26, 2007.

[137] G. Kostenko. Efficiency of heat processes. *Promishlenaya Teplotechnika*, 4:70–73, 1983.

[138] M. Sorin and V.M. Brodyansky. A method of efficiency definition for power and chemical systems. *Izvestia Vuzov Energetika*, pages 78–88, 1985.

[139] D.R. Wilson and T.R. Martinez. Improved heterogeneous distance function. *Journal of Artificial Intelligence Research*, 6:1–34, 1997.

[140] H. Abdi. The eigen-decomposition: Eigenvalues and eigenvectors. *Encyclopedia of measurements and statistics*, 2007.

[141] R. Bronson and G.B. Costa. *Linear algebra: An introduction*. Elsevier, 2 edition, 2007.

[142] E. Kreyszig. *Advanced engineering mathematics*. John Wiley & Sons, Ltd, 8 edition, 1999.

[143] S. van Graan. Graph matching as a means to energy-visualisation of a counter-flow heat exchanger. Master's thesis, Computer and Electronic Engineering, North West University., 2016.

[144] M.M. Kostic. The elusive nature of entropy and its physical meaning. *Entropy*, 16:953–967, 2014.

APPENDIX A

Operational graphs

The Brayton cycle depicted in Figure A.1 was simulated and the operational graphs are presented in this section. The operational graphs are from initial conditions to steady state conditions for normal operating conditions, with the PT output controlled at 100 kJ/s. The power input or output of each component is shown in Figure A.2. The specific enthalpy at each node (1-5) is shown in Figure A.3 and Figure A.4 shows the specific entropy at each node. In Figure A.5 the exergy destroyed in the component is shown. Figure A.6 and Figure A.7, respectively shows the pressure and temperature at the various nodes.

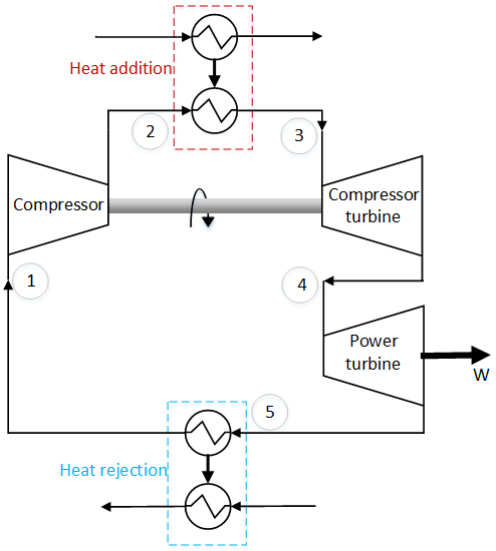

Figure A.1: Brayton cycle

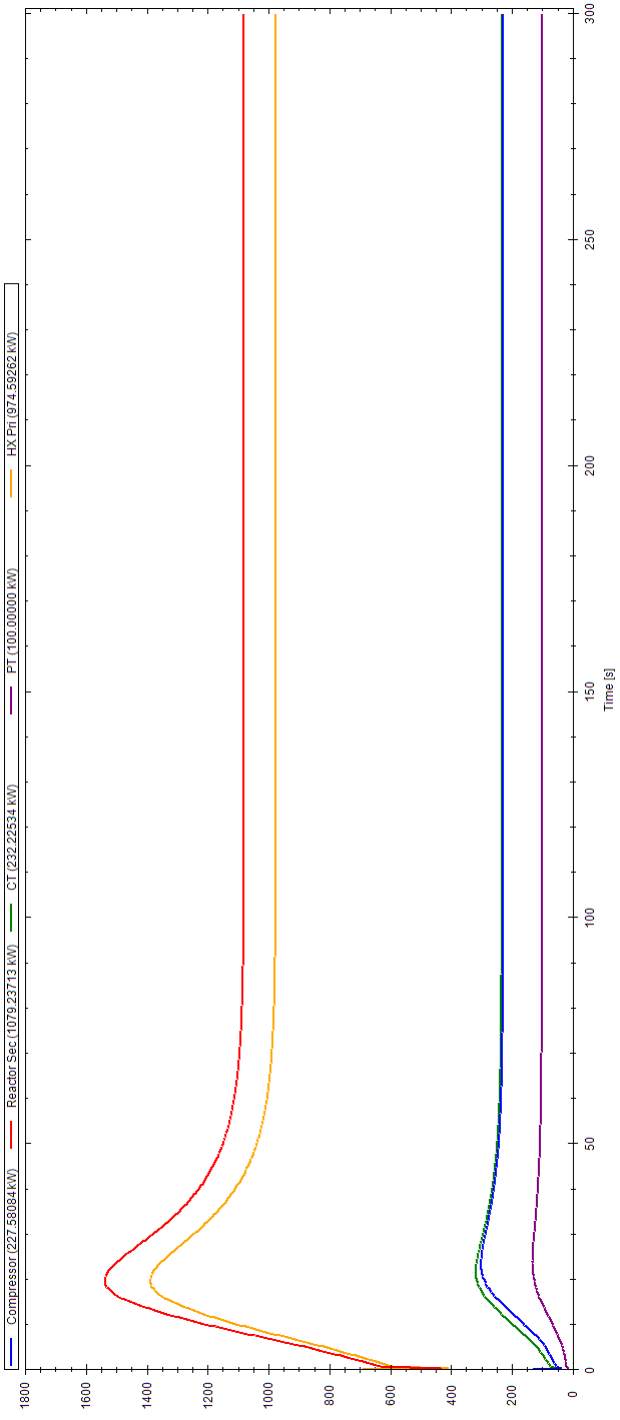

Figure A.2: Power input or output for each component

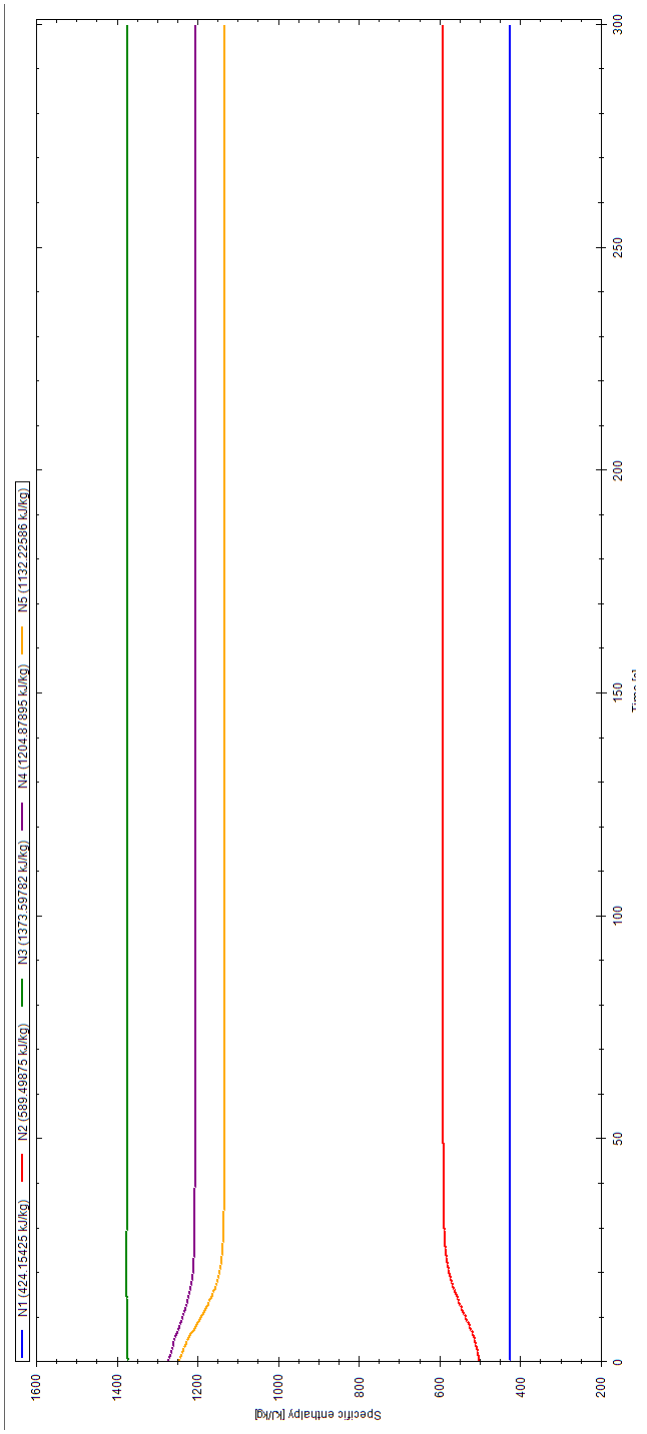

Figure A.3: Specific enthalpy measured at Nodes 1 to 5

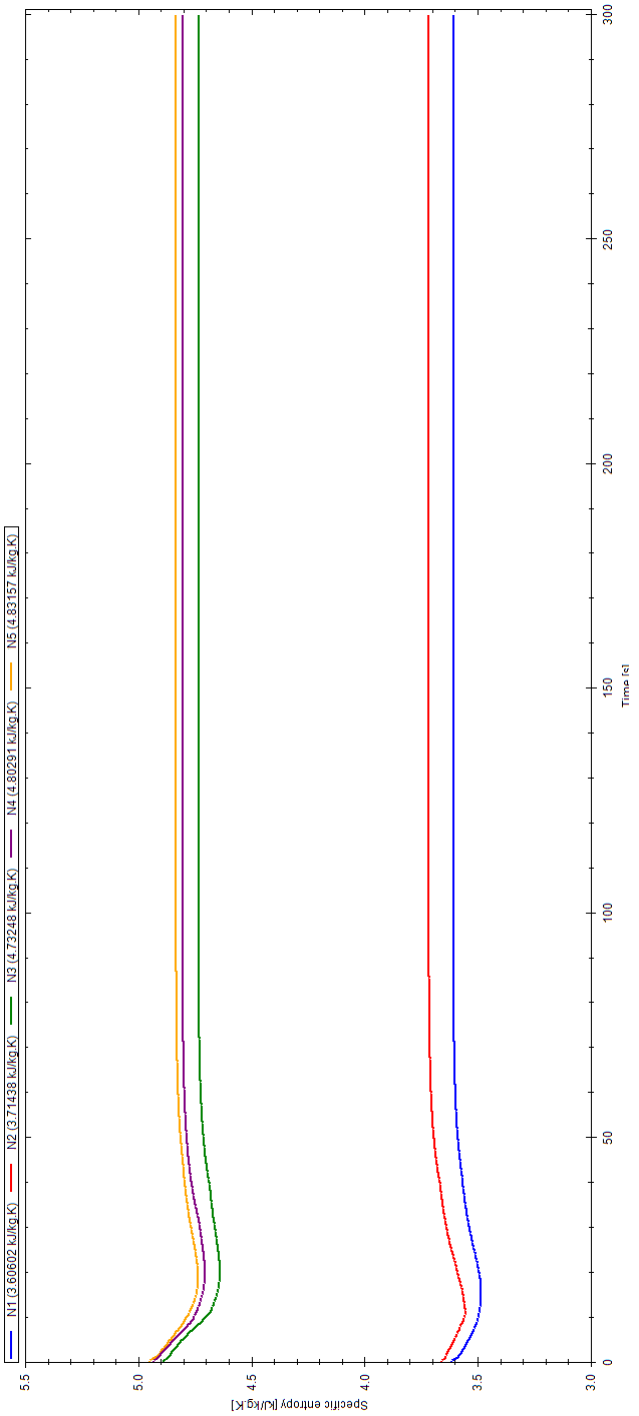

Figure A.4: Specific entropy measured at Nodes 1 to 5

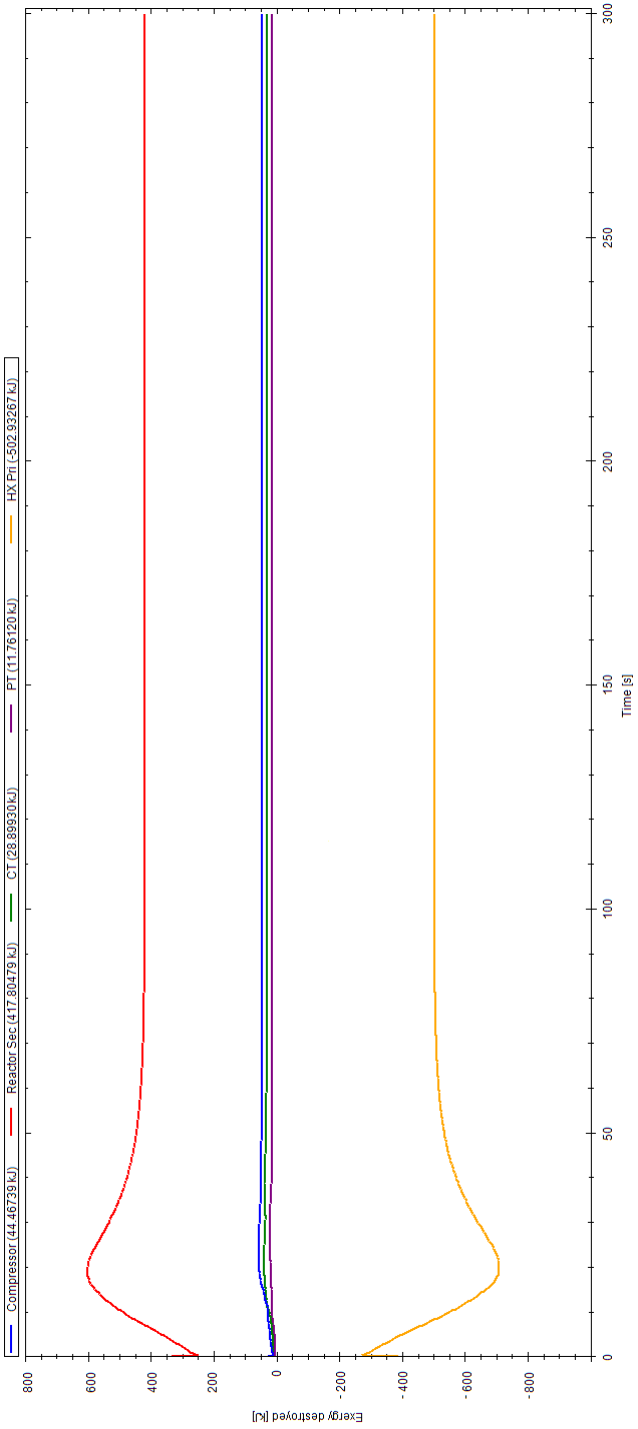

Figure A.5: Exergy destroyed in the components

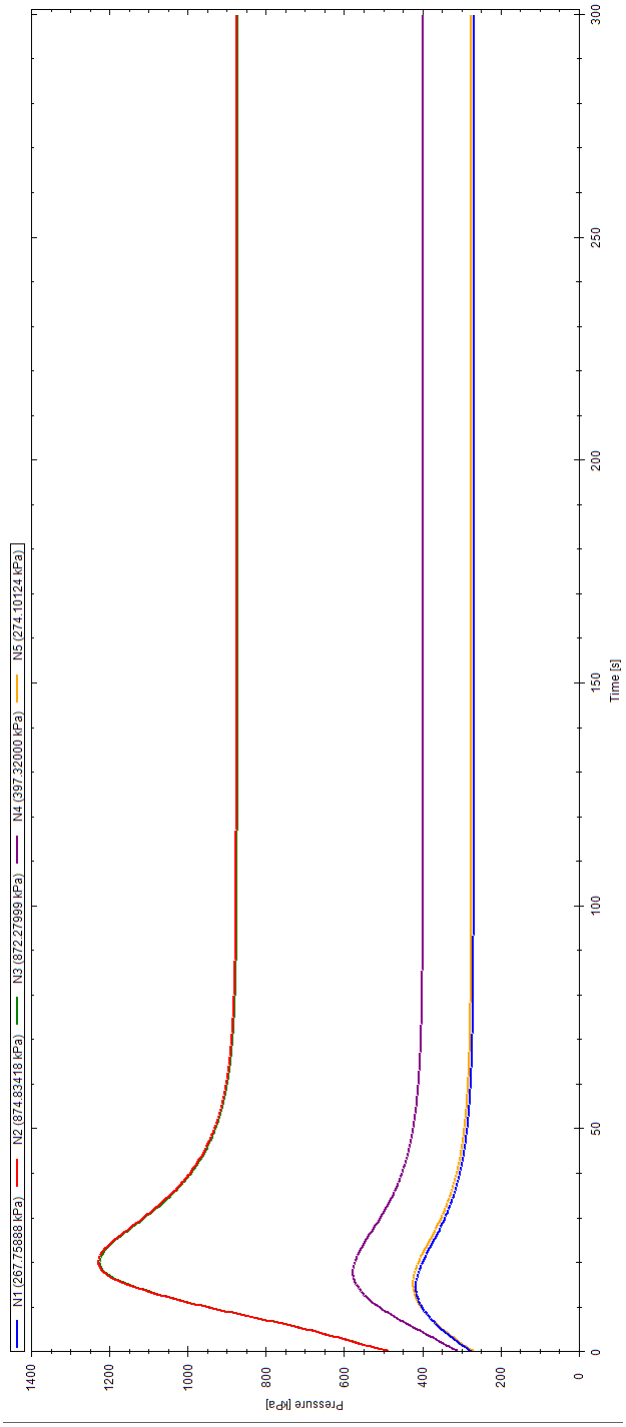

Figure A.6: Pressure measured at Nodes 1 to 5

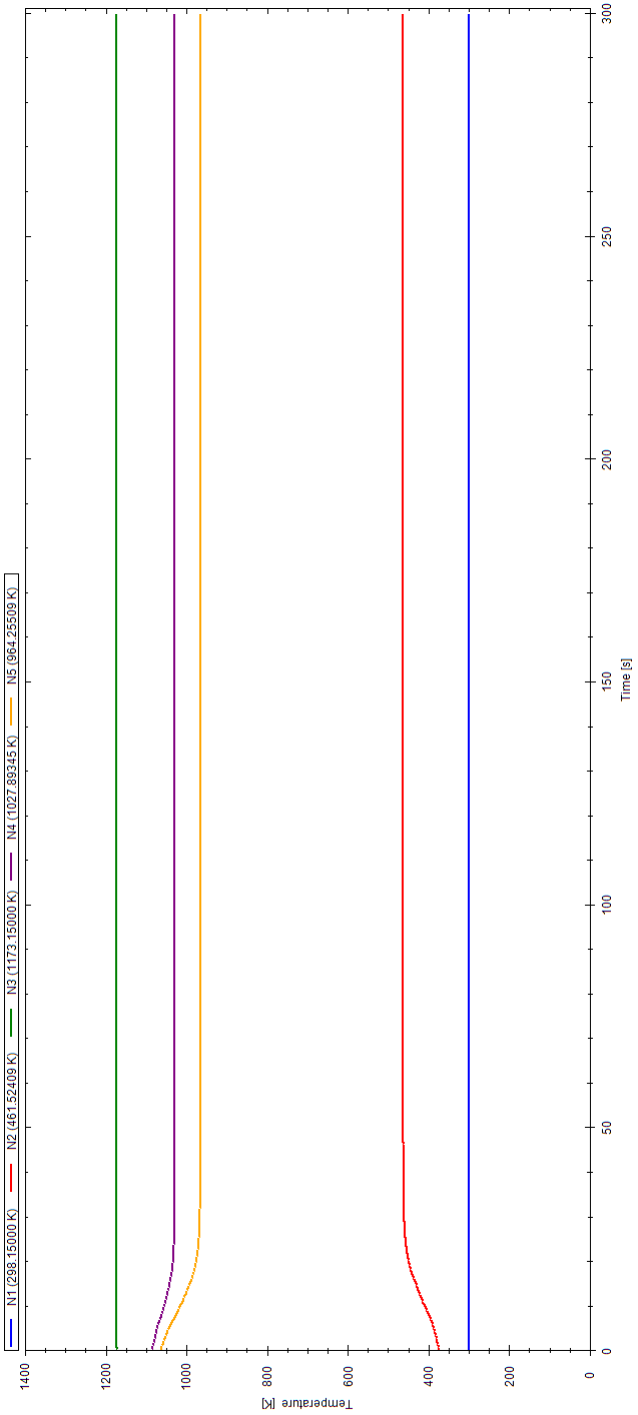

Figure A.7: Temperature measured at Nodes 1 to 5

APPENDIX B

Verification and validation of the representative Brayton cycle model

The Brayton cycle model used in this study is only a representative model of a Brayton cycle. This representative model is not based on a real Brayton cycle PCU, in terms of operating conditions or component performance. For the purpose of this study, which is to use energy and exergy to detect and isolate faults, a basic model is required that is representative of a Brayton cycle in terms of its behaviour. The representative model, as discussed in Chapter 4, is shown again in Figure B.1, and will be referred to as the basic model.

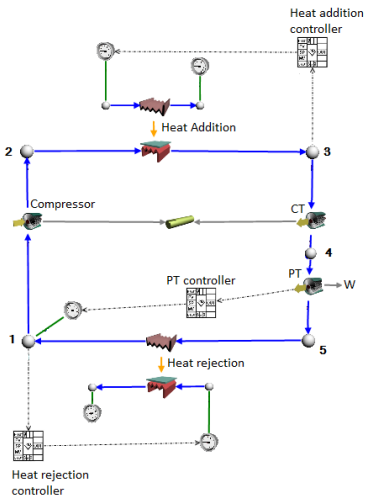

Figure B.1: Flownex® model of a basic Brayton cycle

In the following sections, the basic model will be verified and validated. The components in the basic model are verified by comparing simulated results with analytical results. The basic model will be validated by comparing the behaviour of the basic model with that of a validated Brayton cycle.

Verification

The simulated temperature and pressure results of the cycle under steady state conditions, with a PT setpoint of 100 kJ/s, are presented in Table B.1. The temperature and pressure data are used to calculate the operating conditions of the components and compared in order to verify the components.

Table B.1: Simulated temperature and pressure results

Node	**Temperature** (K)	**Pressure** (kPa)
1	298.15	267.76
2	461.52	874.83
3	1173.15	872.28
4	1027.89	397.32
5	964.25	274.1

Compressor

The compressor is verified using the equations presented in Chapter 4 and summarised in Table B.2. The calculated results are also shown in Table B.2.

Table B.2: Summary of compressor variables

Variable	Description	Equation	Value
P_{inlet}	Inlet pressure		267.76 kPa
P_{outlet}	Outlet pressure		874.83 kPa
T_{inlet}	Inlet temperature	Fixed inlet temperature	298.15 K
T_{outlet}	Outlet temperature	$T_{inlet} + \Delta T$	459.507 K
N	Shaft speed		96.823 r/sec
$\grave{m}$	Corrected mass flow	From performance maps	8.89
$\grave{N}$	Corrected shaft speed	$\frac{N}{\sqrt{T_{inlet}}}$	96.823
$\dot{m}$	Mass flow	$\frac{\grave{m}P_{inlet}}{\sqrt{T_{inlet}}}$	1.379 kg/s
W	Power	$\dot{m}C_p(T_{inlet} - T_{outlet})$	-225.404 W
γ	Specific heat ratio	$\frac{C_p}{C_v}$	1.404
P_{ratio}	Pressure ratio	$\frac{P_{outlet}}{P_{inlet}}$	3.267
ΔT	Temperature difference	$\frac{T_{inlet}}{\eta_{comp}}\left(1 - P_{ratio}^{\left(\frac{\gamma-1}{\gamma}\right)}\right)$	161.357 K
η	Isentropic efficiency	From performance maps	0.75

The calculated and simulated results of the compressor are summarised in Table B.3 with the percentage error indicated.

Table B.3: Verification of compressor results

Variable	Calculated results	Simulated results	% error
$\dot{m}$	1.379 kg/s	1.376 kg/s	-0.21
ΔT	161.357 K	163.37 K	1.2
W	225.403 W	227.58 W	0.96
T_{outlet}	459.507 K	461.52 K	0.4

The calculated and simulated results for the CT and PT are summarised in Tables B.4 and B.5.

Table B.4: Verification of CT results

Variable	Calculated results	Simulated results	% error
$\dot{m}$	1.379 kg/s	1.376 kg/s	-0.21
ΔT	145.566 K	145.26 K	-0.21
W	-233.857 W	-232.225 W	0.69
T_{outlet}	1027.584 K	1027.89 K	0.03

Table B.5: Verification of PT results

Variable	Calculated results	Simulated results	% error
$\dot{m}$	1.379 kg/s	1.376 kg/s	-0.21
ΔT	63.31 K	63.63 K	0.5
W	-100.9 W	-100 W	-0.89
T_{outlet}	964.57 K	964.255 K	-0.03

Heat addition element

The heat addition element is verified based on the heat transfer. The steady state conditions for the heat addition element are given in Table B.6. The calculated result for the heat transfer ($\dot{Q}$) is also shown in Table B.6

Table B.6: Summary of heat addition element variables

Variable	Description	Equation	Value
$\dot{m}$	Mass flow		1.379 kg/s
C_p	Specific heat at constant pressure		1.099 kJ/kg·K
T_{inlet}	Inlet temperature		459.507 K
T_{outlet}	Outlet temperature		1173.15 K
$\dot{Q}$	Heat transfer	$\dot{m}C_p(T_{outlet} - T_{inlet})$	1078.49 W

The calculated and simulated results for the heat addition element are shown in Table B.7.

Table B.7: Verification of heat addition results

Variable	Calculated results	Simulated results	% error
$\dot{Q}$	1078.49 W	1078.92 W	0.04

The calculated and simulated results for the heat rejection element are shown in Table B.8

Table B.8: Verification of heat addition results

Variable	Calculated results	Simulated results	% error
$\dot{Q}$	-973.672 W	-974.593 W	0.09

The simulated results are verified, as evident from the small error between the simulated and calculated results.

Validation

The behaviour of the basic model will be validated in terms of temperature and pressure, using four validation techniques[1].

Traces:

With this technique, the temperature and pressure are traced through the cycle. The following behaviour is expected:

- The temperature and pressure will increase through the compressor.
- The temperature will increase through the heat addition component, with a small decrease in the pressure.
- The temperature and pressure will decrease through the CT and PT.
- The temperature will decrease through the heat rejection element, with a small decrease in the pressure.

The temperature and pressure behaviour of the basic model is illustrated in Figure B.2. The behaviour of the basic model is the same as what was expected. Based on this technique, it is concluded that the basic model is validated.

[1] R.G. Sargent. Verification and validation of simulation models. Proceedings of the 2001 winter simulation conference, pages 183–198, 2001

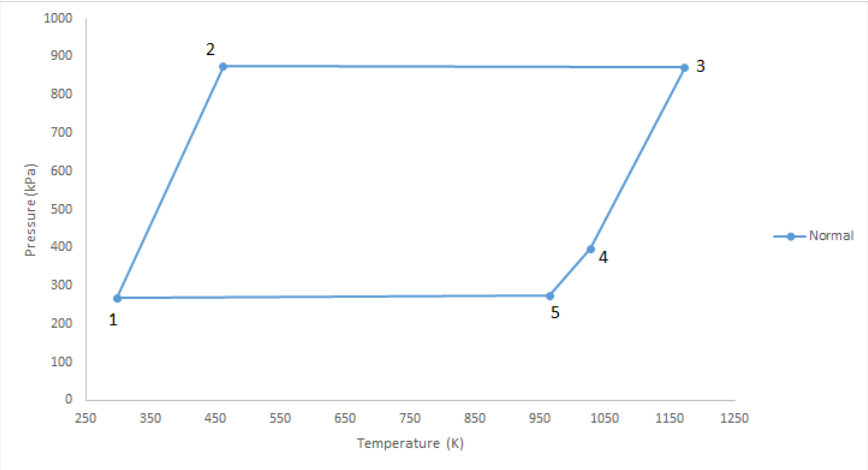

Figure B.2: Temperature-pressure graph of the basic model

Face validity:

From literature it is known that a closed-loop Brayton cycle, at minimum, consists of a compressor, a heat addition element, a turbine and a heat rejection element, in that order. This is the layout of the basic model (see Figure B.1). The layout of the Rankine cycle is however similar, with the biggest difference being that the Rankine cycle is a vapour cycle (the working fluid changes between liquid and vapor), while the Brayton cycle is a gas cycle (the working fluid is a gas). From the simulation, the working fluid remained in a gas phase, with no phase changes occurring through the cycle. Based on this technique, the basic model is validated.

Internal validity:

The basic model was simulated numerous times under the same conditions and the results of each simulation compared. This was explained in Section 4.2.3 as part of determining the numerical noise. The maximum difference in the data between multiple simulations was 1.251×10^{-12}. Since the difference between simulations is small, it is concluded that the basic model is validated based on internal validity.

Comparison to other models:

The basic model (Figure B.1), is a simplification of the three shaft Brayton cycle used in the PBMR. The Flownex® model of the three shaft closed-loop Brayton cycle, available as a demonstration in Flownex®, is shown in Figure B.3. This model will be referred to as the complex model. The complex model is based on the PBMR. The verification and validation of the three shaft Brayton cycle used in the PBMR are presented in the work of van Niekerk et al.[2]

[2]W.M.K. van Niekerk, P.G. Rousseau, and G.P. Greyvenstein. Operation and simulation of a three-shaft,

The simplification of the model was done in order to reduce the number of nodes and therefore the size of the attributed graph matrix representing the cycle. The complex cycle consists of two compressor-turbine pairs with an intercooler between the compressors and, a precooler and a heat recovery unit (recuperator) between the power turbine and low-pressure compressor. The temperature at the inlet to the high-pressure turbine is fixed at 993.15 K. The power turbine is connected to a compressor (PT-compressor) of which the outlet pressure is controlled to 170 kPa (normal operating condition) by means of regulating the pressure at the precooler inlet. The working fluid in the complex model is air, simulated as a single phase gas. The temperature and pressure are measured before the low-pressure compressor (Node 1), after the high-pressure compressor (Node 2), before the high-pressure turbine (Node 3), after the low-pressure turbine (Node 4) and after the power turbine (Node 5). This coincides with the nodes of the basic model.

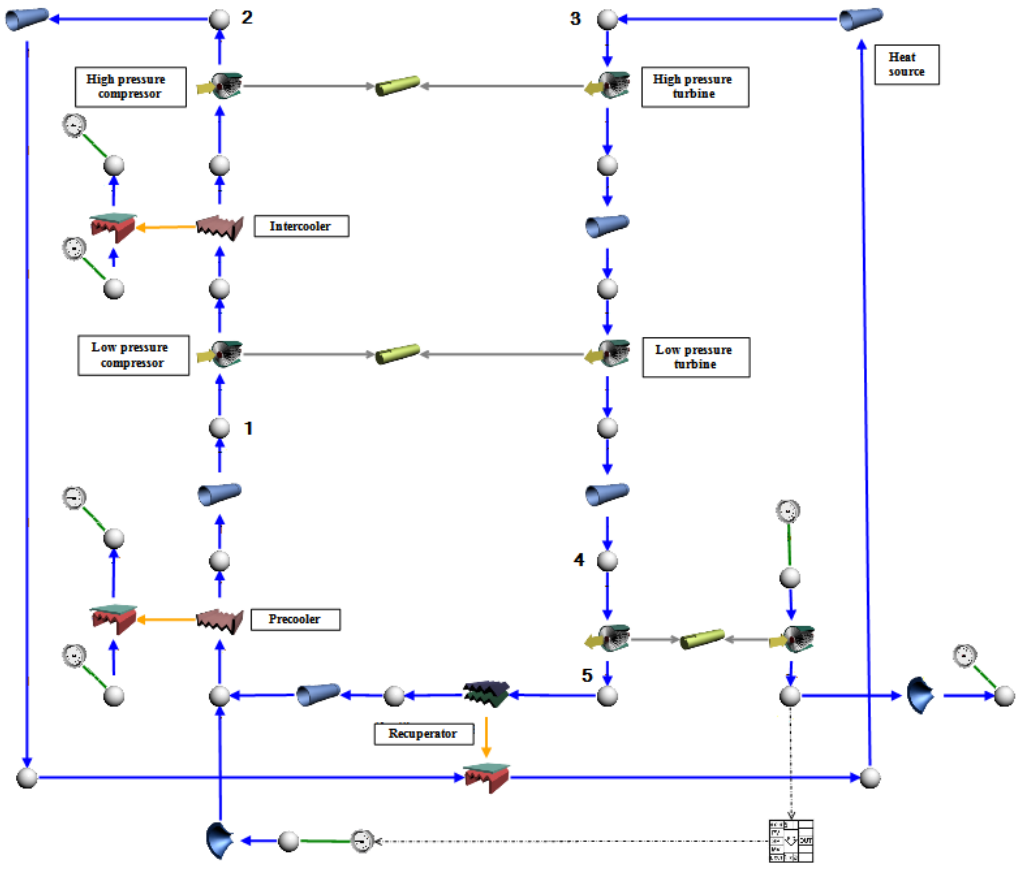

Figure B.3: Flownex® model of the PBMR

closed-loop, Brayton cycle model of the PBMR power plant. In Proceedings of International Congress on Advances in Nuclear Power Plants, 2003.

In order to validate that the basic model is representative of a Brayton cycle, the behaviour of the basic and complex models, in terms of temperature and pressure, are compared. The operating conditions of the basic model were experimentally determined, based on the components available in Flownex® and used in the complex model. The complex model, available with Flownex®, will be used to validate the basic model. The components available in Flownex® have been verified, therefore only the interactions of the components in the basic model have to be validated. The temperature-pressure diagram of the complex model is given in Figure B.4. The temperature-pressure diagram of the basic and complex model are similar. The exact temperatures and pressure will differ as the models have different operating conditions but the temperature and pressure behaviour are similar.

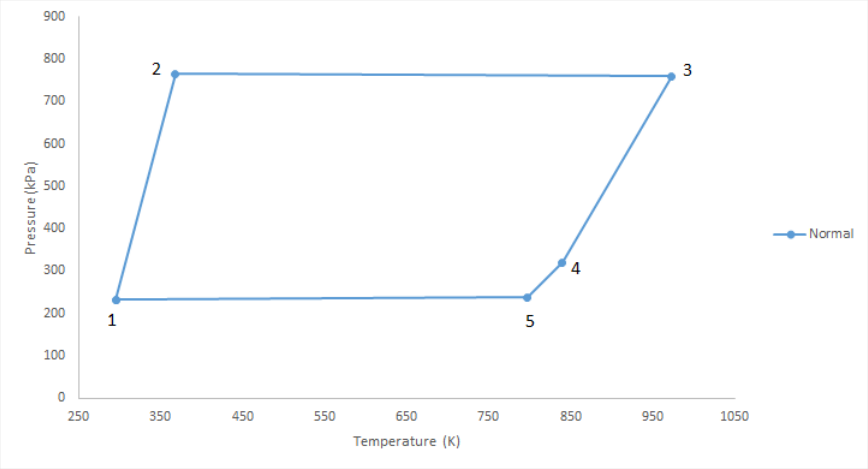

Figure B.4: Pressure-temperature graph of the complex model

The operating setpoints of both models were changed and the temperature-pressure diagrams for the different setpoints are shown in Figure B.5a and b, for the basic and complex models respectively. The exact change in the setpoint is not important. What is important, is how the temperature and pressure change, with an increase and decrease in the setpoint. The temperatures and pressures are presented in Table B.9.

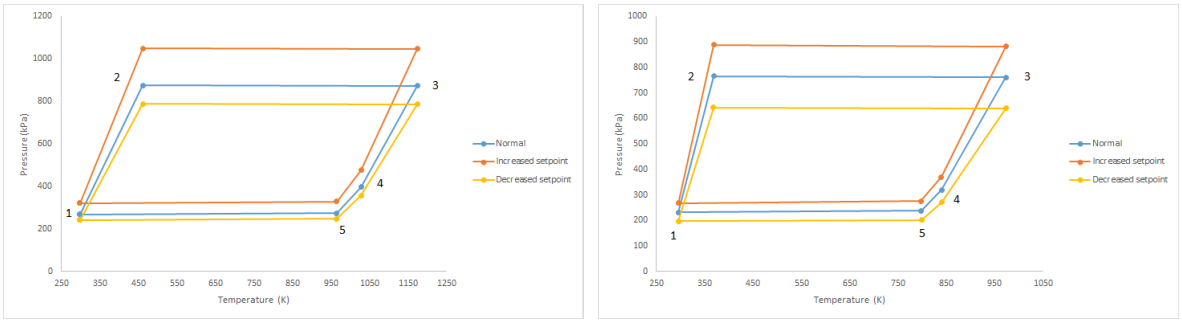

(a) Basic model

(b) Complex model

Figure B.5: Pressure-temperature graphs at different operating setpoints

Table B.9: Pressure and temperature values at different setpoints

(a) Basic model

Node	Decreased setpoint		Normal		Increased setpoint	
	Pressure (kPa)	Temperature (K)	Pressure (kPa)	Temperature (K)	Pressure (kPa)	Temperature (K)
1	241.07	298.15	267.75	298.15	321.09	298.15
2	787.56	461.52	874.83	461.52	1049.25	461.53
3	785.26	1173.15	872.27	1173.15	1046.19	1173.15
4	357.69	1027.86	397.31	1027.89	476.51	1027.95
5	246.77	964.23	274.10	964.25	328.70	964.30

(b) Complex model

Node	Decreased setpoint		Normal		Increased setpoint	
	Pressure (kPa)	Temperature (K)	Pressure (kPa)	Temperature (K)	Pressure (kPa)	Temperature (K)
1	196.28	295.28	232.05	295.16	268.26	295.17
2	643.09	367.92	764.86	368.19	887.85	368.39
3	638.88	973.15	759.97	973.14	882.25	973.14
4	270.49	840.35	320.34	839.68	370.78	839.25
5	201.47	798.84	237.91	797.40	274.84	796.84

In the work of du Rand[3] the temperature and pressure data of the PBMR were presented. The temperature-pressure diagram for the PBMR is shown in Figure B.6, for the normal operating conditions and with an increase in the operating setpoint. The pressure-temperature diagram and the behaviour of the basic model is similar to that of the PBMR.

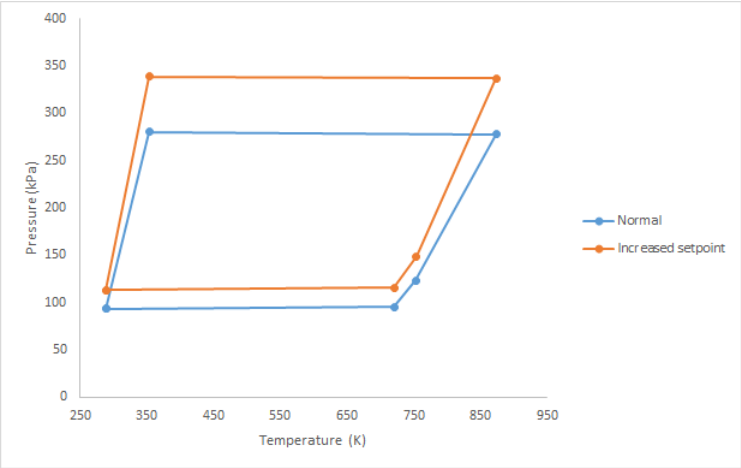

Figure B.6: Pressure-temperature graph of the PBMR at different operating setpoints

The basic model is validated, based on the comparative technique since:

- The temperature-pressure diagram of the basic model is similar to the complex model and PBMR.
- The basic model's response to a change in the operating setpoint is similar to that of the complex model and PBMR.

The basic model was verified and validated and it is therefore concluded that the basic model is representative of a Brayton cycle.

[3]C.P. du Rand. Health monitoring of a Brayton cycle-based power conversion unit. PhD thesis, Computer and Electronic Engineering. North West University, 2007

APPENDIX C

Energy and Exergy changes

The changes in the energy and exergy flow through each component in the cycle as well as the change in the exergy of the surroundings due to the interaction between the component and its surroundings are presented in this section. The energy and exergy changes under normal operating conditions for changes in the PT setpoint are given in Table C.1. The energy and exergy changes for each of the fault conditions are given in Table C.2 to Table C.5. For each of the fault conditions the output of the PT was controlled at 100 kJ/s.

Table C.1: Energy and exergy result for normal operating conditions at different PT setpoints

Normal operating condition at 90 kJ/s			
Component	Δ Energy flow (kJ/s)	Δ Exergy flow (kJ/s)	Δ Exergy flow (kJ/s) external to the cycle due to the component
Compressor	204.87	163.49	-204.87
Heat addition	971.42	595.39	-1005.52
CT	-209.05	-232.99	209.05
PT	-90.00	-101.61	90.00
Heat rejection	-877.24	-424.28	41.32
Net	0.00	0.00	-870.02

(a)

Normal operating condition at 100 kJ/s			
Component	Δ Energy flow (kJ/s)	Δ Exergy flow (kJ/s)	Δ Exergy flow (kJ/s) external to the cycle due to the component
Compressor	227.52	188.76	-227.52
Heat addition	1078.92	658.53	-1102.77
CT	-232.16	-258.99	232.16
PT	-100.00	-114.90	100.00
Heat rejection	-974.28	-473.38	44.05
Net	0.00	0.00	-954.08

(b)

Normal operating condition at 120 kJ/s			
Component	Δ Energy flow (kJ/s)	Δ Exergy flow (kJ/s)	Δ Exergy flow (kJ/s) external to the cycle due to the component
Compressor	272.97	222.91	-272.97
Heat addition	1294.84	793.76	-1231.22
CT	-278.54	-314.21	278.54
PT	-120.00	-137.49	120.00
Heat rejection	-1169.27	-564.97	117.15
Net	0.00	0.00	-988.50

(c)

Table C.2: Energy and exergy result for Fault-1 to Fault-3

Fault-1 with 5% fault magnitude			
Component	Δ Energy flow (kJ/s)	Δ Exergy flow (kJ/s)	Δ Exergy flow (kJ/s) external to the cycle due to the component
Compressor	224.33	180.97	-224.33
Heat addition	1057.21	647.88	-1092.11
CT	-228.91	-257.14	228.91
PT	-100.00	-111.80	100.00
Heat rejection	-952.63	-459.90	51.50
Net	0.00	0.00	-936.03

(a)

Fault-2 with 5% fault magnitude			
Component	Δ Energy flow (kJ/s)	Δ Exergy flow (kJ/s)	Δ Exergy flow (kJ/s) external to the cycle due to the component
Compressor	231.28	185.17	-231.28
Heat addition	1104.30	676.44	-1098.59
CT	-236.00	-265.83	236.00
PT	-100.00	-111.27	100.00
Heat rejection	-999.58	-484.51	70.74
Net	0.00	0.00	-923.13

(b)

Fault-3 with 5% fault magnitude			
Component	Δ Energy flow (kJ/s)	Δ Exergy flow (kJ/s)	Δ Exergy flow (kJ/s) external to the cycle due to the component
Compressor	244.01	194.07	-244.01
Heat addition	1190.75	728.19	-1158.88
CT	-248.99	-281.96	248.99
PT	-100.00	-112.74	100.00
Heat rejection	-1085.77	-527.56	93.08
Net	0.00	0.00	-960.82

(c)

Fault-1 with 10% fault magnitude			
Component	Δ Energy flow (kJ/s)	Δ Exergy flow (kJ/s)	Δ Exergy flow (kJ/s) external to the cycle due to the component
Compressor	221.75	179.68	-221.75
Heat addition	1039.78	637.81	-1053.50
CT	-226.28	-253.70	226.28
PT	-100.00	-112.35	100.00
Heat rejection	-935.26	-451.44	55.05
Net	0.00	0.00	-893.92

(d)

Fault-2 with 10% fault magnitude			
Component	Δ Energy flow (kJ/s)	Δ Exergy flow (kJ/s)	Δ Exergy flow (kJ/s) external to the cycle due to the component
Compressor	235.65	187.49	-235.65
Heat addition	1133.99	694.21	-1119.32
CT	-240.46	-271.38	240.46
PT	-100.00	-110.58	100.00
Heat rejection	-1029.18	-499.73	78.30
Net	0.00	0.00	-936.21

(e)

Fault-3 with 10% fault magnitude			
Component	Δ Energy flow (kJ/s)	Δ Exergy flow (kJ/s)	Δ Exergy flow (kJ/s) external to the cycle due to the component
Compressor	258.09	201.24	-258.09
Heat addition	1347.02	819.97	-1267.25
CT	-263.35	-295.45	263.35
PT	-100.00	-116.72	100.00
Heat rejection	-1241.75	-609.04	136.56
Net	0.00	0.00	-1025.42

(f)

Table C.3: Energy and exergy result for Fault-4 to Fault-6

Fault-4 with 5% fault magnitude			
Component	Δ Energy flow (kJ/s)	Δ Exergy flow (kJ/s)	Δ Exergy flow (kJ/s) external to the cycle due to the component
Compressor	217.02	174.83	-217.02
Heat addition	1081.54	659.34	-1102.65
CT	-221.38	-248.08	221.38
PT	-100.00	-111.80	100.00
Heat rejection	-977.19	-474.29	64.49
Net	0.00	0.00	-933.80

(a)

Fault-5 with 5% fault magnitude			
Component	Δ Energy flow (kJ/s)	Δ Exergy flow (kJ/s)	Δ Exergy flow (kJ/s) external to the cycle due to the component
Compressor	231.28	185.17	-231.28
Heat addition	1104.30	676.44	-1098.59
CT	-236.00	-265.83	236.00
PT	-100.00	-111.27	100.00
Heat rejection	-999.58	-484.51	70.74
Net	0.00	0.00	-923.13

(b)

Fault-6 with 5% fault magnitude			
Component	Δ Energy flow (kJ/s)	Δ Exergy flow (kJ/s)	Δ Exergy flow (kJ/s) external to the cycle due to the component
Compressor	239.55	193.58	-239.55
Heat addition	1136.14	696.28	-1120.83
CT	-244.44	-276.14	244.44
PT	-100.00	-113.37	100.00
Heat rejection	-1031.25	-500.35	78.90
Net	0.00	0.00	-937.04

(c)

Fault-4 with 10% fault magnitude			
Component	Δ Energy flow (kJ/s)	Δ Exergy flow (kJ/s)	Δ Exergy flow (kJ/s) external to the cycle due to the component
Compressor	201.52	161.73	-201.52
Heat addition	1086.74	659.86	-1086.32
CT	-205.64	-229.66	205.64
PT	-100.00	-112.16	100.00
Heat rejection	-982.63	-479.78	65.64
Net	0.00	0.00	-916.56

(d)

Fault-5 with 10% fault magnitude			
Component	Δ Energy flow (kJ/s)	Δ Exergy flow (kJ/s)	Δ Exergy flow (kJ/s) external to the cycle due to the component
Compressor	250.33	200.90	-250.33
Heat addition	1105.11	680.87	-1098.93
CT	-255.43	-288.59	255.43
PT	-100.00	-111.17	100.00
Heat rejection	-1000.00	-482.01	71.24
Net	0.00	0.00	-922.59

(e)

Fault-6 with 10% fault magnitude			
Component	Δ Energy flow (kJ/s)	Δ Exergy flow (kJ/s)	Δ Exergy flow (kJ/s) external to the cycle due to the component
Compressor	252.85	205.31	-252.85
Heat addition	1199.35	734.99	-1164.91
CT	-258.01	-292.97	258.01
PT	-100.00	-115.99	100.00
Heat rejection	-1094.19	-531.34	95.61
Net	0.00	0.00	-964.14

(f)

Table C.4: Energy and exergy result for Fault-7 to Fault-10

Fault-7 with a 50 kW heat loss			
Component	Δ Energy flow (kJ/s)	Δ Exergy flow (kJ/s)	Δ Exergy flow (kJ/s) external to the cycle due to the component
Compressor	227.60	183.13	-227.60
Heat addition	1079.37	661.50	-1137.19
CT	-232.25	-261.15	232.25
PT	-100.00	-111.76	100.00
Heat rejection	-974.72	-471.73	64.51
Net	0.00	0.00	-968.03

(a)

Fault-8 with 5% fault magnitude			
Component	Δ Energy flow (kJ/s)	Δ Exergy flow (kJ/s)	Δ Exergy flow (kJ/s) external to the cycle due to the component
Compressor	229.38	184.75	-229.38
Heat addition	1091.41	668.72	-1089.60
CT	-234.06	-263.41	234.06
PT	-100.00	-111.53	100.00
Heat rejection	-986.73	-478.53	67.45
Net	0.00	0.00	-917.46

(b)

Fault-10			
Component	Δ Energy flow (kJ/s)	Δ Exergy flow (kJ/s)	Δ Exergy flow (kJ/s) external to the cycle due to the component
Compressor	230.13	185.28	-230.13
Heat addition	1082.07	663.59	-1089.57
CT	-234.83	-264.40	234.83
PT	-100.00	-111.71	100.00
Heat rejection	-977.37	-472.76	65.38
Net	0.00	0.00	-919.50

(c)

Fault-7 with a 100 kW heat loss			
Component	Δ Energy flow (kJ/s)	Δ Exergy flow (kJ/s)	Δ Exergy flow (kJ/s) external to the cycle due to the component
Compressor	227.62	183.15	-227.62
Heat addition	1079.50	661.57	-1195.05
CT	-232.26	-261.17	232.26
PT	-100.00	-111.76	100.00
Heat rejection	-974.85	-471.79	64.54
Net	0.00	0.00	-1025.86

(d)

Fault-8 with 10% fault magnitude			
Component	Δ Energy flow (kJ/s)	Δ Exergy flow (kJ/s)	Δ Exergy flow (kJ/s) external to the cycle due to the component
Compressor	231.18	186.39	-231.18
Heat addition	1103.64	676.05	-1098.13
CT	-235.90	-265.71	235.90
PT	-100.00	-111.29	100.00
Heat rejection	-998.92	-485.45	70.57
Net	0.00	0.00	-922.84

(e)

Fault-9			
Component	Δ Energy flow (kJ/s)	Δ Exergy flow (kJ/s)	Δ Exergy flow (kJ/s) external to the cycle due to the component
Compressor	230.21	185.81	-230.21
Heat addition	1150.77	702.54	-1131.00
CT	-241.95	-273.23	241.95
PT	-100.00	-110.39	100.00
Heat rejection	-1039.04	-504.74	81.47
Net	0.00	0.00	-937.80

(f)

Table C.5: Energy and exergy result for Fault-11 and Fault-12

(a)

Fault-11			
Component	Δ Energy flow (kJ/s)	Δ Exergy flow (kJ/s)	Δ Exergy flow (kJ/s) external to the cycle due to the component
Compressor	292.77	226.95	-292.77
Heat addition	1361.99	836.08	-1277.68
CT	-298.75	-334.11	298.75
PT	-100.00	-117.51	100.00
Heat rejection	-1256.01	-611.41	142.36
Net	0.00	0.00	-1029.34

(b)

Fault-12			
Component	Δ Energy flow (kJ/s)	Δ Exergy flow (kJ/s)	Δ Exergy flow (kJ/s) external to the cycle due to the component
Compressor	279.23	216.99	-279.23
Heat addition	1352.93	828.02	-1271.41
CT	-284.93	-318.28	284.93
PT	-100.00	-117.98	100.00
Heat rejection	-1247.23	-608.74	139.29
Net	0.00	0.00	-1026.42

APPENDIX D

Graphs matrices

The graph matrices for the different fault conditions and normal operating conditions are presented in this section. The subscripts (eg. F1.5) of the graph matrix (G) refers to Fault-1 at 5% fault magnitude, F2.10 refers to Fault-2 at 10% fault magnitude. In the case of Fault-7, the subscripts refer to a heat loss of either 50 kJ/s or 100 kJ/s.

$$\mathbf{G}_{F1.5} = \begin{bmatrix} 134.259 & 0 & 590.365 & 0 & 0 & -424.175 & -166.191 \\ 480.241 & -590.365 & 0 & 1373.583 & 0 & 0 & -783.218 \\ -190.381 & 0 & -1373.583 & 0 & 1204.001 & 0 & 169.582 \\ -83.061 & 0 & 0 & -1204.001 & 0 & 1129.917 & 74.084 \\ -341.058 & 424.175 & 0 & 0 & -1129.917 & 0 & 705.743 \\ -668.174 & 166.191 & 783.218 & -169.582 & -74.084 & -705.743 & 0 \end{bmatrix}$$

$$\mathbf{G}_{F2.5} = \begin{bmatrix} 131.641 & 0 & 588.55 & 0 & 0 & -424.131 & -164.419 \\ 480.89 & -588.55 & 0 & 1373.614 & 0 & 0 & -785.064 \\ -188.98 & 0 & -1373.614 & 0 & 1205.84 & 0 & 167.774 \\ -79.105 & 0 & 0 & -1205.84 & 0 & 1134.748 & 71.092 \\ -344.446 & 424.131 & 0 & 0 & -1134.748 & 0 & 710.617 \\ -656.27 & 164.419 & 785.064 & -167.774 & -71.092 & -710.617 & 0 \end{bmatrix}$$

$$\mathbf{G}_{F3.5} = \begin{bmatrix} 126.495 & 0 & 583.454 & 0 & 0 & -424.051 & -159.404 \\ 482.763 & -583.454 & 0 & 1373.67 & 0 & 0 & -790.215 \\ -182.702 & 0 & -1373.67 & 0 & 1210.999 & 0 & 162.57 \\ -75.419 & 0 & 0 & -1210.999 & 0 & 1144.824 & 66.187 \\ -351.272 & 424.051 & 0 & 0 & -1144.824 & 0 & 720.914 \\ -635.936 & 159.404 & 790.215 & -162.57 & -66.187 & -720.914 & 0 \end{bmatrix}$$

$$\mathbf{G}_{F4.5} = \begin{bmatrix} 127.57 & 0 & 582.812 & 0 & 0 & -424.14 & -158.652 \\ 482.891 & -582.812 & 0 & 1373.595 & 0 & 0 & -790.773 \\ -181.594 & 0 & -1373.595 & 0 & 1211.738 & 0 & 161.934 \\ -81.745 & 0 & 0 & -1211.738 & 0 & 1138.621 & 73.042 \\ -346.978 & 424.14 & 0 & 0 & -1138.621 & 0 & 714.492 \\ -667.845 & 158.652 & 790.773 & -161.934 & -73.042 & -714.492 & 0 \end{bmatrix}$$

$$\mathbf{G}_{F5.5} = \begin{bmatrix} 136.214 & 0 & 596.079 & 0 & 0 & -424.165 & -171.915 \\ 479.088 & -596.079 & 0 & 1373.602 & 0 & 0 & -777.522 \\ -194.812 & 0 & -1373.602 & 0 & 1198.215 & 0 & 175.387 \\ -79.862 & 0 & 0 & -1198.215 & 0 & 1127.252 & 70.964 \\ -340.627 & 424.165 & 0 & 0 & -1127.252 & 0 & 703.087 \\ -655.895 & 171.915 & 777.522 & -175.387 & -70.964 & -703.087 & 0 \end{bmatrix}$$

$$\mathbf{G}_{F6.5} = \begin{bmatrix} 133.613 & 0 & 589.463 & 0 & 0 & -424.122 & -165.341 \\ 480.578 & -589.463 & 0 & 1373.635 & 0 & 0 & -784.172 \\ -190.595 & 0 & -1373.635 & 0 & 1204.919 & 0 & 168.715 \\ -78.479 & 0 & 0 & -1204.919 & 0 & 1135.898 & 69.021 \\ -345.048 & 424.122 & 0 & 0 & -1135.898 & 0 & 711.777 \\ -646.752 & 165.341 & 784.172 & -168.715 & -69.021 & -711.777 & 0 \end{bmatrix}$$

$$\mathbf{G}_{F7.50} = \begin{bmatrix} 133.036 & 0 & 589.494 & 0 & 0 & -424.154 & -165.34 \\ 480.547 & -589.494 & 0 & 1373.598 & 0 & 0 & -820.427 \\ -189.711 & 0 & -1373.598 & 0 & 1204.884 & 0 & 168.714 \\ -81.187 & 0 & 0 & -1204.884 & 0 & 1132.239 & 72.645 \\ -342.685 & 424.154 & 0 & 0 & -1132.239 & 0 & 708.085 \\ -703.224 & 165.34 & 820.427 & -168.714 & -72.645 & -708.085 & 0 \end{bmatrix}$$

$$\mathbf{G}_{F8.5} = \begin{bmatrix} 132.809 & 0 & 589.036 & 0 & 0 & -424.146 & -164.89 \\ 480.717 & -589.036 & 0 & 1373.606 & 0 & 0 & -784.57 \\ -189.355 & 0 & -1373.606 & 0 & 1205.351 & 0 & 168.255 \\ -80.177 & 0 & 0 & -1205.351 & 0 & 1133.465 & 71.886 \\ -343.993 & 424.146 & 0 & 0 & -1133.465 & 0 & 709.319 \\ -659.523 & 164.89 & 784.57 & -168.255 & -71.886 & -709.319 & 0 \end{bmatrix}$$

$$\mathbf{G}_{F1.10} = \begin{bmatrix} 135.222 & 0 & 591.074 & 0 & 0 & -424.19 & -166.883 \\ 479.988 & -591.074 & 0 & 1373.572 & 0 & 0 & -782.498 \\ -190.922 & 0 & -1373.572 & 0 & 1203.283 & 0 & 170.289 \\ -84.55 & 0 & 0 & -1203.283 & 0 & 1128.027 & 75.256 \\ -339.738 & 424.19 & 0 & 0 & -1128.027 & 0 & 703.837 \\ -672.731 & 166.883 & 782.498 & -170.289 & -75.256 & -703.837 & 0 \end{bmatrix}$$

$$\mathbf{G}_{F2.10} = \begin{bmatrix} 129.979 & 0 & 587.474 & 0 & 0 & -424.103 & -163.371 \\ 481.275 & -587.474 & 0 & 1373.633 & 0 & 0 & -786.159 \\ -188.141 & 0 & -1373.633 & 0 & 1206.929 & 0 & 166.705 \\ -76.664 & 0 & 0 & -1206.929 & 0 & 1137.602 & 69.327 \\ -346.449 & 424.103 & 0 & 0 & -1137.602 & 0 & 713.498 \\ -649.047 & 163.371 & 786.159 & -166.705 & -69.327 & -713.498 & 0 \end{bmatrix}$$

$$\mathbf{G}_{F3.10} = \begin{bmatrix} 119.092 & 0 & 576.616 & 0 & 0 & -423.885 & -152.732 \\ 485.247 & -576.616 & 0 & 1373.763 & 0 & 0 & -797.147 \\ -174.842 & 0 & -1373.763 & 0 & 1217.915 & 0 & 155.849 \\ -69.076 & 0 & 0 & -1217.915 & 0 & 1158.736 & 59.179 \\ -360.421 & 423.885 & 0 & 0 & -1158.736 & 0 & 734.851 \\ -606.831 & 152.732 & 797.147 & -155.849 & -59.179 & -734.851 & 0 \end{bmatrix}$$

$$\mathbf{G}_{F4.10} = \begin{bmatrix} 119.204 & 0 & 572.627 & 0 & 0 & -424.094 & -148.533 \\ 486.35 & -572.627 & 0 & 1373.604 & 0 & 0 & -800.977 \\ -169.267 & 0 & -1373.604 & 0 & 1222.04 & 0 & 151.564 \\ -82.668 & 0 & 0 & -1222.04 & 0 & 1148.336 & 73.705 \\ -353.619 & 424.094 & 0 & 0 & -1148.336 & 0 & 724.241 \\ -675.749 & 148.533 & 800.977 & -151.564 & -73.705 & -724.241 & 0 \end{bmatrix}$$

$$\mathbf{G}_{F5.10} = \begin{bmatrix} 140.724 & 0 & 599.513 & 0 & 0 & -424.166 & -175.346 \\ 476.934 & -599.513 & 0 & 1373.613 & 0 & 0 & -774.1 \\ -202.153 & 0 & -1373.613 & 0 & 1194.688 & 0 & 178.925 \\ -77.869 & 0 & 0 & -1194.688 & 0 & 1124.641 & 70.047 \\ -337.636 & 424.166 & 0 & 0 & -1124.641 & 0 & 700.474 \\ -646.246 & 175.346 & 774.1 & -178.925 & -70.047 & -700.474 & 0 \end{bmatrix}$$

$$\mathbf{G}_{F6.10} = \begin{bmatrix} 134.253 & 0 & 589.423 & 0 & 0 & -424.086 & -165.338 \\ 480.607 & -589.423 & 0 & 1373.675 & 0 & 0 & -784.252 \\ -191.574 & 0 & -1373.675 & 0 & 1204.964 & 0 & 168.712 \\ -75.844 & 0 & 0 & -1204.964 & 0 & 1139.574 & 65.39 \\ -347.443 & 424.086 & 0 & 0 & -1139.574 & 0 & 715.488 \\ -630.45 & 165.338 & 784.252 & -168.712 & -65.39 & -715.488 & 0 \end{bmatrix}$$

$$\mathbf{G}_{F7.100} = \begin{bmatrix} 133.034 & 0 & 589.489 & 0 & 0 & -424.154 & -165.335 \\ 480.543 & -589.489 & 0 & 1373.598 & 0 & 0 & -856.746 \\ -189.707 & 0 & -1373.598 & 0 & 1204.889 & 0 & 168.709 \\ -81.176 & 0 & 0 & -1204.889 & 0 & 1132.253 & 72.636 \\ -342.694 & 424.154 & 0 & 0 & -1132.253 & 0 & 708.099 \\ -745.144 & 165.335 & 856.746 & -168.709 & -72.636 & -708.099 & 0 \end{bmatrix}$$

$$\mathbf{G}_{F8.10} = \begin{bmatrix} 132.581 & 0 & 588.58 & 0 & 0 & -424.138 & -164.442 \\ 480.88 & -588.58 & 0 & 1373.614 & 0 & 0 & -785.034 \\ -188.999 & 0 & -1373.614 & 0 & 1205.816 & 0 & 167.798 \\ -79.159 & 0 & 0 & -1205.816 & 0 & 1134.684 & 71.131 \\ -345.303 & 424.138 & 0 & 0 & -1134.684 & 0 & 710.547 \\ -656.428 & 164.442 & 785.034 & -167.798 & -71.131 & -710.547 & 0 \end{bmatrix}$$

$$\mathbf{G}_{F9} = \begin{bmatrix} 126.163 & 0 & 579.295 & 0 & 0 & -430.553 & -155.23 \\ 463.891 & -579.295 & 0 & 1340.457 & 0 & 0 & -761.162 \\ -179.212 & 0 & -1340.457 & 0 & 1182.059 & 0 & 158.398 \\ -71.899 & 0 & 0 & -1182.059 & 0 & 1117.837 & 64.221 \\ -333.668 & 430.553 & 0 & 0 & -1117.837 & 0 & 686.883 \\ -616.666 & 155.23 & 761.162 & -158.398 & -64.221 & -686.883 & 0 \end{bmatrix}$$

$$\mathbf{G}_{F10} = \begin{bmatrix} 138.545 & 0 & 595.573 & 0 & 0 & -458.532 & -171.439 \\ 478.376 & -595.573 & 0 & 1373.64 & 0 & 0 & -778.066 \\ -198.235 & 0 & -1373.64 & 0 & 1198.702 & 0 & 174.937 \\ -75.598 & 0 & 0 & -1198.702 & 0 & 1130.848 & 67.854 \\ -324.495 & 458.532 & 0 & 0 & -1130.848 & 0 & 671.887 \\ -646.672 & 171.439 & 778.066 & -174.937 & -67.854 & -671.887 & 0 \end{bmatrix}$$

$$\mathbf{G}_{F11} = \begin{bmatrix} 130.26 & 0 & 591.99 & 0 & 0 & -423.93 & -168.05 \\ 479.9 & -591.99 & 0 & 1373.76 & 0 & 0 & -781.77 \\ -191.78 & 0 & -1373.76 & 0 & 1202.28 & 0 & 171.48 \\ -67.45 & 0 & 0 & -1202.28 & 0 & 1144.88 & 57.39 \\ -350.94 & 423.93 & 0 & 0 & -1144.88 & 0 & 720.94 \\ -590.84 & 168.05 & 781.77 & -171.48 & -57.39 & -720.94 & 0 \end{bmatrix}$$

$$\mathbf{G}_{F12} = \begin{bmatrix} 126.27 & 0 & 586.42 & 0 & 0 & -423.92 & -162.49 \\ 481.87 & -586.42 & 0 & 1373.76 & 0 & 0 & -787.34 \\ -185.22 & 0 & -1373.76 & 0 & 1207.94 & 0 & 165.81 \\ -68.66 & 0 & 0 & -1207.94 & 0 & 1149.75 & 58.19 \\ -354.26 & 423.92 & 0 & 0 & -1149.75 & 0 & 725.83 \\ -597.33 & 162.49 & 787.34 & -165.81 & -58.19 & -725.83 & 0 \end{bmatrix}$$

The graph matrices under normal operating conditions with PT setpoints of 90 kJ/s, 100 kJ/s and 120 kJ/s are shown below.

$$\mathbf{G}_{90} = \begin{bmatrix} 131.939 & 0 & 589.556 & 0 & 0 & -424.216 & -165.34 \\ 480.505 & -589.556 & 0 & 1373.528 & 0 & 0 & -783.972 \\ -188.033 & 0 & -1373.528 & 0 & 1204.814 & 0 & 168.715 \\ -82.004 & 0 & 0 & -1204.814 & 0 & 1132.18 & 72.633 \\ -342.407 & 424.216 & 0 & 0 & -1132.18 & 0 & 707.964 \\ -702.139 & 165.34 & 783.972 & -168.715 & -72.633 & -707.964 & 0 \end{bmatrix}$$

$$\mathbf{G}_{100} = \begin{bmatrix} 133.038 & 0 & 589.499 & 0 & 0 & -424.154 & -165.345 \\ 480.551 & -589.499 & 0 & 1373.598 & 0 & 0 & -784.099 \\ -189.715 & 0 & -1373.598 & 0 & 1204.879 & 0 & 168.719 \\ -81.198 & 0 & 0 & -1204.879 & 0 & 1132.225 & 72.653 \\ -342.675 & 424.154 & 0 & 0 & -1132.225 & 0 & 708.071 \\ -662.576 & 165.345 & 784.099 & -168.719 & -72.653 & -708.071 & 0 \end{bmatrix}$$

$$\mathbf{G}_{120} = \begin{bmatrix} 135.026 & 0 & 589.384 & 0 & 0 & -424.032 & -165.352 \\ 480.819 & -589.384 & 0 & 1373.732 & 0 & 0 & -784.348 \\ -190.331 & 0 & -1373.732 & 0 & 1205.006 & 0 & 168.726 \\ -83.284 & 0 & 0 & -1205.006 & 0 & 1132.316 & 72.69 \\ -342.229 & 424.032 & 0 & 0 & -1132.316 & 0 & 708.284 \\ -598.785 & 165.352 & 784.348 & -168.726 & -72.69 & -708.284 & 0 \end{bmatrix}$$

APPENDIX E

Exergy ratios

The exergy ratios of the individual components for the different fault conditions and fault magnitudes are given in Table E.1 to Table E.3. The exergy ratios for different operational conditions are given in Table E.4 and the exergy ratios for Fault-1 at an operational setpoint of 120 kJ/s are given in Table E.5.

Table E.1: Exergy ratios for Fault-1 and Fault-2

(a) Fault-1

Fault	Compressor	Heat addition	CT	PT	Heat rejection
Fault-1.10	0.81	0.613	0.892	0.89	2.072
Fault-1.5	0.808	0.613	0.891	0.892	2.069

(b) Fault-2

Fault	Compressor	Heat addition	CT	PT	Heat rejection
Fault-2.10	0.796	0.612	0.886	0.904	2.059
Fault-2.5	0.801	0.613	0.888	0.899	2.063

Table E.2: Exergy ratios for Fault-3 to Fault-8

(a) Fault-3

Fault	Compressor	Heat addition	CT	PT	Heat rejection
Fault-3.10	0.78	0.609	0.891	0.857	2.039
Fault-3.5	0.808	0.613	0.885	0.879	2.063

(b) Fault-4

Fault	Compressor	Heat addition	CT	PT	Heat rejection
Fault-4.10	0.803	0.607	0.895	0.892	2.048
Fault-4.5	0.804	0.611	0.892	0.894	2.059

(c) Fault-5

Fault	Compressor	Heat addition	CT	PT	Heat rejection
Fault-5.10	0.803	0.616	0.885	0.9	2.075
Fault-5.5	0.792	0.616	0.9	0.889	2.064

(d) Fault-6

Fault	Compressor	Heat addition	CT	PT	Heat rejection
Fault-6.10	0.812	0.613	0.881	0.862	2.059
Fault-6.5	0.808	0.613	0.885	0.879	2.063

(e) Fault-7

Fault	Compressor	Heat addition	CT	PT	Heat rejection
Fault-7.10	0.806	0.613	0.888	0.899	2.058
Fault-7.5	0.805	0.613	0.889	0.897	2.062

(f) Fault-8

Fault	Compressor	Heat addition	CT	PT	Heat rejection
Fault-8.10	0.805	0.561	0.889	0.895	2.066
Fault-8.5	0.805	0.586	0.889	0.895	2.066

Table E.3: Exergy ratios for Fault-9 and Fault-10

(a) Fault-9

Fault	Compressor	Heat addition	CT	PT	Heat rejection
Fault-9	0.812	0.61	0.883	0.893	2.058

(b) Fault-10

Fault	Compressor	Heat addition	CT	PT	Heat rejection
Fault-10	0.808	0.614	0.882	0.897	2.07

Table E.4: Exergy ratios for different operational setpoints

Setpoint	Compressor	Heat addition	CT	PT	Heat rejection
90 kJ/s	0.798	0.613	0.897	0.886	2.068
120 kJ/s	0.817	0.613	0.886	0.872	2.07
150 kJ/s	0.805	0.613	0.891	0.888	2.067

Table E.5: Exergy ratios for Fault-1 at an operational setpoint of 120 kJ/s

Fault	Compressor	Heat addition	CT	PT	Heat rejection
Fault-1.10	0.823	0.614	0.879	0.891	2.075
Fault-1.5	0.82	0.613	0.882	0.883	2.073